Investigation of Cysteine and Methionine Oxidation Using X-Ray Absorption Spectroscopy

by

Anusha Karunakaran

B.Sc., Simon Fraser University, 2000

M.Sc., University of Sussex, 2002

A THESIS SUBMITTED IN PARTIAL FULFILLMENT OF THE

REQUIREMENTS FOR THE DEGREE OF

DOCTOR OF PHILOSOPHY

in

THE FACULTY OF GRADUATE STUDIES

(Chemistry)

THE UNIVERSITY OF BRITISH COLUMBIA

(Vancouver)

April 2010

ABSTRACT

Cysteine (Cys) and methionine (Met) are sulfur containing amino acids with various oxidation forms. Oxidation of Cys yields cysteinyl radicals that have been postulated as intermediates in several biological contexts including enzymatic catalysis, long-range electron transfer, peptide post-translational modification and cellular redox signaling. The challenges of detecting sulfur-based radicals with electron paramagnetic resonance (EPR) have led to the development of Sulfur K-edge X-ray absorption spectroscopy (S K-edge XAS) as a spectroscopic tool. The reactivity of sulfur-based radicals was studied in a *Pseudomonas aeruginosa* azurin protein system to probe the electronic structure of isolated cysteinyl radicals, which are characterized by S 3p ← 1s pre-edge transition. S K-edge XAS has shown to be a sensitive method in detecting these cysteinyl radicals in hydrophobic and hydrophilic protein environments. The pre-edge feature of the cysteinyl radicals in hydrophobic environments was lower in energy than their hydrophilic counterparts due to hydrogen bonding interactions.

Additionally, S K-edge XAS was employed to study the redox photochemistry of Met and its oxidized forms methionine sulfoxide (MetSO) and methionine sulfone ($MetSO_2$). Met is easily photooxidized to MetSO and $MetSO_2$ in the presence of O_2. In the absence of O_2, photoirradiation leads to the one-electron-oxidized Met cation radical ($MetS^{\bullet+}$), suggesting an alternative mechanism for photooxidation of thioethers through direct oxidation. The photoirradiation of MetSO leads back to Met under both aerobic and anaerobic conditions while $MetSO_2$ is photochemically inert. These findings provide new insights into the formation of age-related cataracts.

Finally, the metal-induced Met oxidation in amyloid-β (Aβ) peptide was investigated. Much of the research to date has focused on the redox chemistry of Cu^{2+} in Aβ peptide with inconsistent findings with regards to the role of Met_{35} and the oxidation state of the Met_{35}. Findings reported here indicate that in the presence of Cu^{2+} alone, Met_{35} was oxidized to MetSO, but surprisingly Fe^{3+} failed to oxidize the Met. These differences in the oxidation behaviour lead to the investigation of the metal binding site in Aβ. Fe^{3+} found to be in a six-coordinate environment with oxygen-rich ligands while Cu^{2+} is in a five-coordinate environment with histidine-rich ligands.

TABLE OF CONTENTS

LIST OF TABLES

LIST OF FIGURES

LIST OF SCHEMES

LIST OF EQUATIONS

ABBREVIATIONS AND SYMBOLS

-	minus; covalent bond
=	equals; double bond
±	plus or minus
~	approximately
←	to (indicates transition)
δ	chemical shift in ppm (NMR)
$\delta_a(k)$	absorberphase shift functions (EXAFS)
Δ	change in
ε_r	dielectric constant
σ_i^2	mean-square deviation in R_i(EXAFS)
μ	absorption; dipole moment, D
$\mu(E)$	total absorption coefficient (XAS)
$\mu_0(E)$	smooth atomic background (spline function; XAS)
ν	frequency
θ	angle in degrees
$\chi(E)$	chi = oscillatory fine structure (EXAFS)
λ	wavelength
$\lambda(k)$	photoelectron mean free path function (EXAFS)
$\phi_i(k)$	total EXAFS phase shift function (EXAFS)
$\psi_i(k)$	scattererphase shift functions (EXAFS)
A	absorber atom
Å	angstrom
$A_i(k)$	backscattering amplitude function (EXAFS)
Aβ	amyloid-β
AD	Alzheimer's disease
ac-Met-NH_2	N-acetyl-L-methionine amide
APP	amyloid precursor protein
BSA	bovine serum albumin
BSS	benzylsuccinate synthase
CaM	calmodulin
cm^{-1}	wavenumber(s)
CN	coordination number
Cys	cysteine
Cys-SOH	sulfenic acid
d	lattice spacing
D	Debye (dipole moment units)
DAO	D-amino acid oxidase
dmphen	dimethylphenanthroline
DNA	deoxyribonucleic acid
E	incident photon energy (XAS)
E_0	ionisation (threshold) energy (XAS; see also *IE*)
EDTA	ethylenediaminetetraacetic acid

EGF	epidermal growth factor
EPR	electron paramagnetic resonance
ERK	extracellular signal regulated kinase
ESR	electron spin resonance
eV	electronvolt(s)
EXAFS	extended x-ray absorption fine structure
FEFF	ab initio code (EXAFS)
$f_i(k)$	EXAFS amplitude function (EXAFS)
GRx	glutaredoxin
GSH	glutathione
GSNO	S-nitrosoglutathione
GSOH	glutathione sulfenic acid
GSSG	glutathione disulfide
h	Planck's constant
$\hbar$	$h/2\pi$
HPLC	high performance liquid chromatography
HSA	human serum albumin
HIV	human immunodeficiency virus
HOTf	triflic acid
I_0	incident light
I_1	transmitted light (after sample; XAS)
I_2	transmitted light (after reference; XAS)
IFEFFIT	command line program (EXAFS)
IPTG	isopropyl-β-thiogalacto-pyranoside
JNK	c-Jun NH_2-terminal kinase
k	photoelectron wavenumber
LB	Luria-Bertani medium
m	mass of the photoelectron
Met	methionine
$MetS^{\bullet+}$	methionine radical cation
Met-SO	methionine sulfoxide
min.	minute(s)
MS	multiple scattering
Msr	methionine sulfoxide reductase
MWCO	molecular weight cut-off
n	harmonic order
N_i	number of atom i scatterers (EXAFS)
NADPH	nicotinamide adenine dinucleotide phosphate (reduced form)
NAPS	nucleic acid protein service
NHase	nitrile hydratase
NMR	nuclear magnetic resonance
OD	optical density
OTf^-	triflate anion = $CF_3SO_3^-$
PBS	phosphate buffered saline
PC	principle component
PCA	principle component analysis

PD	Parkinson’s disease
PDI	protein disulfide isomerase
PeakFit	software for fitting data
PFL	pyruvate formate lyase
pK_a	-log of the acid dissociation constant
Prx	peroxiredoxin
PSH	protein with Cys residue
PSOH	protein sulfenic acids
PSSP	disulfides between 2 proteins
PSSG	S-glutathionylated protein
PTK	protein tyrosine kinase
PTP	protein tyrosine phosphatase
Q_o	Oxidative quencher
R	interatomic distance
R_i	absorber-backscatterer distance for atom *i* (EXAFS)
RNR	ribonucleotide reductases
RNS	reactive nitrogen species
ROS	reactive oxygen species
s	second(s)
S	Scatterer atom
S_0^2	total amplitude reduction factor (EXAFS)
$S_i(k)$	amplitude reduction function (EXAFS)
SHE	standard hydrogen electrode
SixPACK	graphical user interface for XAS data processing and analysis
SOD	superoxide dismutase
SOD1	copper-zinc superoxide dismutase
Srx	sulfiredoxin
SS	single scattering
SSRL	Stanford Synchrotron Radiation Lightsource
TB	terrific broth (media)
Trx	thioredoxin
TrxR	thioredoxin reductase
UBC	University of British Columbia
UV	ultra-violet
Vis	visible
XANES	x-ray absorption near-edge structure
XAS	x-ray radiation spectroscopy
Z	atomic number (atom identity for EXAFS)

ACKNOWLEDGEMENTS

I would like to express my sincere gratitude first and foremost to Pierre for being an excellent supervisor. I really appreciate his flexibility and the freedom that he gave me to adapt projects in the direction that I wanted. Thank you for always having time to discuss research and other interesting topics. Your support, patience, encouragement, and understanding has been vital in my experience as a graduate student.

Joining a new start-up lab has been a great experience because of Vlad, Mario, and Kendra. Thank you for your company and friendship which have made the grad school experience enjoyable. I am very thankful that you have created the right atmosphere in the lab. I want to thank Vlad for keeping me entertained especially during the trips to Stanford. It was great to bounce off ideas with him and I am thankful for his feedback in my research and in preparation of this thesis. I also want to thank Mario for giving a helpful hand whenever I needed, especially developing a program that was essential in my EXAFS analysis. Finally joining our core initial group is the organized Kendra, I am grateful that she was always willing to give a hand in the lab and sharing lab duties. There are plenty of things for which to thank you guys, but above all, I am thankful for our friendship and the bond we now have. I was fortunate to work with three best summer and co-op students Wendy, Alison, and Stephanie. You guys were a pleasure to supervise, and helped me so much with molecular biology work in this thesis. I also want to thank the

present group members Danielle, Thamy, Tulin, and Wei, although it was a short overlap, but it was a memorable one.

I thank Dr. William Wehbi and Prof. Harry Gray for kindly providing me the mutant plasmid to start the Azurin work. I want to thank Dr. Jinhe Pan for synthesis of the amyloid-β peptide.

I would also like to thank the UBC Chemistry department support staff in particular Elena Polishchuk, Candice Martin and Jie Chen for accommodating me in Biological Services, John Ellis for his help with acquisition orders, Pat Olsthoom for his help with sample shipments to SSRL and Marshall Lapawa for the mass spec data collection. Special thanks to Anka Lekhi for having a positive impact and giving great feedback on my teaching skills.

I would like to express my appreciation to the staff at the Stanford Synchrotron Radiation Lightsource (SSRL) for technical and scientific support during data collection. Special thanks to Dr. Serena DeBeer Geroge, who always been ready to help at any time and Dr. Matthew Lattimer for his help with the experimental setup for our photo-irradiation studies.

Finally, I would like to thank my family - Mom and Dad for encouraging and supporting in all my decisions and my grandmother for providing me with her special after-walk snacks and our tea-time which I took for granted during my years at living home. I thank Satesh for being the best brother and always pushing me to the next level. Of course special thanks go to my best biochemistry lab partner and my best friend, my husband Neil for his enduring support and tolerance. He was there for me

throughout the lows and the highs and patiently listening to me rant and rave about everything. I am grateful for all his valuable lessons and always seeing the bigger picture. I feel lucky to have a great loving family and friends. To all of them go my sincerest thanks, respect and appreciation.

This research is funded by NSERC (Canada). Start-up funds and infrastructure support were provided by UBC. Portions of this research were carried out at SSRL, a national user facility operated by Stanford University on behalf of the United States Department of Energy, Office of Basic Energy Sciences. The SSRL Structural Molecular Biology Program is supported by the Department of Energy, Office of Biological and Environment Research, and by the National Institutes of Health, National Center for Research Resources Biomedical Technology Program.

CHAPTER 1: INTRODUCTION

1.1 Thesis Overview

This thesis seeks to address fundamental questions regarding the redox chemistry and biochemistry of cysteine (Cys) and methionine (Met), two sulfur-containing natural amino acids. The work presented herein explores the use of X-ray absorption spectroscopy (XAS) as a tool to probe the redox state of these two important biological molecules and, in doing so, provides new insights into the relevance of sulfur redox processes in disease, particularly in age-related cataracts and Alzheimer's disease.

The present chapter introduces the Cys and Met oxidation in biology highlighting the wealth of oxidative modifications of these two amino acids and their biological implications. It summarises the level of understanding that exists in the current scientific literature. Chapter 2 provides the background and theory of XAS. The data analysis procedures and experimental setup are also described in this chapter. In the subsequent chapters (chapter 3-6), applications of this spectroscopic technique to specific topics have been discussed. This thesis covers three distinct projects that focus on Cys and Met oxidation.

Chapter 3 covers the first project which describes the synthesis and characterization of cysteinyl radical. Currently, there is a lack of a sensitive detection method for cysteinyl radicals. Therefore, sulfur K-edge XAS was used in

this project as a spectroscopic method to investigate cysteinyl radicals in distinct hydrophilic and hydrophobic protein environments. Chapter 4 describes the second project that focused on the photochemistry of methionine, methionine sulfoxide, and methionine sulfone and their importance in age-related cataract formation. The final project is divided into two chapters, chapter 5 and 6. Chapter 5 describes the work on the metal-induced methionine oxidation in amyloid-β peptide and chapter 6 describes the copper(II) and iron(III) binding in amyloid-β peptide. Finally, chapter 7 provides a conclusion of the work herein and considers future directions.

1.2 The Chemistry of Cysteine and Methionine

Cys and Met are the two naturally occurring sulfur containing amino acids typically found in peptides and proteins (Figure 1.1). In humans, Met is an essential amino acid, obtained by dietary intake while Cys is non-essential and a metabolite of Met metabolism. The Cys side chain is distinguished by a thiol functional group. The large, polarizable sulfur atom in a thiol is electron-rich and quite nucleophilic; its nucleophilicity is enhanced in its deprotonated thiolate form. The thiol group is mildly acidic and its pK_a is dependent on the structure and local environment. The pK_a of free Cys in aqueous solution is ~8 but varies considerably in proteins, ranging from as low as 3.5 to a high of 8.7.[1,2] The Met side chain contains a terminal methyl group to form a dialkyl thioether. For this reason, Met possesses a unique combination of hydrophobic properties provided by the terminal methyl group and nucleophilic reactivity provided by the two lone pairs on the sulfur atom. Together Cys and Met fulfill a wide range of essential biological functions.

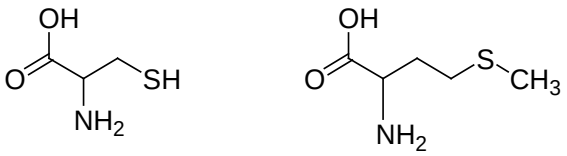

Cysteine (Cys) Methionine (Met)

Figure 1.1 Structures of cysteine and methionine

Cys residues are involved in a number of proteins and enzymes, playing both catalytic and structural functions. Catalytic Cys residues are seen in the active sites of proteases, phosphatases, and proteinases.[3-5] More indirectly, Cys residues are often found as ligands to catalytically active transition metal centres, as observed in nitrile hydratase[6], aconitase[7], and some heme enzymes such as cytochrome P450[8]. The structural role of Cys is observed in protein disulfide bonds[9] as well as in Zn fingers[10]. In addition, Cys also plays a role in cell signaling and antioxidant defence.[9,11,12]

Met plays a mandatory role as an initiator in protein synthesis. Met can also play an important role in stabilizing protein structure, although in a different manner to Cys; due to its hydrophobic properties, Met residues are usually located in the hydrophobic core of proteins, thus stabilizing their tertiary structure.[13] In addition to their structural role, Met residues are found as ligands to metal centres, as seen in cytochrome *c*, azurin and plastocyanin.[14-17] Similarly to Cys, Met also plays a role in antioxidant defence[18] and cell signaling.[19] Of these various functions, antioxidant defence and cell signaling rely on the rich reduction-oxidation (redox) chemistry of

Cys and Met, generally initiated by reactive oxygen and nitrogen species (ROS/RNS).

1.3 Reactive Oxygen and Nitrogen Species

Reactive oxygen species form as a natural by-product of the normal metabolism of dioxygen. ROS include singlet oxygen ($^1O_2$), hydrogen peroxide (H_2O_2), superoxide ($O_2^{\bullet-}$), hydroperoxyl radical ($HO_2^{\bullet}$), hydroxyl radicals ($^{\bullet}OH$), hypochlorous acid (HOCl), chloroamine (RNHCl), and related species.[20-22] A general scheme depicting the generation and metabolism of ROS is given in Scheme 1.1. Mitochondrial respiration is a major source of $O_2^{\bullet-}$, although enzymatic reactions such as those of NADPH oxidase and xanthine oxidase are also important.[23-25] Although $O_2^{\bullet-}$ is a strong oxidant, its conjugate acid ($HO_2^{\bullet}$) is even stronger.[26,27] H_2O_2 and O_2 are formed by dismutation of $O_2^{\bullet-}$ catalyzed by superoxide dismutases (SOD).[28] H_2O_2 may be converted by neutrophil myeloperoxidase or eosinophil peroxidise to a more reactive oxidant HOCl, which can further react with an amine to form chloroamine (RNHCl).[29] ROS are also produced by ionizing and UV radiation. For example, $^1O_2$ is formed upon photoexcitation of endogenous photosensitizers and energy transfer to ground state $^3O_2$.[22] Also, ROS attack on metalloproteins frequently results in the release of their metal ions, such as Zn^{2+}, $Fe^{2+/3+}$, and $Cu^{1+/2+}$. The redox active iron and copper are able to participate in Fenton-type reactions to reduce H_2O_2 to form $^{\bullet}OH$.[30]

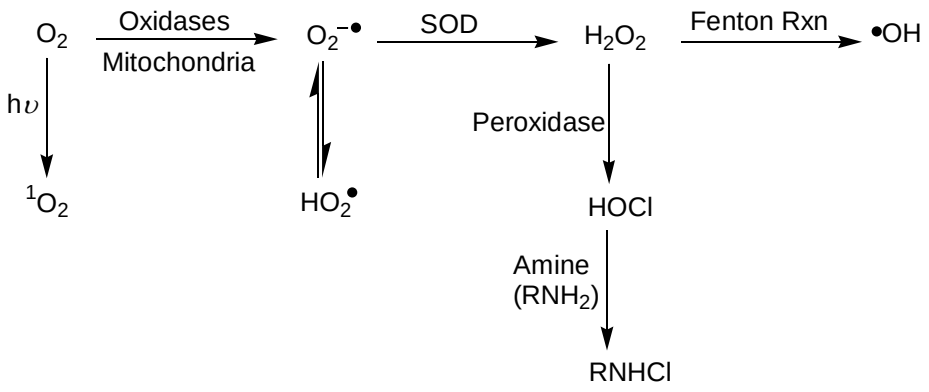

Scheme 1.1 Generation and interconversion of ROS

Analogous to ROS, RNS include nitric oxide radicals ($NO^{\bullet}$) and NO-derived species such as peroxynitrite ($ONOO^-$) and dinitrogen trioxide (N_2O_3). The main source of $NO^{\bullet}$ is via enzymatic oxidation of L-arginine by NO synthase.[31] $NO^{\bullet}$ is unstable in an oxygen environment, therefore it can further react with O_2 to give N_2O_3 and with O_2^- to give $ONOO^-$ (Scheme 1.2).[32]

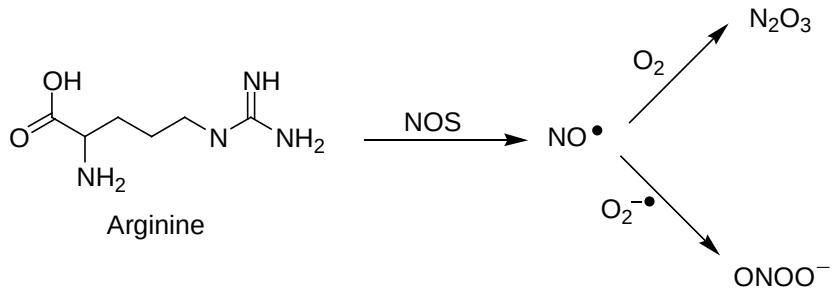

Scheme 1.2 Generation and interconversion of RNS

ROS and RNS play an integral role in the modulation of several physiological functions but can also be potentially destructive if produced in excessive amounts. ROS and RNS are subject to the limitations of the Bertrand diagram[33] (Figure 1.2). Moderate levels of ROS and RNS are essential for normal cell function such as defence against infectious agents, maturation of cellular structures, cell signaling pathways, and the induction of mitogenic response.[34-38] When ROS and RNS levels exceed the cellular antioxidant capacity, a deleterious condition known as oxidative/nitrosative stress occurs. It is a status in which cellular antioxidant defences are insufficient to keep the levels of ROS/RNS below their toxic threshold. This can lead to DNA damage[39], lipid peroxidation[40], and protein modification via oxidation of amino acids[41]. Oxidation of amino acids is associated with either irreversible loss or reversible regulation of protein function.

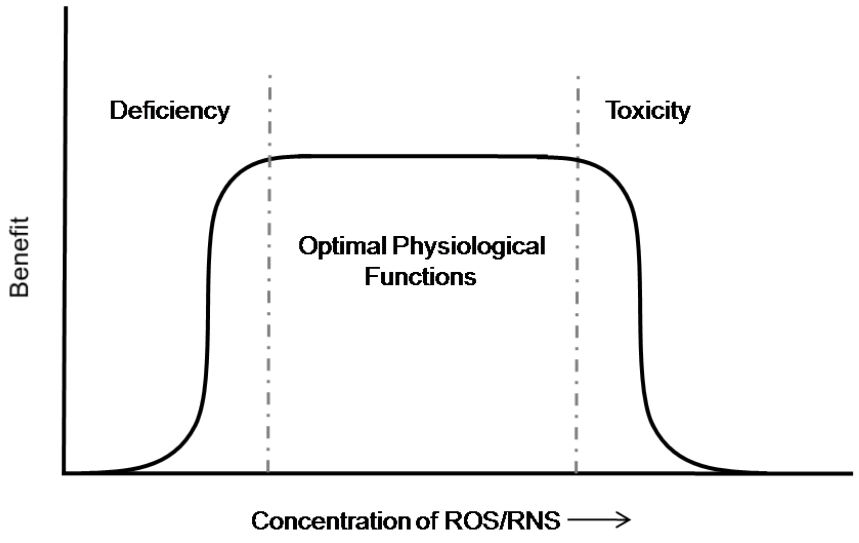

Figure 1.2 Bertrand diagram indicating the benefit of ROS/RNS depends on its concentrations.

To cope with oxidative and nitrosative stress, cells have developed defence strategies at the level of damage repair and antioxidant defence. Key antioxidants are glutathione (GSH), Vitamins C and E, β-carotene, proteins such as albumin as well as enzymatic ROS-metabolizing systems including superoxide dismutase (SOD), catalase, peroxiredoxin (Prx) and GSH peroxidase.[42-44] Repair mechanisms include various protein disulfide reductase enzymes as well as other reducing enzymes such as thioredoxin reductase (TrxR), methionine sulfoxide reductase (Msr) and sulfiredoxin (Srx).[45-49] When ROS and RNS are not tightly controlled by these defence mechanisms, oxidative and nitrosative stress plays a role in the development of chronic and degenerative ailments such as cancer, autoimmune disorders, rheumatoid arthritis, cataract, aging, cardiovascular and neurodegenerative diseases.[34-37,50-53]

1.4 Cysteine Oxidation

Cys has long been recognized as being easily oxidized *in vivo*. The polarizable sulfur atom in Cys is subject to numerous oxidative post-translational modifications in the cellular milieu as shown in Figure 1.3. Oxidation of Cys within proteins may result in various changes to the protein's structure and function, not all of which are detrimental. Oxidative activation and inactivation of proteins can be biologically reversible or irreversible, depending on the Cys oxidation state that is formed.

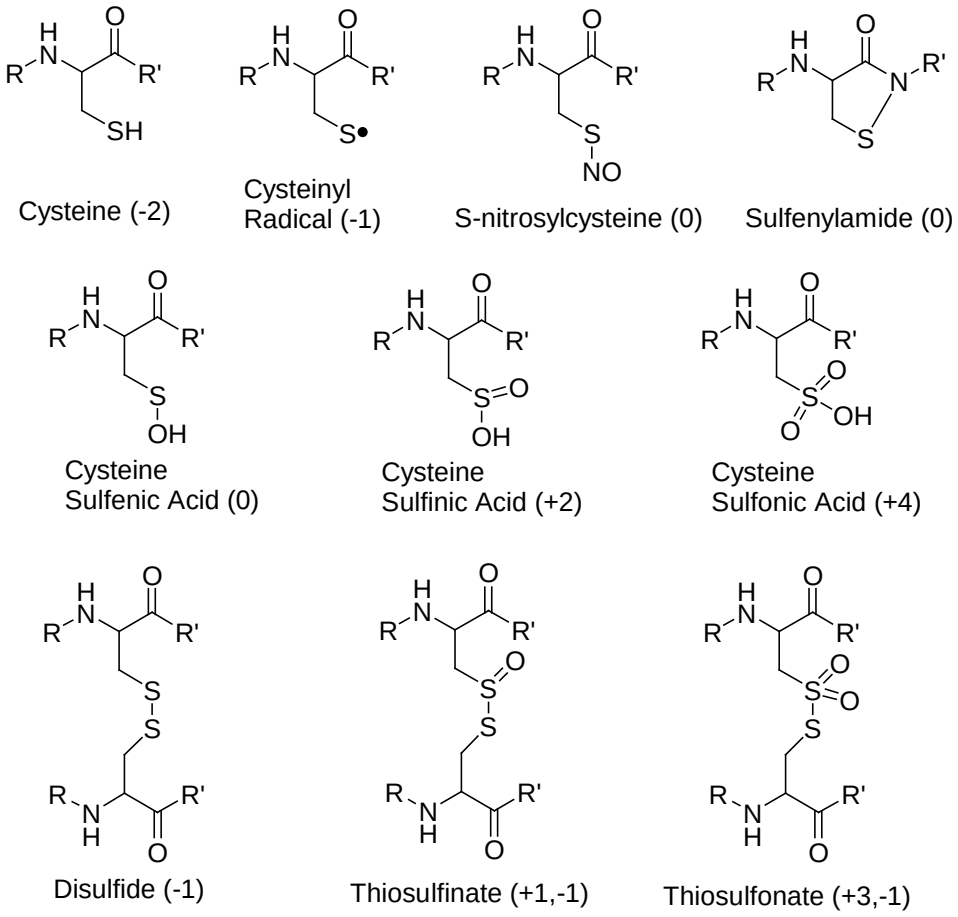

Figure 1.3 Common oxidative modifications of cysteine in proteins that have been observed or proposed to occur *in vivo*. (Formal oxidation states for the sulfur atom(s) in these species are given in parentheses.)

1.4.1 Intra- and Intermolecular Disulfides

The most extensively studied oxidative modification of Cys involves the formation of intramolecular and intermolecular disulfide bonds. The formation of intramolecular disulfide bonds stabilizes the conformation of proteins and is a crucial element of maintaining the tertiary structure of proteins. The disulfide-linked folding in proteins is assisted by protein disulfide isomerase (PDI), a protein that can

catalyze disulfide formation and reduction as well as isomerisation of incorrect disulfides.[54] PDI is found in the endoplasmic reticulum of eukaryotes. In prokaryotes, several periplasmic proteins are involved in protein disulfide formation; such proteins include DsbA, DsbB and DsbC.[55-57] Both disulfide bond formation and isomerase activities occur by thiol-disulfide exchange reactions (Equation 1.1). The ability of PDI and DsbA to catalyze thiol-disulfide exchange reaction is correlated with a presence of a Cys-Xaa_1-Xaa_2-Cys motif in the active site.[58] When the cysteines in the active site are present in the disulfide form, PDI or DsbA can directly oxidize thiol groups of target proteins into disulfide bridges. The reduced DsbA is then reoxidized by DsbB[59] whereas PDI is reoxidized by a protein called Ero1.[60] In contrast, the isomerase activity of PDI relies on the reduced form of the cysteines in the active site, which is suitable for disulfide reshuffling.[61] The isomerase activity in prokaryotes is assisted by DsbC.[62] Thiol-disulfide exchange reactions are nucleophilic substitutions. A thiol or thiolate act as a nucleophilic agent on a disulfide bond. These reactions are not only used to form and destroy structural disulfides in proteins but also to regulate enzyme activity, control cellular signaling pathways and to maintain the cellular redox balance.

Equation 1.1 Thiol-disulfide exchange reaction

$$RSSR + R'SH \rightleftarrows R'SSR + RSH$$

Intermolecular disulfides can form between two proteins (PSSP), which can have regulatory functions. For example, type I protein kinase A contains protein thiols that operate as redox sensor, forming an interprotein disulfide bond between its two regulatory RI subunits in response to cellular H_2O_2.[63] In order to serve as a

redox sensor, disulfide formation must be reversible. In addition to PDI, glutaredoxin (GRx) and thioredoxin (Trx) are involved in reduction of disulfides, however, Trx is more effective in reducing the disulfides in proteins.[64] Trx also contains the Cys-Xaa_1-Xaa_2-Cys motif in the active site, which is involved in reducing disulfide bonds in target proteins through thiol-disulfide exchange reactions, and forms an intramolecular disulfide at the active site in the process. Oxidized Trx relies on thioredoxin reductase (TrxR) for regeneration of its reduced state.[65] The reduction of protein disulfides by the Trx/TrxR system is depicted in Scheme 1.3.

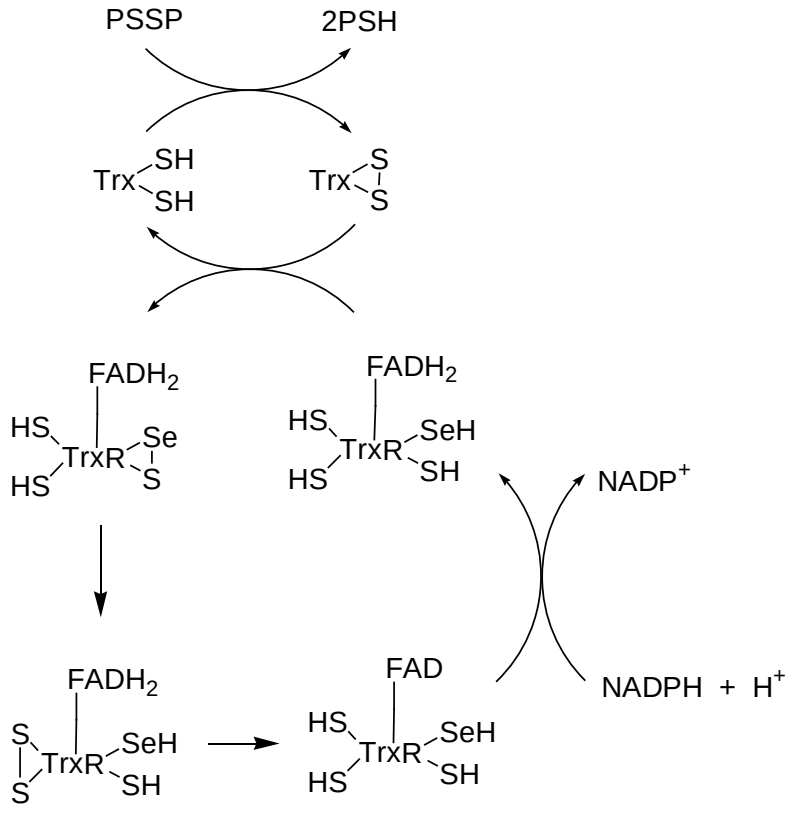

Scheme 1.3 Reduction of protein disulfide bond by thioredoxin/thioredoxin reductase system.[65] PSSP is interprotein disulfide bond and PSH is the reduced protein

Another well known example of a biologically important intermolecular disulfide is that of glutathione disulfide (GSSG). The tripeptide glutathione (GSH) is the most abundant and important low-molecular weight thiol, and is ubiquitously distributed at millimolar concentrations in cells. It has essential roles as an antioxidant and intracellular redox buffer.[66-68] GSH scavenges to remove ROS and during the detoxification of ROS produces GSSG, which can be reduced back to GSH by NADPH-dependent enzyme GSSG reductase.[69] In addition, GSH is involved in cell signaling processes and regulation of protein activity through modifications of the oxidation state of protein cysteines. GSH can form mixed disulfides with the protein Cys residues (PSHs) to generate S-glutathionylated proteins (PSSGs).[70-72] Several mechanisms (Scheme 1.4) have been proposed for the formation of PSSG. Among them is the thiol-disulfide exchange reaction (Scheme 1.4, reaction A), where the thiol group of a Cys residue in protein reacts with the GSSG.[66,73,74] The other proposed mechanisms (Scheme 1.4, reactions B-E) will be discussed in subsequent sections.

Regardless of the route of S-glutathionylation, the process can be reversed by means of a reaction catalyzed by the thiol-disulfide oxidoreductase glutaredoxin (GRx).[75,76] GRx has a conserved active site sequence Cys-Xaa_1-Xaa_2-Cys or Cys-Xaa_1-Xaa_2-Ser and a GSH recognition site.[77] GRx operates via a nucleophilic, double displacement mechanism where the thiolate of GRx initiates a nucleophilic attack on the mixed disulfide of PSSG, leading to formation of a new disulfide between GRx and GSH and the release of the protein substrate in the reduced form. The mixed disulfide between GRx and GSH can be reduced by GSH through

another nucleophilic attack on the disulfide to form GSSG and reduced GRx as the final products (Scheme 1.5).[78-80] Although other enzymes such as PDI, Srx and Trx can carry out this reversible process, GRx is preferentially used for this reaction.[76,81,82]

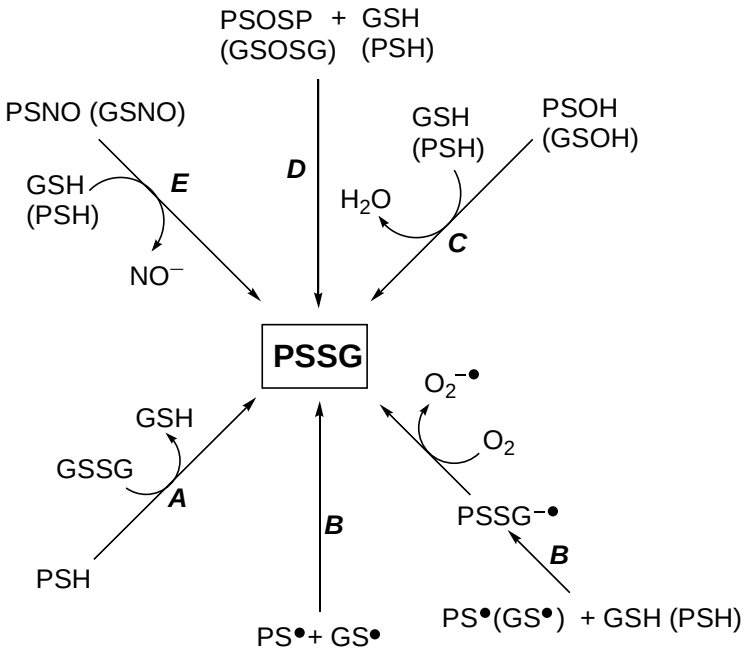

Scheme 1.4 Formation of protein S-glutathionylation, A) Thiol-disulfide exchange, B) Cysteinyl radical, C) Cysteine sulfenic acid, D) Thiosulfinate, E) S-nitrosylcysteine.

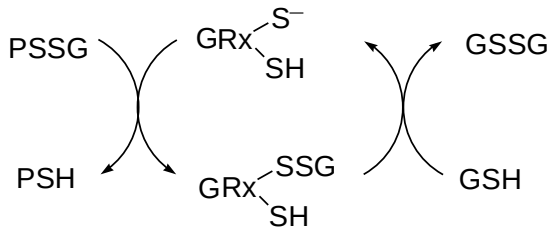

Scheme 1.5 Mechanism of GRx-catalyzed protein deglutathionylation.[80]

The existence of enzymes that selectively reverse S-glutathionylation (deglutathionylation) emphasizes the importance of S-glutathionylation in regulatory mechanisms. S-glutathionylation regulates the structure and function of a wide range of proteins, including enzymes, signaling molecules, transcription factors and ion channels.[72] An example of S-glutathionylation is the regulation of actin polymerization. Actin is a widely distributed cytoskeletal protein that is found to shuttle between monomeric and polymeric forms in cells. In normal cellular conditions, a portion of G-actin (globular actin, monomer) is S-glutathionylated at Cys_{374}, which likely inhibits polymerization into F-actin (filamentous actin). In the presence of epidermal growth factor (EGF), deglutathionylation of Cys_{374} catalyzed by GRx leads to increase in polymerization of G-actin into filaments.[83,84] This shows that cytoskeletal arrangements are regulated by the reversible S-glutathionylation of actin.

At resting levels, S-glutathionylated proteins account for ~1% of the total. Oxidative stress leads to a significant increase in S-glutathionylation,[85] which suggests that S-glutathionylation might also have a secondary role. In addition to its regulatory role, S-glutathionylation may serve as a means of storing GSH and of protection when the cell experiences oxidative/nitrosative stress, by preventing irreversible oxidation of critical Cys residues. This may often occur at the expense of a temporary loss of protein activity.[66] This hypothesis is supported by S-glutathionylation of γ-glutamyl transpeptidase, which appears to protect this membrane-bound enzyme from irreversible oxidation[86] and the S-glutathionylation of α-ketoglutarate dehydrogenase that causes a reversible inactivation in response to

alterations in the mitochondrial GSH status.[87] Although PSSG provides protection from overoxidation, these disulfides can be oxidized further to thiosulfinates (disulfide-S-dioxides, RS(O)SR) and thiosulfonates (disulfide-S-dioxides, $RS(O)_2SR$) under highly oxidative conditions.[88,89] However, even such overoxidation of disulfides can be reversed. In the presence of reducing thiols such as GSH, thiosulfinates are readily converted to sulfenic acids (RSOH) which can then be reduced back to a thiol.[90,91] Such a redox cascade is depicted in Scheme 1.6. The formation and fate of oxidized disulfides *in vivo*, however, still remain unclear.

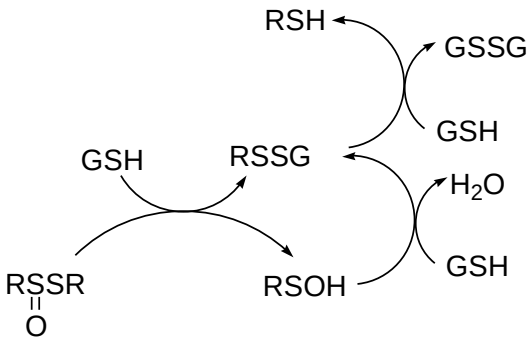

Scheme 1.6 Stepwise reduction of thiosulfinate.

1.4.2 Sulfenic Acids

Cysteines can readily be oxidized to sulfenic acids (CysSOH), which are unstable and highly reactive. The formation of sulfenic acids is dependent on the Cys ionization state as thiolates are more nucleophilic than their protonated counterparts, thiols. CysSOH is formed by several different mechanisms as shown

in Scheme 1.7. CysSOH is formed predominately by the reaction of thiolate with H_2O_2 and other biological oxidants such as $ONOO^-$, and HOCl.[22,92-94] Four other less common reactions include the hydrolysis of protein disulfide bond through an enzyme-facilitated mechanism to generate one thiol and one sulfenic acid.[95] A second mechanism involves the oxidized disulfide, thiosulfinate, which can react with a thiol group to generate a new disulfide bond and CysSOH.[89] Thirdly, cysteinyl radicals can react with O_2 or $^{\bullet}OH$ to form CysSOH.[96] Finally, sulfenic acid is postulated to be formed by the hydrolysis of S-nitosothiols.[97]

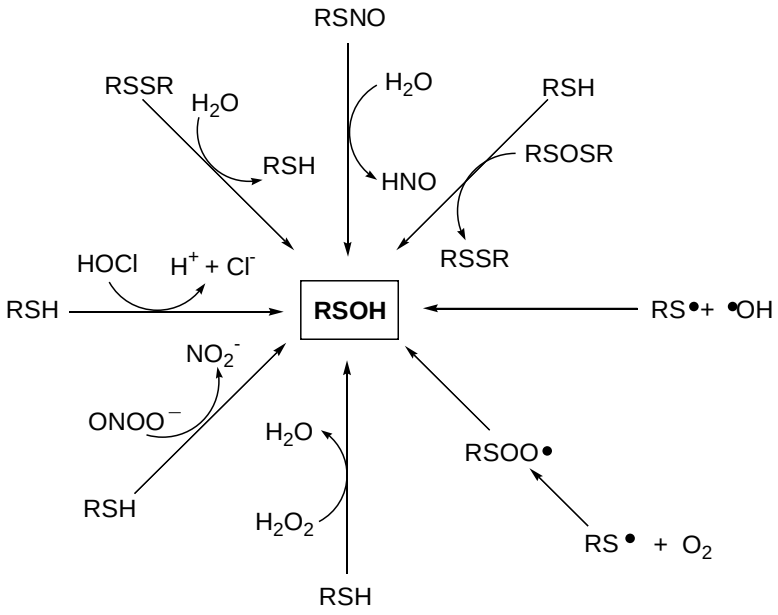

Scheme 1.7 Formation of cysteine sulfenic acid.

Once formed, sulfenic acids can generate other forms of reversibly or irreversibly modified cysteinyl groups. Sulfenic acids are notoriously difficult to study because they are highly unstable, thus evidence for the existence of stable CysSOH in

proteins are limited. Crystallographic evidence of CysSOH has been presented in NADH peroxidase.[98] The stability of CysSOH is highly dependent on its environment. The primary factor in its stability is the absence of proximal Cys group as CysSOH easily reacts with the vicinal thiol to form an intramolecular disulfide bond. CysSOH can also interact with GSH to form S-glutathionylated protein. Likewise, the sulfenated form of GSH (GSOH) can react with Cys in protein to form PSSG.[99] When fixed in close proximity, the sulfur atom in CysSOH can also react with an amide nitrogen in the protein to form a cyclic sulfenamide (Scheme 1.8). This unusual modification was first observed directly in the crystal structure of the protein tyrosine phosphatase-1B[100] and recently in the receptor protein tyrosine phosphatase-α.[101] Sulfenamide can react with GSH to form the S-glutathionylated protein, therefore sulfenic acids play an important role in glutathionylation, which is a reversible process.

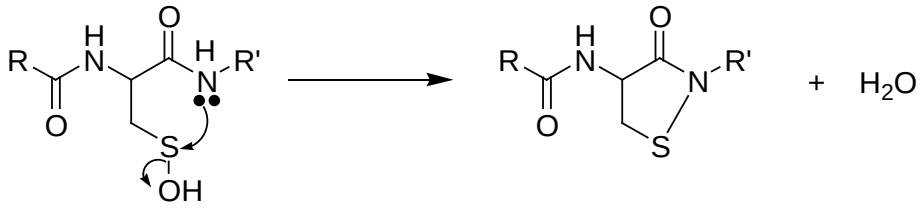

Scheme 1.8 Formation of cyclic sulfenamide.

There are a number of proteins that are involved in sulfenic acid formation that play roles in enzyme catalysis, antioxidant defence, and cell signaling. A noteworthy example of sulfenic acids in enzyme catalysis and in antioxidant defence

comes from peroxiredoxins (Prx), a ubiquitous family of antioxidant enzymes that catalyze the reduction of H_2O_2 and other hydroperoxides. Prx enzymes possess one or two Cys residues in their active site (1-Cys and 2-Cys, respectively) and are divided into three classes: typical 2-Cys Prx, atypical 2-Cys Prx, and 1-Cys Prx.[102] All Prxs share the same basic catalytic mechanism in which the active site Cys residue is oxidized to CysSOH by the peroxide substrate. The recycling of the CysSOH back to a thiol is what distinguishes them into different classes (Scheme 1.9). In 1-Cys Prx, the sulfenic acid likely reacts with a thiol-containing small molecule forming a mixed disulfide bond which is then reduced by a second molecule of the reductant. The identity of the thiol-containing small molecule is not clear but GSH and lipoic acid have been proposed.[102,103] In typical 2-Cys Prxs, the CysSOH from one subunit is attacked by the Cys residue of another subunit forming an intermolecular disulfide bond, which is then reduced by a disulfide oxidoreductase such as Trx.[104,105] Finally, atypical 2-Cys Prxs have a similar mechanism as typical 2-Cys but the Cys residue that is attacking the CysSOH comes within the same subunit forming an intramolecular disulfide bond.[103,106]

The capacity of Cys to cycle between its oxidized sulfenate and its fully reduced thiol form makes it a candidate as a regulatory mechanism in protein function, as has been proposed in protein tyrosine phosphatases (PTP). Reversible phosphorylation of proteins is an important regulatory mechanism. Within the cell, the level of phosphorylation at serine, threonine, and tyrosine residues are under the strict control of protein kinases (phosphorylation) and protein phosphatases (dephosphorylation). These enzymes are in turn regulated by diverse mechanisms.

PTPs catalyze the hydrolysis of phosphotyrosine from specific signal-transducing proteins. PTPs along with protein tyrosine kinases (PTKs) are responsible for maintaining a normal tyrosine phosphorylation status *in vivo*. Figure 1.4 shows the mechanism in which the activity of PTPs themselves may be regulated. Upon activation of a receptor PTK by interaction with epidermal growth factor (EGF) causes an increase in intracellular H_2O_2. This increase in H_2O_2 inhibits phosphatase activity of PTP due to the formation of CysSOH of the active site Cys residue.[107,108] This reversible oxidation of Cys residue plays an important regulatory mechanism for downregulating PTP, thus enhancing tyrosine phosphorylation of proteins including receptor PTK. Dephosphorylation takes place after degradation of H_2O_2 and the subsequent reactivation of PTP by electron donors such as Trx.

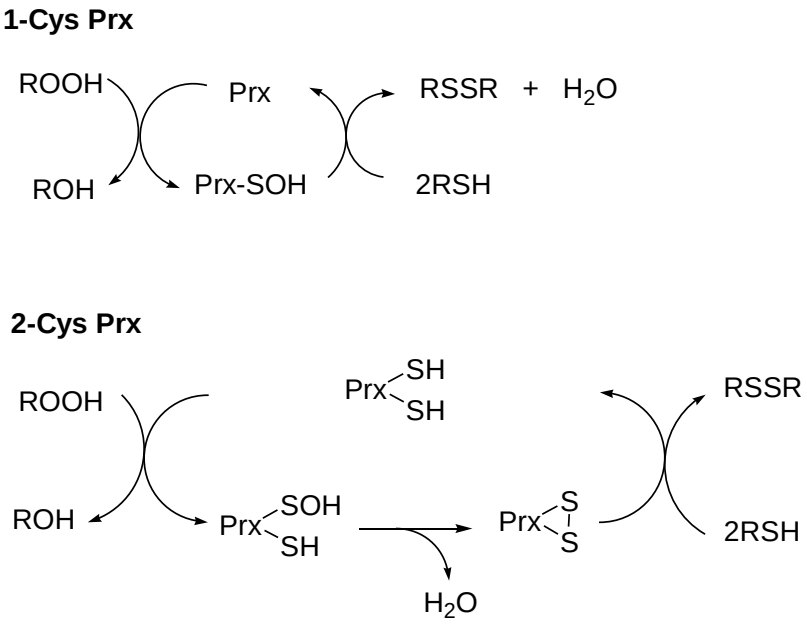

Scheme 1.9 Mechanism of 1-Cys and 2-Cys peroxiredoxins.[102]

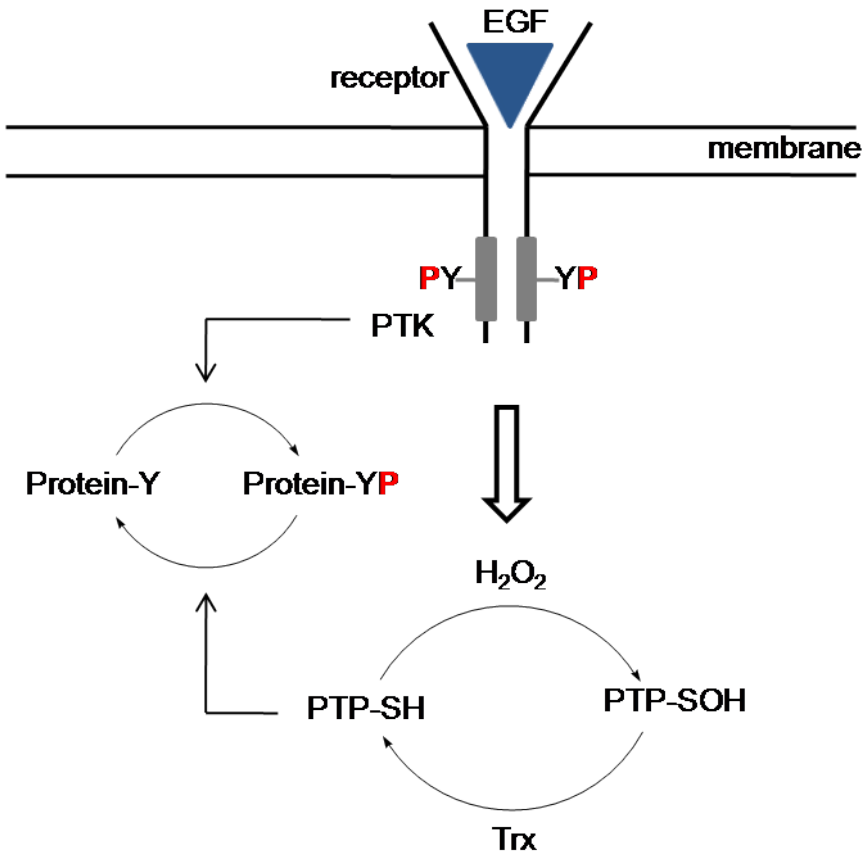

Figure 1.4 Mechanism of PTP activity regulated by H_2O_2. Y is tyrosine residue in protein and receptor. YP and PY are phosphorylated tyrosine residues.[107]

1.4.3 Sulfinic and Sulfonic Acids

Sulfinic acid ($CysSO_2H$) can be formed from sulfenic acid reacting with ROS such as H_2O_2 or via cysteinyl radical interactions with dioxygen (see Section 1.4.5). Unlike sulfenic acids, sulfinic acids do not undergo self-condensation reactions or react with thiols under physiological conditions. Functional roles for sulfinic acid have been identified in numerous proteins including D-amino acid oxidase (DAO),[109] Parkinson's disease protein DJ-1,[110] and copper-zinc superoxide dismutase

(SOD1).[111] In addition, $CysSO_2H$ acts as a ligand to the metal site in nitrile hydratase (NHase), which catalyzes the transformation of nitriles to amides. In this protein, two Cys residues coordinated to the metal are modified to $CysSO_2H$ and CysSOH which is essential for catalytic activity.[6,112] Sulfinic acid has received the most attention in the family of Prxs because of its reversibility by Sulfiredoxin (Srx).[113,114]

Unlike sulfenic acids, sulfinic acids cannot be reduced by major cellular reductants such as GSH and Trx. For this reason, it was generally believed that sulfinylation of proteins was irreversible until the relatively recent discovery of the ATP-dependent enzyme, Srx.[115] However, Srx activity is limited to the reduction of $CysSO_2H$ in Prx proteins and does not provide a general route to desulfinylation. The mechanism of Srx-catalyzed sulfinic acid reduction in Prx proposed by Biteau *et al.*[115] is shown in Scheme 1.10. The first step of the Srx reaction involves phosphorylation of sulfinic acid to form sulfinic acid phosphoryl ester because under physiological conditions, the hydroxyl group of $CysSO_2H$ (pK_a ~ 2.1) is fully deprotonated and cannot serve as the leaving group. Therefore, phosphorylation of the sulfinic acid serves to improve its leaving group ability. The sulfinic acid phosphoryl ester is reductively cleaved by thiols such as GSH or Trx to produce a thiosulfinate. The thiosulfinate is further reduced to the thiol form of Prx after oxidizing three thiol equivalents.

Formation and reversal of sulfinic acid in Prx indicates that Prx might play a role in cell signaling, a unique role for the eukaryotic Prxs. As mentioned above, Prx detoxifies H_2O_2 using the Cys/CysSOH redox cycle. In the presence of extreme

oxidative stress, the concentration of H_2O_2 exceeds the capacity of the enzyme and leads to $CysSO_2H$ formation. Once Prx is converted to $CysSO_2H$, it is no longer enzymatically active, losing its antioxidant role and allowing for the build-up of H_2O_2.[116] H_2O_2 starts the signaling cascade of various proteins[117,118] and is considered to function as an intracellular messenger at subtoxic concentrations. Therefore, Prx acts as a regulator of H_2O_2 mediated cell signaling.

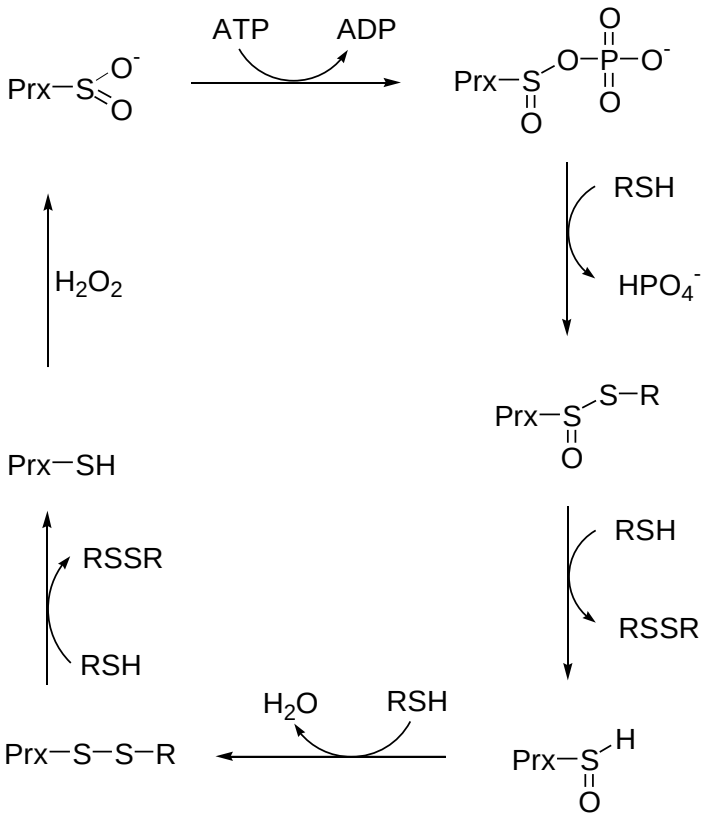

Scheme 1.10 Proposed mechanism of sulfiredoxin catalyzed sulfinic acid in peroxiredoxin.[119]

Sulfinic acids are stable intermediates, but are readily oxidized to sulfonic acid ($CysSO_3H$) by ROS. Under intolerable oxidative stress, Prx loses its antioxidant

function and the cell signaling function due to formation of irreversible $CysSO_3H$. The formation of sulfinic and sulfonic acids depends on the degree of oxidative stress. Other than the sulfinic acid in Prx, both, sulfinic and sulfonic acids are considered irreversibly oxidized forms of Cys; as such, they can impact protein function and homeostasis in many ways. These highly oxidized species with a negative charge distribution and steric requirements can impact protein structure and can inhibit enzyme activity of enzymes that require a thiolate for catalysis.

1.4.4 S-Nitrosylation

S-nitrosylation is a ubiquitous modification of the cysteine thiol by nitric oxide ($NO^{\bullet}$). There is no evidence of a reaction of $NO^{\bullet}$ itself with Cys residues under physiological conditions, but the formation of $NO^{\bullet}$ quickly yields N_2O_3 and $ONOO^-$, as mentioned earlier, both of which react with Cys residues to form S-nitrosylated proteins. Once formed, S-nitrosylated Cys can undergo reductive denitrosylation (catalyzed by Trx/TrxR)[120] or form other reversibly oxidized Cys modifications. It can also promote disulfide formation with neighbouring thiols or react with GSH to form S-glutathionylated protein. Transnitrosylation (transfer of NO group) by low molecular weight S-nitrosothiols such as GSNO (S-nitrosoglutathione) has also been suggested as a possible mechanism for protein S-nitrosylation in a manner analogous to thiol/disulfide exchange (see Section 1.4.1).[121,122] Reversibility of this Cys modification makes S-nitrosylation an ideal candidate for cellular regulatory mechanisms.

The physiological relevance of S-nitrosylation has been confirmed in mammalian plasma where S-nitrosoalbumin and S-nitrosoglutathione possess vasodilatory activity as well as the ability to inhibit platelet aggregation.[123] S-nitrosylation is implicated in cell signaling events within the cell. Critical signaling kinases such as extracellular signal regulated kinase (ERK), p38 and c-Jun NH_2-terminal kinase (JNK) are activated by nitrosylation.[124] Ion channels such as N-methyl-D-aspartate receptor channel complexes, Ca^{2+}-activated K^+ channels, cyclic nucleotide-gated channels, and cardiac Ca^{2+} release channels, are also postulated to be regulated by S-nitrosylation.[125-128] S-nitrosylation is involved in host defence as well. For example, inactivation of the human immunodeficiency virus (HIV)-1 protease can be achieved due to Cys nitrosylation. HIV-1 protease action is modulated by the redox equilibrium of Cys residues at position 67 and 95 and the nitrosylation of these Cys residues inactivates the protease activity which is essential for the life cycle of HIV.[129]

1.4.5 Cysteinyl Radical

There are several routes for the formation of cysteinyl radicals in biology. The general mechanism of GSH antioxidant activity is known to occur through abstraction of the S-bound H atom by carbon-centred radicals with concomitant formation of the cysteine-based radical of GSH.[130] Reaction of Cys with ROS and RNS such as $^{\bullet}OH$ and $ONOO^-$ also generates cysteinyl radicals.[131-133] Cysteinyl radicals also occur in important enzymes such as the ribonucleotide reductase (RNR) superfamily, pyruvate formate lyase (PFL), and benzylsuccinate synthase

(BSS). Cysteinyl radicals in these enzymes are formed by one of two mechansims: (i) long-range one-electron transfer from the Cys or (ii) short range H-atom donation from the Cys.[91] Long-range one-electron transfer occurs in aerobic Fe-dependent (class I) RNR from *E.coli*, which generates a cysteinyl radical by electron transfer from Cys to a remote tyrosyl radical.[134] Active site cysteinyl radical formation in anaerobic formate-dependent (class III) RNR from bacteriophage T4 and in anaerobic PFL from *E.coli* proceeds through a short-range hydrogen-atom donation from Cys residue to a glycyl radical.[135] Furthermore, cysteinyl radicals can be generated in the presence of iron or copper ions.[136,137]

Once formed, a cysteinyl radical can participate in a number of different reactions, (Scheme 1.11). They can be reduced back to Cys through H-atom abstraction. In RNR the hydrogen atom is abstracted either from external dithiols (for class I) or formate (for class III), which are ultimately oxidized to disulfides or CO_2, respectively.[138] However, cysteinyl radicals can also abstract hydrogen from nearby amino acids, which may be a starting point for protein aggregation and/or fragmentation that lead to irreversible protein damage. In addition, cysteinyl radicals can react with thiolates or thiols to form disulfide radical anions ($RSSR^{\bullet -}$), which in turn can react with oxygen to form a disulfide and superoxide that can be removed by SOD.[139] This is a possible mechanism for the formation of S-glutathionylated protein in which cysteinyl radical ($PS^{\bullet}$ or $GS^{\bullet}$) react with GSH or PSH, respectively. Cysteinyl radical could alternatively be intercepted by $^{\bullet}OH$ or $NO^{\bullet}$ to yield sulfenic acid or S-nitrosothiol, respectively.[96,140]

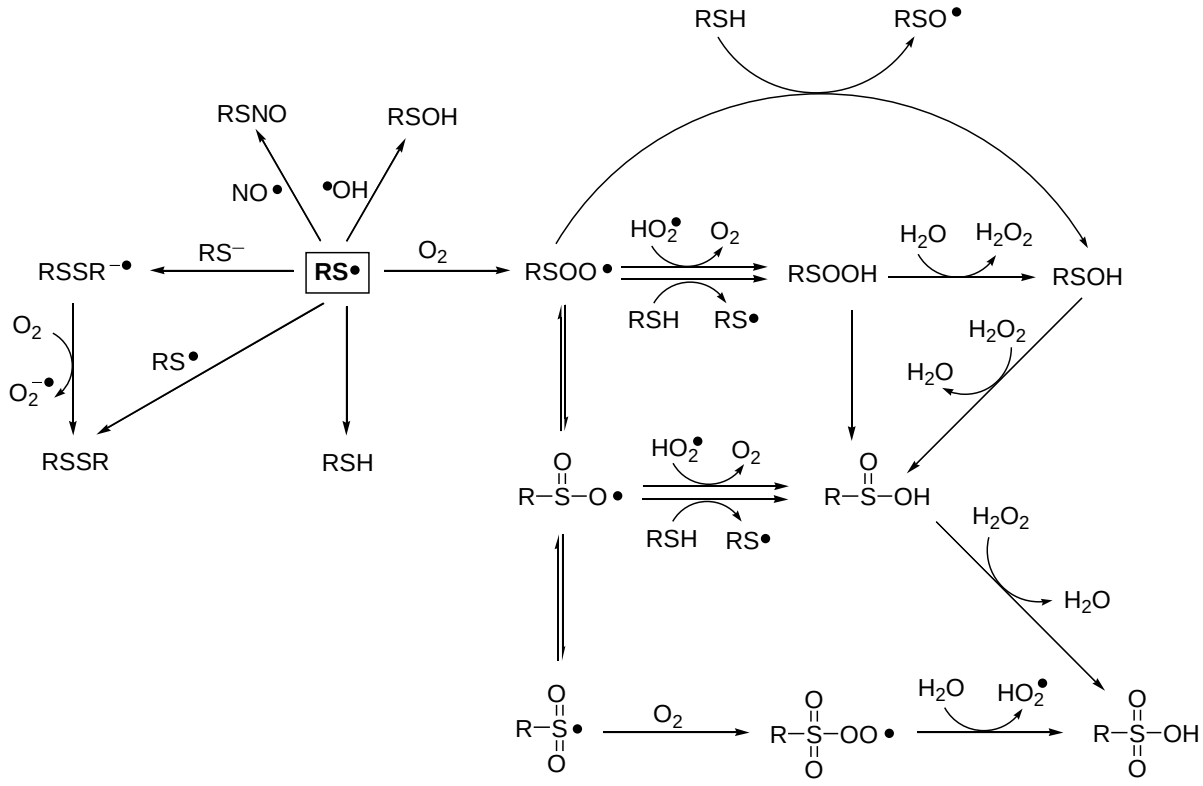

Scheme 1.11 Reactions of cysteinyl radicals.

Cysteinyl radicals can also react with oxygen to form thiyl peroxyl radical ($RSOO^{\bullet}$). $RSOO^{\bullet}$ can further react to form a number of other highly reactive species. $RSOO^{\bullet}$ can isomerize to the fully sulfur-centered, thermodynamically favoured sulfonyl radical ($RSO_2^{\bullet}$). $RSO_2^{\bullet}$ may subsequently react with another oxygen and give rise to sulfonyl peroxyl radical ($RSO_2OO^{\bullet}$).[141] The highly reactive $RSO_2OO^{\bullet}$ intermediate converts ultimately to RSO_3H by reaction with water.[142] $RSOO^{\bullet}$ can also oxidize Cys residues yielding a sulfinyl radical ($RSO^{\bullet}$) and sulfinic acid.[143] All of these radicals species ($RSOO^{\bullet}$, $RSO_2^{\bullet}$, $RSO^{\bullet}$, $RSO_2OO^{\bullet}$) exhibit non-specific oxidizing properties and therefore can be very damaging to cells. Moreover,

$RSOO^{\bullet}$ is seen to be the precursor of sulfenic, sulfinic and sulfonic acids and disulfide.[144] Thiyl hydroperoxides (RSOOH) are possibly present as an intermediate in these processes. RSOOH is generated from $RSOO^{\bullet}$ via H-abstraction from another thiol group or via reaction with $HO_2^{\bullet}$.[145] RSOOH can interact with water to yield H_2O_2 and RSOH or it may react with another thiol molecule to form a disulfide. RSOOH can generate RSO_2H via isomerization which can then react with H_2O_2 to yield the highly oxidized Cys, RSO_3H.[146]

Cysteinyl radicals are considered to be highly reactive species that act as intermediates in the reversible or irreversible formation of other Cys oxidation products. Cys radical generation is important for several biological mechanisms, such as the enzymatic functioning of RNR and PFL, cell signaling (as intermediates of S-nitrosylated proteins), PSSG and sulfenic acid, and antioxidant defence mechanism provided by GSH. It is worth mentioning that the antioxidant defence mechanism provided by Cys radicals is counterbalanced by its ability to abstract hydrogen, which can damage other biomolecules such as amino acids, carbohydrates, and lipids.[147-149] Therefore, the Cys radical is considered a double-edge sword in these biological redox processes.

The amino acid Cys has been regarded as a sink for oxidation processes in peptides and proteins. As discussed above, there are various oxidation products of Cys and the mechanism of Cys oxidation is very complex. The complexity of Cys oxidation is illustrated in Figure 1.5 to give an overall view of each Cys oxidation product and how they interplay with each other.

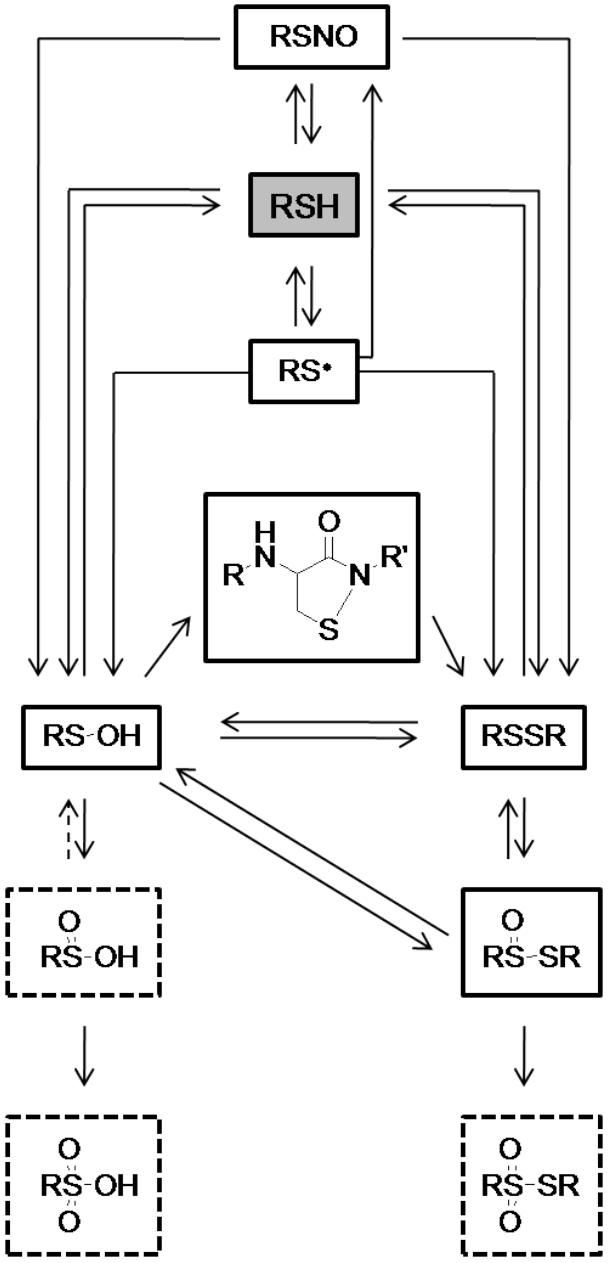

Figure 1.5 Formation of cysteine oxidation products in proteins and peptides. Irreversible oxidation products are framed with dashed lines. The dashed arrow represents one exception where occurs in Prx.

1.5 Methionine Oxidation

Methionine is susceptible to oxidation as well but, unlike Cys, it has fewer oxidized products (Figure 1.6). Met oxidation also involves reversible as well as irreversible oxidation processes.

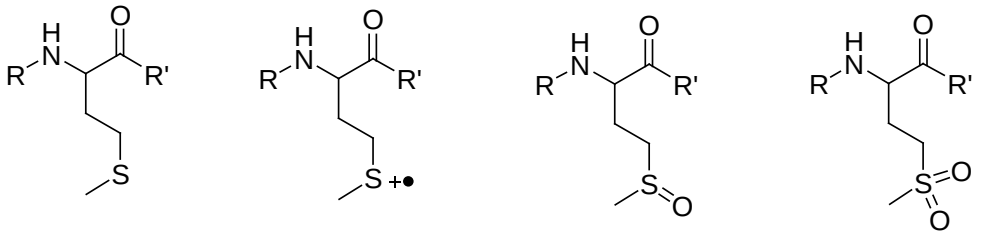

Figure 1.6 Common oxidative modifications of methionine in proteins that have been observed or proposed to occur *in vivo*. (Formal oxidation states for the sulfur atom in these species are given in parentheses.)

1.5.1 Formation and Role of Sulfoxide

Methionine is quite easily oxidized to methionine sulfoxide (MetSO). The biological oxidants that mediate the formation of MetSO are superoxide, hydrogen peroxide, hydroxyl radicals, singlet oxygen, hypochlorous acid, and chloramines.[19,22] Met oxidation leads to a mixture of both the S-and R-stereoisomers of MetSO. MetSO can be reduced back to Met by methionine sulfoxide reductases (Msr) in the presence of Trx. Msr are small cytosolic enzymes found in a variety of organisms ranging from bacteria to mammals.[150-153] There are two classes of Msr, depending

on the stereochemistry at the sulfur center. MsrA is specific for the reduction of (S)-MetSO whereas MsrB is for (R)-MetSO.[154,155] Two possible reaction mechanisms for the Msr have been proposed; proceeding either through a series of thiol-disulfide exchange reaction steps or through a sulfenic acid intermediate formation. Scheme 1.12 shows the mechanism of bovine MsrA which undergoes the thiol-disulfide exchange reaction. The mechanism is initiated by the nucleophilic attack on the sulfoxide sulfur atom by the thiolate anion of Cys_{72} which leads to the formation of a thiosulfinate intermediate. Subsequent attack by the thiolate anion of Cys_{218} and a proton transfer to the sulfoxide oxygen leads to loss of water and formation of Met along with formation of a disulfide bond between Cys_{72} and Cys_{218}. The initial (reduced) state of the active site is then restored with a thiol-disulfide exchange between Cys_{227} and Cys_{218} followed by the reduction of this disulfide bond with Trx.[156] In the case of *E. coli* MsrA (Scheme 1.13), the initial intermediate that is formed by Cys_{51} attack on the sulfur atom of sulfoxide rearranges to a sulfenic acid. During this process Met is released with the oxygen atom transfer from Met to the Cys_{51}. Cys_{198} then attacks Cys_{51} to form a disulfide bond and release of water. The active site is then restored by thiol-disulfide exchange, first by Cys_{206} then by Trx.[157]

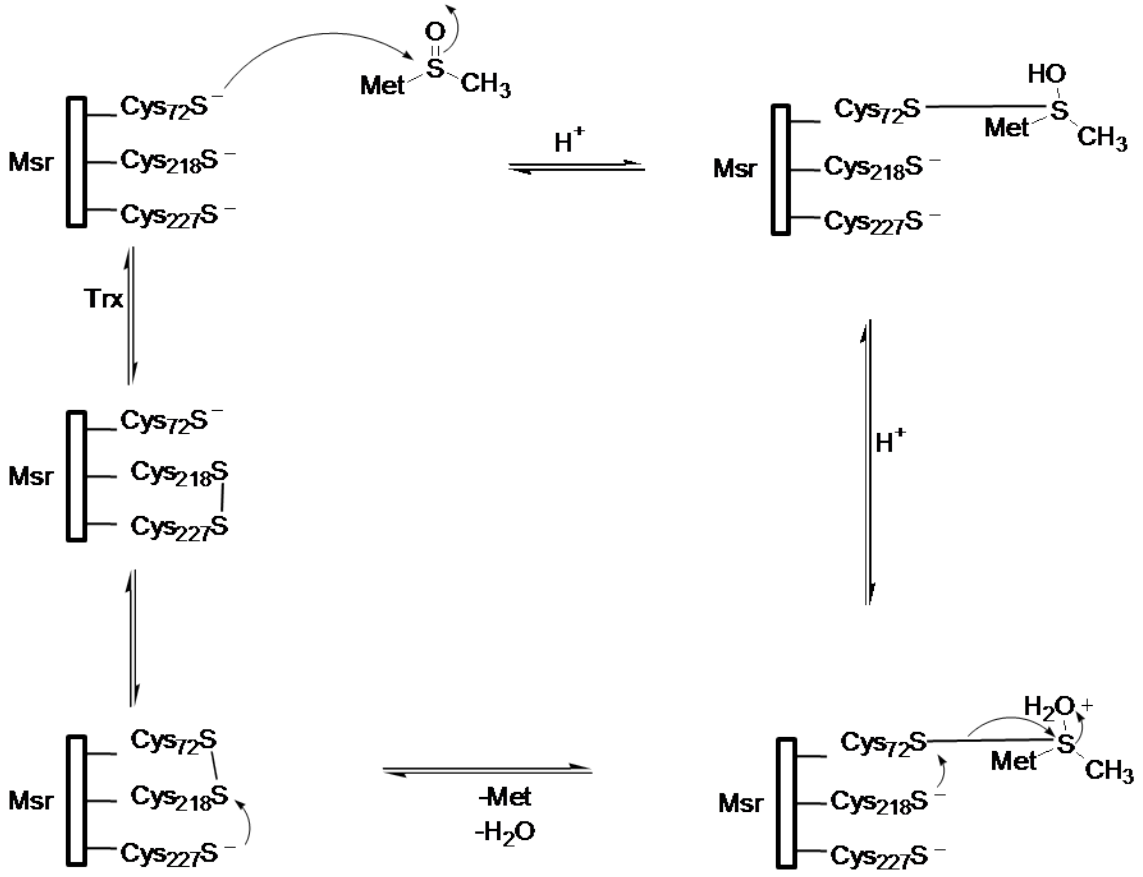

Scheme 1.12 Proposed mechanism of bovine methionine sulfoxide reductase.[156]

The reversibility of MetSO back to Met suggests that MetSO has a biochemical and physiological role. Met oxidation to MetSO can serve as an antioxidant.[158] Surface Met residues in proteins act as protection against oxidation of other residues that are vital for activity. This protective role is observed in glutamine synthetase where 8 of the 16 Met residues are oxidized to MetSO without significantly affecting the enzyme activity. The Met residues near active sites can prevent autoxidation of other amino acids by substrates, products, or cofactors.[18] A further example of Met serving as an antioxidant comes from α-2-macroglobulin, a physiologically important proteinase inhibitor, which acts at sites of inflammation

where ROS and RNS are in relatively high concentration. In such oxidizing environments, Met residues in α-2-macroglobulin get oxidized to MetSO without the loss of antiproteinase activity. However, prolonged exposure to this oxidizing environment causes a single tryptophan (Trp) residue to be oxidized with concomitant loss of antiproteinase activity. This suggests that Met residues serve to protect the critical Trp from damage.[159,160]

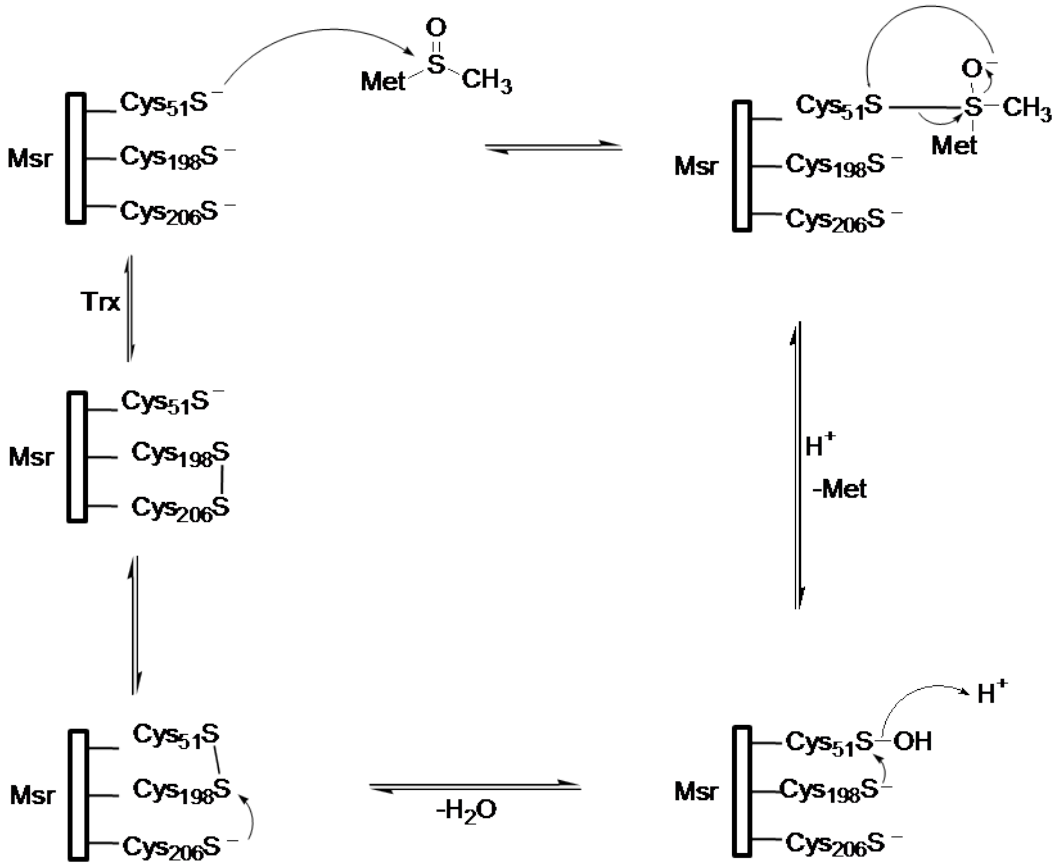

Scheme 1.13 Proposed mechanism for *E.coli* methionine sulfoxide reductase.[157]

The reversibility of MetSO formation also suggests that it may play a role in cell regulation. Evidence for this comes from the Ca^{2+} binding protein calmodulin (CaM). CaM is involved in many cellular processes as it controls the function of a number of enzymes, ion channels, pumps, and other signaling proteins that depend on Ca^{2+}. Upon C-terminal Met oxidation to MetSO in CaM, the protein loses its conformational stability and therefore loses its function.[161] Msr can restore CaM function by reducing MetSO back to Met.[162] This cyclic oxidation and reduction of the specific Met in CaM constitutes a regulatory system by which the activity of numerous cellular signaling systems can be controlled.

1.5.2 Formation and Role of Sulfone

Methionine sulfoxides can be further oxidized by H_2O_2 to methionine sulfones ($MetSO_2$), which are the most oxidized form of Met; no biologically-relevant reduction of $MetSO_2$ has been observed. The biological role of $MetSO_2$ is less apparent. Evidence of $MetSO_2$ is usually observed in pathophysiological states.[110,163] However in a unique example, $MetSO_2$ is shown to act as a ligand and portray a beneficial role. In catalase of *Proteus mirablis PR*, a peroxide resistant mutant of *P. mirabilis* which contains a heme group that interacts with a $MetSO_2$. Catalase, an enzyme found in almost all aerobic organisms catalyzes the dismutation of H_2O_2. The oxidation of Met_{53} could result from the action of H_2O_2 and the presence of $MetSO_2$ does not significantly affect the activity of the catalase. It has been proposed that this formation of $MetSO_2$ could produce some steric hindrance impairing the accessibility of large substrates or inhibitors to the iron containing active site. *P.*

mirabilis PR catalase is less sensitive to aminotriazole, a specific inhibitor of catalase known to bind covalently to the essential distal iron coordinated by histidines.[164]

1.5.3 Methionine Radical Cation

Formation of the methionine radical cation ($MetS^{\bullet+}$) has been suggested, but concrete evidence of such formation *in vivo* is still lacking. Like the cysteinyl radical, $MetS^{\bullet+}$ may act as an intermediate in the formation of MetSO. $MetS^{\bullet+}$ is proposed to be formed via metal-induced oxidation and by ROS such as $^{\bullet}OH$.[165-167]

One example where the biological relevance of $MetS^{\bullet+}$ has been proposed is in the chemistry of amyloid-β (Aβ) peptide and its relevance to Alzheimer's disease (AD). AD is a progressive neurodegenerative disorder with two characteristic features, extracellular deposits of amyloid-β (Aβ) peptide and neurofibrillary tangles.[168-170] Evidence suggests that the aggregation of Aβ is caused by abnormal interactions with metal ions such as Zn^{2+}, Cu^{2+} and Fe^{3+}. Aβ is a relatively small 40 to 42 amino acid long membrane protein with metal binding sites in the N-terminal region.[171] Binding of redox-active metal ions (i.e., Cu^{2+} or Fe^{3+}) is believed to result in the oxidation of Met at position 35. Although, thermodynamically the one-electron transfer from Met_{35} to Cu^{2+} is not favoured, it is enhanced by neighbouring isoleucine (Ile) at position 31. Pulse radiolysis studies have shown that sulfide radical cations can be stabilized through complexation with Lewis bases.[172] Also, one-electron oxidation of the model compound N-acetyl-L-methionine amide has shown that the

thioether radical cation is stabilized through complexation with the amide bond forming a cyclic structure (Scheme 1.14).[167] Thus, it is hypothesized that one-electron oxidation of Met_{35} in Aβ is stabilized through complexation with carbonyl oxygen of C-terminal of Ile_{31} forming a S-O bonded cyclic radical.[165,173]

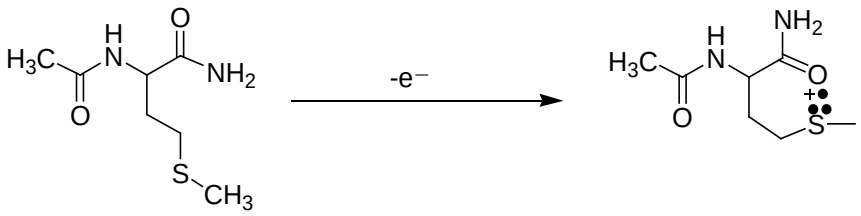

Scheme 1.14 One electron oxidation of N-acetyl-L-methionine amide.

The formation of $MetS^{\bullet+}$ is hypothesized as a possible explanation of how a membrane bound peptide is found to be in the extracellular space of AD individuals. Structural studies indicate that residues 28-36 of Aβ form a helix, which is embedded into the membrane. Oxidation of Met_{35} disrupts the helical conformation and causes Aβ to be dislodged from the membrane forming insoluble aggregates.[174] Evidence of MetSO in Aβ plaques have been observed[175] which suggest that perhaps $MetS^{\bullet+}$ is the intermediate in the metal-induced oxidation of MetSO. AD is not the only unique case where Met oxidation is implicated. Cys and Met oxidation are thought to be involved directly or indirectly in various disease states.

1.6 Implications of Cys and Met Oxidation in Diseases

The irreversible oxidation of Cys and Met in proteins and peptides may lead to loss of function and therefore to pathophysiological states. Similarly poor regulation of reversible Cys and Met oxidation would have similar consequences. When ROS and RNS are produced in excessive amounts, oxidative and nitrosative stress occurs, respectively. Cells try to cope with the oxidative and nitrosative stress through sophisticated antioxidant defence mechanisms, including enzymatic and non-enzymatic processes, and through specific repair mechanisms discussed previously.

Glutathione, one of the major antioxidants involved in detoxifying ROS and RNS, gets oxidized to GSSG. GSSG accumulates in stressed cells and an imbalance in the ratio of GSH/GSSG occurs if cellular processes cannot effectively reduce GSSG back to GSH; the GSH/GSSG ratio has therefore been used as an indicator of oxidative/nitrosative stress in an organism.[176] A high concentration of GSSG may damage many enzymes oxidatively. GSH is also a cofactor for several detoxifying enzymes against oxidative stress such as glutathione peroxidase and glutathionetransferase. Thus, the unavailability of the reduced GSH affects these enzymes and causes more accumulation of ROS and RNS. Under oxidative/nitrosative conditions, an increase in S-glutathionylated proteins occurs to protect the Cys residues in the proteins from irreversible oxidation. A significant increase in PSSGs have been found in diseases such as cancer, HIV, and diabetes mellitus.[177-179] There is also evidence of low GSH levels in lymphocytes of HIV patients.[180] HIV-infected cells have decreased ability to dethiolate PSSGs[178], as

mentioned earlier, dethiolation is dependent on free GSH. Thus, S-glutathionylated proteins have been investigated as possible biomarkers of oxidative stress in correlation with disease. Since the blood concentration of PSSGs may reflect the state of oxidative stress status even in inaccessible tissues, hemoglobin is used as a biomarker for some human diseases.[181] For example, glutathionylated hemoglobin is increased in patients suffering from type I and type II diabetes, Friedreich's ataxia, hyperlipidemia, and uremia.[182-184]

Similarly, alterations in the balance between thiols and their S-nitrosylated forms are believed to be indicative of disease states. Significant increase in S-nitrosylated proteins has been observed in joints of arthritis patients due to the increased level of NO production.[185] In diabetes mellitus, elevated levels of nitrosylated hemoglobin in red blood cells have been observed, which impairs the vascular relaxing activity.[186] Human serum albumin (HSA), the most abundant thiol-containing molecule in plasma, is endogenously S-nitrosylated.[187] Accumulation of nitrosylated HSA in pre-eclamptic women contributes to hypertension because nitrosylated HSA is a weak vasodilator.[188,189]

Antioxidant enzymes such as SOD, Prx and GSH peroxidase can also be affected by ROS/RNS as well.[116,190,191] For example, copper-zinc superoxide dismutase (SOD1) plays a protective role against oxidative stress, however it becomes a major target of oxidative damage itself leading to pathogenicity in various neurodegenerative diseases, including familial amyotrophic lateral sclerosis.[190] SOD1 in humans has a reactive Cys residue, Cys_{111}, at the surface of the SOD1, which is selectively oxidized to the Cys sulfinic acid and to Cys sulfonic acid.[192]

Imbalance between ROS/RNS production and antioxidant enzymes causes an increase in Cys and Met oxidation. This imbalance has been shown to play a role in the pathogenesis of a number of diseases.[193-195]

In addition to overwhelming the antioxidant defence mechanism under extreme oxidative/nitrosative stress, repair mechanisms can also be affected and as a result can increase the oxidation of Cys and Met. Several studies indicate that the level of Msr declines with age-related diseases such as Alzheimer's disease, Parkinson's disease and cataractous lenses.[163,196-198] This decrease in Msr causes accumulation of MetSO which has the potential to be oxidized to the irreversible $MetSO_2$. There is also an increase of MetSO in human skin collagen and erythrocytes[199-201] These various studies are consistent with a generalized age-dependent increase in MetSO content in proteins.

Finally, an increase in ROS and RNS can oxidize Cys and Met to the irreversible forms, which can lead to loss of protein function and hence to the formation of disease. Oxidative damage is thought to be a major factor in the development of age-related cataracts, a leading cause of blindness in the world.[202] Characteristics of age-related cataracts include extensive oxidation, cross-linking, and insolubilization of lens proteins.[203] α-Crystallin is one of the most abundant lens proteins that are found extensively in cataract protein aggregates. Its function is to maintain proper refractive index and to function as a molecular chaperone, helping to prevent formation of large light-scattering aggregates.[204,205] Oxidation affects its chaperone activity which suggests that oxidation may have important consequences for protein aggregation in the lens.[206] Among the amino acids that are oxidized, Cys

and Met are found to be in oxidized forms to a large extent. Cys is oxidized to sulfinic and sulfonic acid and Met is oxidized to the sulfoxide and the sulfone forms.[163]

As mentioned in the previous section, Met oxidation is implicated in AD but Met oxidation is also implicated in other neurodegenerative diseases such as Parkinson's disease (PD). Like other neurodegenerative disease, PD also has the characteristic feature of protein fibril (amyloid) deposits. α-Synuclein is a small, natively unfolded and soluble protein that is found in cytosol and is associated with presynaptic vesicles.[207] The normal function of this protein is not known, but it is found in the aggregates characteristic for several neurological diseases and therefore thought to be a key player in the pathogenesis. Numerous observations suggest that oxidative stress may be associated with PD, and the aggregation of α-synuclein is a critical component in the etiology of PD. The lack of Trp and Cys residues leaves few alternatives for the oxidation of α-synuclein and thus Met is found to be oxidized to MetSO. Formation of MetSO increases the degree of unfolding of this protein.[208] However, the relationship between protein oxidation, protein aggregation and neurodegeneration in PD is still unclear.

CHAPTER 2: X-RAY ABSORPTION SPECTROSCOPY

2.1 Background and Theory

X-ray absorption spectroscopy (XAS) results from the absorption of a high energy X-ray by an atom in a sample. As X-rays with increasing energy are passed through the sample, absorption will occur at a specific energy (threshold) through the process of exciting a core electron into empty or partially-empty bound electronic states or can be ionized to the continuum of unbound states. The ionization to the continuum is a characteristic feature of XAS termed "edge".[209,210] Thus, XAS measures the absorption, μ, by a sample as function of photon energy, *E* which is usually expressed in units of electron-Volts (eV). The shell and the subshell from which the electron is ejected gives rise to the edge's name. The principle quantum number is represented as an uppercase letter and the specific absorption line as a subscript number. For example 1s = K, 2s = L_1, $2p_{1/2}$ = L_2, $2p_{3/2}$ = L_3, 3s = M_1 and so on.[211,212]

XAS is an element specific technique since the energies of the edges (ionization energies) are generally well separated from their nearest neighbours. For example, the S K-edge occurs at approximately 2472 eV, whereas the P and Cl K-edges are at 2146 eV and 2822 eV, respectively.[211] The core electron excitation depends not only on the element but also its chemical environment, so XAS shows also chemical specificity. Therefore, XAS is sensitive to oxidation state, coordination number, and geometry. XAS can be used for almost any element in the periodic

table. Importantly, crystallinity is not a requirement for XAS measurements, thus non-crystalline and highly disordered materials can be probed. Its sensitivity allows the XAS investigation of dilute solutions as well.

A typical XAS spectrum is commonly divided into two main regions: the X-ray absorption near-edge structure (XANES) and the extended X-ray absorption fine structure (EXAFS) (Figure 2.1). Together, XANES and EXAFS can provide complementary information, yet the analysis techniques in these two regions are completely different. The XANES region consists of the pre-edge and the edge. The EXAFS region typically starts at ~40 eV above the edge and can extend to several hundred electron volts above the edge.[213]

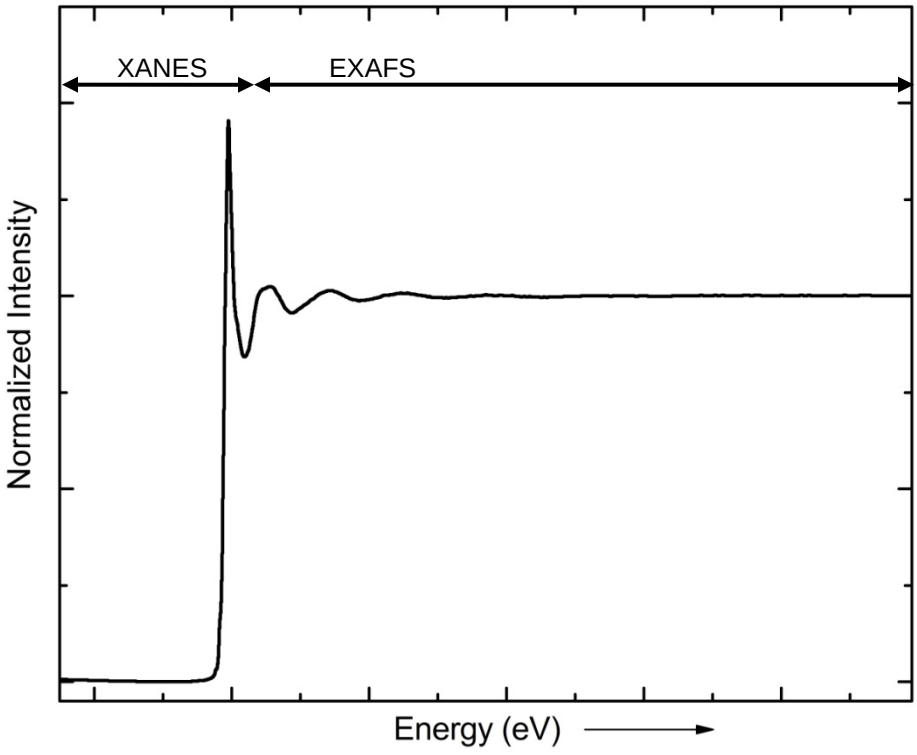

Figure 2.1 XAS spectrum depicting XANES and EXAFS regions.

2.1.1 X-Ray Absorption Near-Edge Structure (XANES)

The XANES region, as mentioned, consists of bound-state transitions (pre-edge) and ionization (edge). The pre-edge transitions normally follow dipole selection rules, i.e., $\Delta l = \pm 1$, but electric quadrupole-allowed transitions can also be visible, particularly at metal edges. For the first-row transition metal K-edge XANES, dipole allowed 4p ←1s and electric quadrupole allowed but dipole forbidden 3d←1s transitions may be observed. The quadrupolar peaks are observed below the absorption threshold (edge). These pre-edge transitions are due to empty valence d-orbitals of the metal which participate in bonding and they are split in energy depending on the ligand field around the absorbing metal.[214] The intensity of pre-edge peaks is generally weak, but can provide information on the coordination environment and charge of transition metal atoms. The dipole allowed bound-state transitions usually dominate the XANES region. The edge jump, a step-like increase, is a unique XAS feature that corresponds to the ionization of the electron to the continuum. Figure 2.2 shows the transitions observed in XANES region and the spectral features.

The XANES region is sensitive to the oxidation state and speciation of the element of interest, and consequently is often used to determine the oxidation state and coordination environment of materials. XANES is capable of distinguishing species of similar formal oxidation states but different coordination. XANES spectra are commonly compared to standards to determine which species are present in an unknown sample. Sulfur K-edge XAS shows particularly rich pre-edge spectra corresponding to dipole allowed transitions that involve excitation of a 1s electron to

antibonding molecular orbitals, which are formed with significant contribution from the sulfur 3p-orbitals.[215] S K-edge spectrum exhibits sharp linewidths and a large chemical shift range over its range of oxidation states[216] as shown in Figure 2.3. As the formal oxidation state of the sulfur increases, the energy of the dipole allowed major peak of the pre-edge spectrum increases as well. These pre-edge transitions provide a sensitive probe of electronic structure and hence of chemical form.

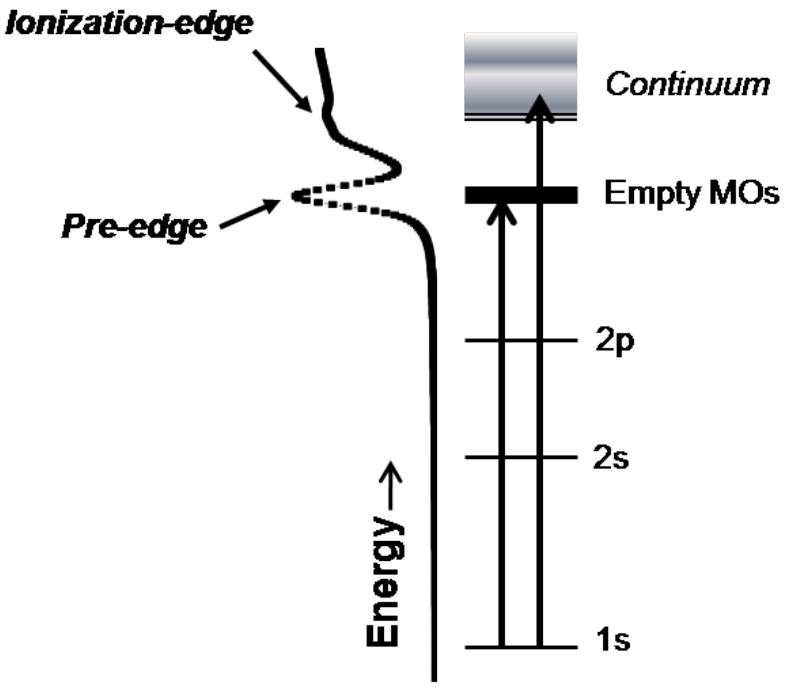

Figure 2.2 XANES transitions and spectral features.

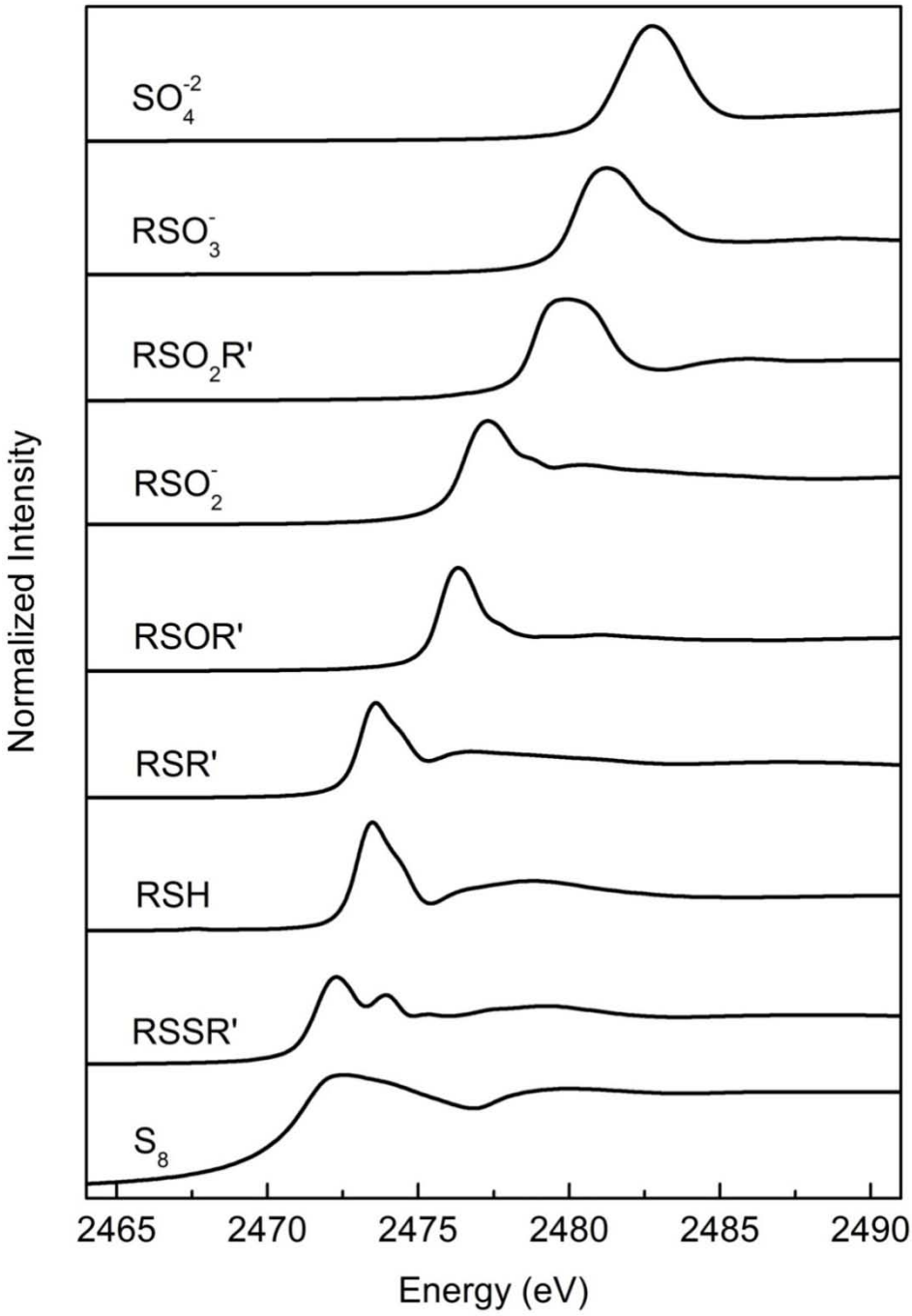

Figure 2.3 Sulfur K-edge spectra of series of oxidized sulfur species.

2.1.2 Extended X-Ray Absorption Fine Structure (EXAFS)

The EXAFS region refers to the sinusoidal waves of the X-ray absorption, μ, observed at energies above the edge as a function of photon energy, *E*. For isolated atoms, μ decreases monotonically as a function of *E* beyond the edge. For atoms either in a molecule or embedded in solid, liquid or matrix, μ displays a fine structure caused by backscattering of the ejected photoelectron from neighbouring atoms.[217] The ejected photoelectron wave propagates out of the central atom (absorber). This propagating electron can be scattered by the neighbouring atoms (scatterers). This scattered wave can either interact constructively or destructively with the outgoing spherical wave resulting in a "peak" or "trough", respectively in the EXAFS region, Figure 2.4.

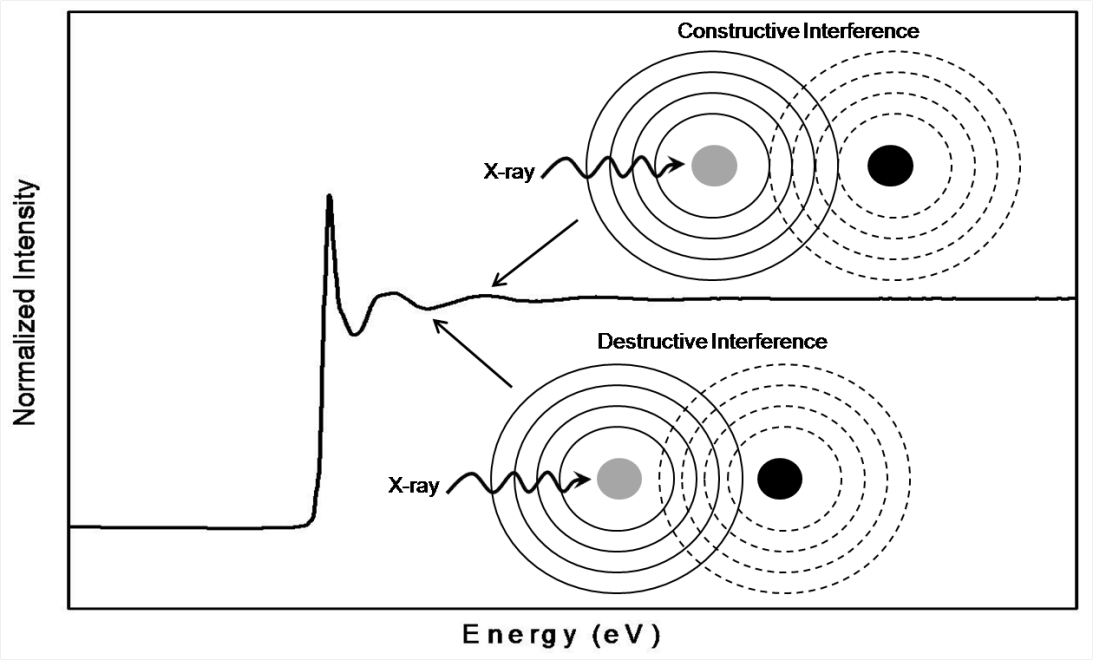

Figure 2.4 The constructive and destructive interference of photoelectron waves that give rise to EXAFS.

Since the oscillation of the X-ray absorption is a direct consequence of the interactions between the photoabsorbing atom and its surrounding environment, EXAFS provides structural information. EXAFS allows quantitative determination of the scatterer's identity (Z ± 1), the number of each type of scatters (N ± 25%), and the interatomic distance between the photoabsorber and scatterers (R ± 0.02 Å).[210]

Because EXAFS results from the wave behaviour of the photoelectron, it is common to convert the X-ray energy to *k*, the wave number of the photoelectron, which is defined as:

Equation 2.1 Photoelectron wavenumber, k

$$k = \sqrt{\frac{2m(E - E_0)}{\hbar^2}}$$

Where:

m = mass of the photoelectron
$\hbar$ = Plank's constant, *h,* divided by 2π
E = incident photon energy
E_0= ionization energy of the core electron

For a single absorber-scatterer path the EXAFS equation can be represented as shown in Equation 2.2. This equation can be broken down into two components, the amplitude and the phase functions. The amplitude of the EXAFS can be dampened by two exponential terms. The first exponential term is related to the mean-free path of the scattered photoelectron and accounts for inelastic loss. The latter is called the Debye-Waller factor, which accounts for the thermal vibrations and static disorder of the system.[210] Lower experimental temperatures reduce the thermal vibration, resulting in larger amplitudes and improved signal to noise ratios. The EXAFS for any absorber-scatterer pair is represented as a damped sine wave with the

amplitude, frequency and phase shift characteristic of the atoms involved. The total EXAFS is the sum of the individual sine waves describing each absorber-scatterer pair interaction. There are two types of parameters present in Equation 2.2: parameters such as S_0^2 and $\lambda(k)$ that are necessary to account for the scattering process and parameters such as N_i, R_i, and σ_i^2 that bear structural information. The structural parameters are relevant in understanding the metal sites in bioinorganic systems. Table 2.1 summarizes the structural information that can be extracted from an EXAFS region.

Equation 2.2 EXAFS single-scattering equation

$$\chi(k) = \underbrace{S_0^2 \sum_i \frac{N_i A_i(k)}{kR_i^2} \exp\left(-2R_i / \lambda(k)\right) \exp\left(-2\sigma_i^2 k^2\right)}_{amplitude\ function} \underbrace{\sin\left[2kR_i + \phi_i(k)\right]}_{phase\ function}$$

Where:

N_i = number of atom i scatterers
R_i = absorber-backscatterer distance for atom i
σ_i^2 = mean-square deviation in R_i (part of the Debye-Waller factor)
S_0^2 = total amplitude reduction factor; accounts for electronic relaxation
$\lambda(k)$ = photoelectron mean free path function
$A_i(k)$ = backscattering amplitude function (including amplitude reduction function, $S_i(k)$ and EXAFS amplitude function, $f_i(k)$); $A_i(k) = S_i(k)f_i(k)$
$\phi_i(k)$ = total EXAFS phase shift function (including scatterer, $\psi_i(k)$, and absorber, $\delta_a(k)$, phase shift functions); $\phi_i(k) = \psi_i(k) + \delta_a(k)$
k = photoelectron wavenumber

Table 2.1 Summary of structural information extracted from EXAFS.

Structural Information	From sine wave
Distance between absorber and scatterer (R_i)	Frequency
Coordination number (N_i)	Amplitude
Scatterer identification (Z)	Phase shift and amplitude
Debye-Waller factor (σ_i^2)	Damping effect

As mentioned above, Equation 2.2 is only applicable to a single-scattering model where each photoelectron is backscattered from one atom. However, in addition to single-scattering, multiple-scattering can also occur in which the photoelectron is scattered by two or more atoms before returning to the absorber. The net effect of scattering by multiple atoms is that the amplitude and phase functions are modified. The strength of a multiple-scattering path depends on the angle between the central atom and the scattering atoms (scattering angle). In most cases, three-body multiple scattering interactions contribute to the EXAFS region (Figure 2.5). For such interactions to have significant intensity, the scattering angle has to be $\geq 150^{o}$. Multiple-scattering is also important for rigid structures such as histidine or tyrosine residues.[209] A combination of all the single- and multiple-scattering processes results in the final EXAFS region. There are several EXAFS fitting programs which incorporate single- and multiple-scattering theory.

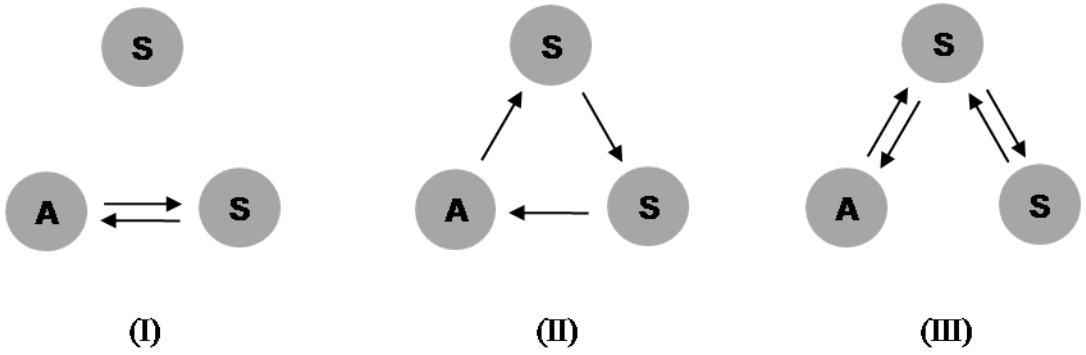

Figure 2.5 Scattering pathways in a three-body configuration consisting of absorber (A) and scatterer (S). (I) is the single-scattering pathway and (II) and (III) are possible multiple-scattering pathways.

2.2 Experimental Set-up

Since the excitation of electrons requires high energies, this technique demands high energy and tunable X-ray sources. As a result, it is done at synchrotron radiation facilities. All the XAS data for this thesis were collected at the Stanford Synchrotron Radiation Lightsource (SSRL).

Synchrotron radiation is the electromagnetic radiation produced by the acceleration of electrons traveling at a velocity close to the speed of light in a magnetic field. Electrons are accelerated in a booster ring to relativistic speeds and directed to the storage ring. Within the storage ring, large dipole magnets guide the electrons around a "curved" orbit. The storage ring in reality is not circular but a many sided shape with straight sections. In these straight sections, insertion devices such as undulators and wigglers, containing a specialised set of magnets are placed to intensify the beam.[218,219] X-ray radiation is emitted tangentially to the electron path in the magnetic fields of the ring. A schematic of the X-ray emission is

shown in Figure 2.6. The emitted photons contain electromagnetic radiation ranges from hard X-ray to infrared wavelengths, and can be tuned to a desired wavelength using various optical devices and filters.[218]

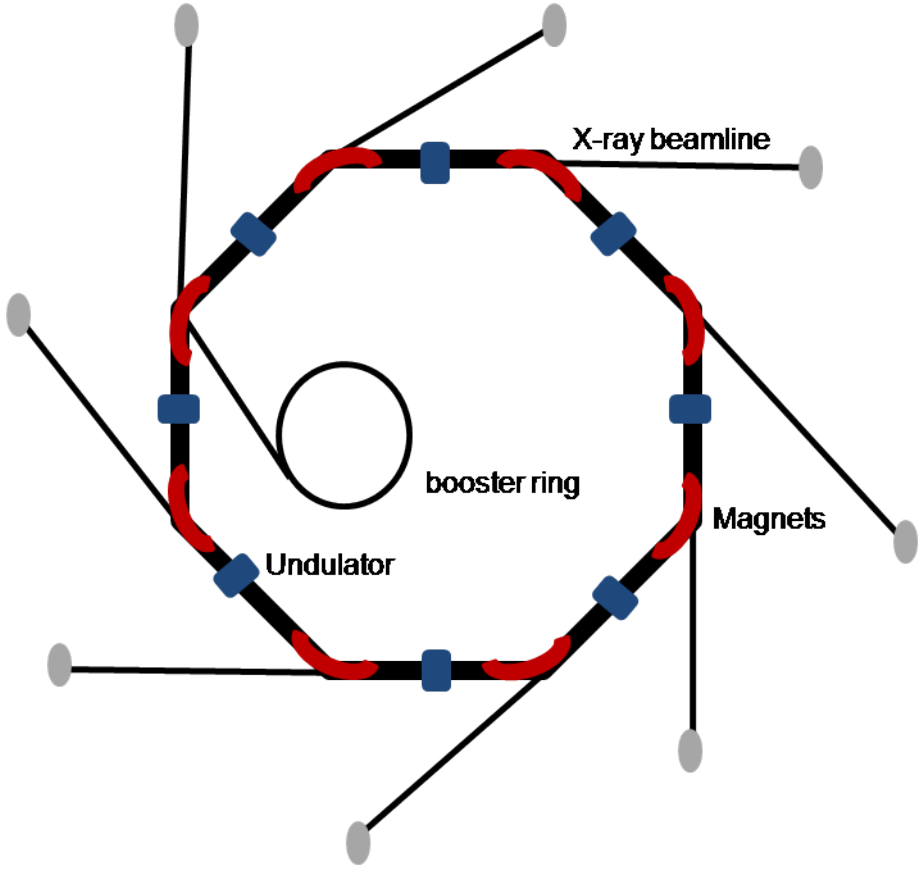

Figure 2.6 Schematic of a synchrotron

The research presented in this thesis was performed at two different beamlines at SSRL. The sulfur K-edge XAS data were collected from beamline 6-2 and the metal K-edge XAS data (hard X-ray) were collected from beamline 7-3. The basic set-up of these beamlines differs slightly. A simplified schematic of the beamlines are shown in Figure 2.7.

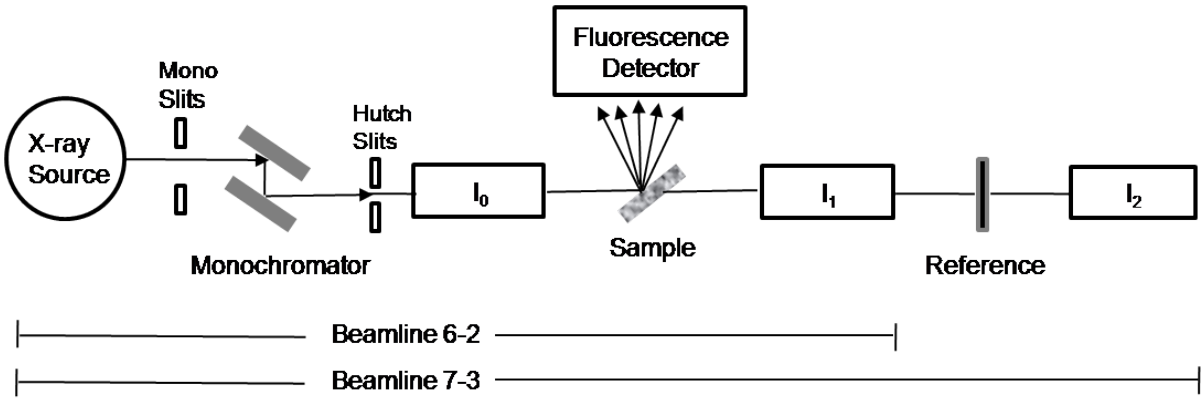

Figure 2.7 XAS experimental set-up

The size of the beam is defined vertically and horizontally using slits before passing through a double crystal monochromator, which is used for energy selection. Two parallel crystals diffract the beam according to Bragg's law:

Equation 2.3 Bragg's Law

$$n\lambda = 2d\sin\theta$$

where λ, n, and d are the wavelength of the diffracted X-rays, the harmonic order, and the lattice spacing at that plane at a Bragg angle θ from the beam direction. The X-ray wavelength is controlled by a computer system, which rotates the monochromator so that θ changes at a constant rate per unit time. Thus measurements over the entire energy region of interest can be taken.

The monochromatized beam is further defined in size using a set of vertical and horizontal slits before it enters the experimental hutch. For beamline 6-2, the beam enters a He-filled ionization chamber (I_0), which is used to measure the intensity of the incident beam. The I_0 chamber in beamline 7-3 is filled with N_2 gas.

The beam then passes through the sample compartment and the transmitted light (I_1) is detected in a second ion chamber providing the transmission data I_1/I_0. For dilute solution samples, the I_1 signal is usually very weak and fluorescence detection mode is used. At beamline 6-2, the S K-edge XAS measurements are only measured using fluorescence mode. A Lytle detector is used to collect the fluorescence from the sample. In the hard X-ray set-up (beamline 7-3), a Ge detector is used which has an array of germanium crystals that simultaneously collect fluorescence data, which are averaged together to reduce noise. In either set-up the fluorescence detector is placed at 90^o to the incident beam and the sample is oriented at a 45^o angle from both the incident beam and to the detector. The spectrum is obtained as FF/I_0. All the data in this thesis were collected in fluorescence mode.

In the case of hard X-ray measurements, internal calibration of the incident beam energy is possible by measuring the absorption of a reference sample using a third ionization chamber I_2, providing the reference transmission data I_2/I_1. In contrast, beamline 6-2 does not provide internal calibration. An external calibrant needs to be run before and after the sample for proper energy calibration. In beamline 7-3, the sample is located in a vacuum chamber with a helium cryostat that maintains a constant low temperature (usually < 20 K), which helps prevent or reduce photoreduction of sensitive samples as well as minimise the disorder. In beamline 6-2, samples can be maintained from room temperature to < 20 K with a helium cryostat, depending on the type of experiment.

2.3 Data Reduction and Analysis

XAS data reduction and analysis requires a number of steps and a variety of computer programs are used.

2.3.1 Sulfur K-edge XANES

SixPACK software was used for S K-edge data reduction.[220] The raw fluorescence data were inspected to eliminate beam or sample induced abnormalities. To ensure that the data were reproducible, two or more sweeps* were run for each sample. The sweeps of a run were averaged together and the energy position was calibrated using reference data. Pre and post-data energy calibration scans were compared, and the energy scale of the data was adjusted by taking the first pre-edge feature of sodium thiosulfate ($Na_2S_2O_3$) and setting this to 2472.02 eV. A smooth second-order polynomial background was fitted for the pre-edge region and subtracted from the entire spectrum. The intensity of the edge jump is concentration dependent, thus normalization is required to enable comparisons between different samples. Normalization of the data was accomplished by fitting a flattened second-order polynomial to the post-edge region and normalizing to an edge jump of 1.0. Energy positions of features in the

* One sweep corresponds to the energy scan from low to high energy for the relevant region, producing an XAS spectrum.

normalized spectrum were obtained from the minima of the second derivative spectrum of the data.

2.3.2 Metal K-edge XANES and EXAFS

ATHENA software[221] was used for Cu and Fe K-edge XANES data reduction. The data processing is similar to the procedures used for analysis of S K-edge. For energy calibration, the lowest-energy maximum of the first derivative of the reference spectra was assigned, for Cu K-edge was set to 8979 eV and for Fe K-edge was set to 7112 eV. The averaged energy calibrated data was used for EXAFS processing but the steps required for this is different from XANES.

The EXAFS region has an oscillatory fine structure described by $\chi(E)$. To process the data in this region, a smooth pre-edge function was first subtracted, then $\chi(E)$ is extracted from the spectra by fitting a spline function, $\mu_0(E)$, above the edge. $\mu_0(E)$ corresponds to the absorption of an isolated atom. In addition, EXAFS data was normalized to the edge jump of the smooth atomic-like background, $\Delta\mu_0$ (Equation 2.4, Figure 2.8A)

Equation 2.4 Oscillatory fine structure, $\chi(E)$

$$\chi(E) = \frac{\mu(E) - \mu_0(E)}{\Delta\mu_0}$$

Once the final $\chi(E)$ function has been extracted, the oscillations can be viewed in k-space ($Å^{-1}$), which is usually weighted as k^3 to emphasize the high k region (Figure 2.8B). The Fourier transformation is used to convert the data from k-

space to R-space (Å), a more conceptually useful depiction (Figure 2.8C). The Fourier transformation gives peaks at the distances between the absorber atom and its neighbours, although slightly shifted from the true value of R.

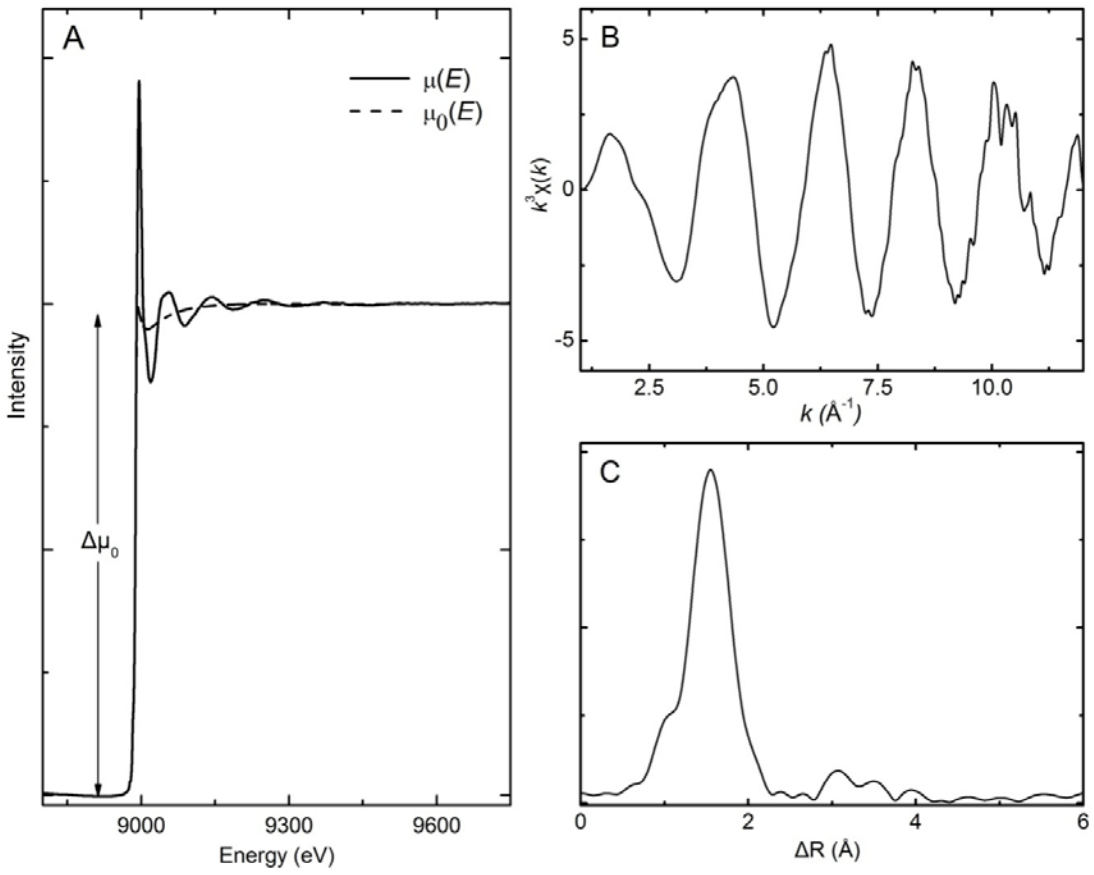

Figure 2.8 EXAFS data processing: A) spline function, B) k^3-space and C) R-space plots**.**

In order to get the structural information from EXAFS, experimental data need to be fit to a hypothetical structure, either theoretically calculated or built up from a known structure. Fitting can be performed in k-space or in R-space. ARTEMIS program,[221] an interface to IFFEFIT[222] is used for EXAFS fitting. Parameters such as amplitude, phase and mean-free path are calculated by FEFF6[223] and are used

for iterative data fitting.[223] The hypothetical model is also refined by varying structural parameters to minimize its difference with the experimental spectrum.[209] Table 2.2 lists the variables that are calculated and those that are refined during the fitting process. The quality of the fit is determined by the goodness-of-fit parameter, R-factor (Equation 2.5), which is automatically calculated by ARTEMIS. The R-factor is essentially the fractional misfit. Values under 0.02 are widely considered to indicate a close match, however, for dilute biological samples values up to 0.2 are considered acceptable.

Equation 2.5 R-factor

$$R = \frac{N}{N-n} \frac{\sum_{i}^{N} \left| \chi(k_i)_{theory} - \chi(k_i)_{\exp} \right|^2 k_i^p}{\sum_{i}^{N} \left| \chi(k_i) \right|^2 k_i^p}$$

Where:
N = number of experimental data points
n = number of fitting parameters (variables)
$\chi(k_i)_{theory}$ = theoretical EXAFS signals
$\chi(k_i)_{\exp}$ = experimental EXAFS signals
k_i^p = k weighting factor (p = 3)

Table 2.2 Calculated and refined parameters in the EXAFS fitting process.

Calculated Parameters		**Refined Parameters**	
Backscattering amplitude function	$A_i(k)$	Interatomic distances	R_i
Total phase shift function	$\phi_i(k)$	Number of scatterers	N_i
Mean free path function	$\lambda(k)$	Disorder parameters	σ_i^2
		Amplitude reduction factor	S_0^2
		Threshold energy	E_0

CHAPTER 3: SYNTHESIS AND CHARACTERIZATION OF CYSTEINYL RADICALS IN *PSEUDOMONAS AERUGINOSA* AZURIN

3.1 Introduction

3.1.1 Implications of Cysteinyl Radicals in Biology

Cysteinyl radicals are involved in a wide assortment of biological processes. They are implicated in enzyme catalysis such as ribonucleotide reductase (RNR), which catalyzes the conversion of ribonucleotides to deoxyribonucleotides, providing the monomeric precursors required for DNA biosynthesis. The general proposed mechanism of RNR requires a cysteinyl radical to initiate nucleotide reduction by abstracting the 3' hydrogen atom of the ribonucleotide substrate.[224,225] Cysteinyl radicals also partake in cellular antioxidant activity. Thiols are abundant in biological systems and are considered protective and antioxidant agents. The main biological thiol is the cysteine-containing tripeptide, glutathione (GSH). GSH acts as a scavenger to remove free radicals formed in normal metabolism. During the scavenging process, a glutathiyl radical is formed by one-electron oxidation of glutathione.[226,227] The importance of cysteinyl radicals is also highlighted in peptide post-translational modifications. As mentioned in chapter 1, cysteinyl radicals are precursors to several well-established cysteine modifications such as S-nitrosylation, S-glutathionylation, cysteine sulfenic acid, cysteine sulfinic acid and cysteine sulfonic

acid. As a result of post-translational modification such as S-nitrosylation, cysteinyl radicals are implicated in cellular signaling as well.[140,228] Although cysteinyl radicals have been postulated for various important biological processes, spectroscopic evidence of protein-based cysteinyl radicals is limited.

3.1.2 Current Spectroscopic Detection

The predominant method used to study radical species is electron paramagnetic resonance (EPR). EPR spectroscopy, also known as electron spin resonance (ESR), is a powerful technique for studying unpaired electrons and their interaction with their environment. The technique is based on the same phenomenon as NMR, the splitting of angular momentum states in the presence of a magnetic field (a.k.a., the Zeeman effect), but instead of nuclear spin states electron spin states are observed. By application of a strong magnetic field, the magnetic moment of an unpaired electron can be oriented either parallel or anti-parallel to the applied field. This creates distinct energy levels for the unpaired electrons, making it possible for net absorption of electromagnetic radiation in the form of microwaves to occur. The energy of the absorbed microwaves corresponds to the Zeeman splitting of the spin states. The field at which resonance occurs is usually reported in terms of g-values, the EPR equivalent of NMR chemical shifts.[229]

EPR has been successfully applied to detect and characterise protein-associated radicals in numerous redox enzymes.[230-232] However, protein-based cysteinyl radicals have been shown to be difficult to observe with EPR compared to tyrosyl radicals or tryptophan radicals due to the large spin-orbit coupling of sulfur* which causes the EPR signal to broaden.[233,234] Direct EPR studies of cysteinyl radicals have been carried out with low molecular-weight thiols such as cysteine and in proteins such as bovine serum albumin (BSA) and *E. coli* RNR (Figure 3.1).[141,235,236] The EPR spectrum of the cysteine sample (Figure 3.1C) shows the dominant feature $g_{\perp}$ at 2.008 and $g_{\parallel}$ at 2.29. The $g_{\parallel}$ component is well separated from the region of overlap with the other radicals and is a diagnostic feature of the cysteinyl radical.[237] The EPR spectrum of the cysteinyl radical in BSA sample (Figure 3.1B) shows a shift of the $g_{\parallel}$ component to 2.18 and a broadening. In the EPR spectrum of RNR (Figure 3.1A), the $g_{\parallel}$ component is broadened even more. The $g_{\parallel}$ component broadening causes difficulty in positively identifying a cysteinyl radical in a protein system.

* The spin-orbit coupling constants for sulfur, oxygen, nitrogen, and carbon are 382, 151, 76, and 28 cm^{-1}, respectively.[233]

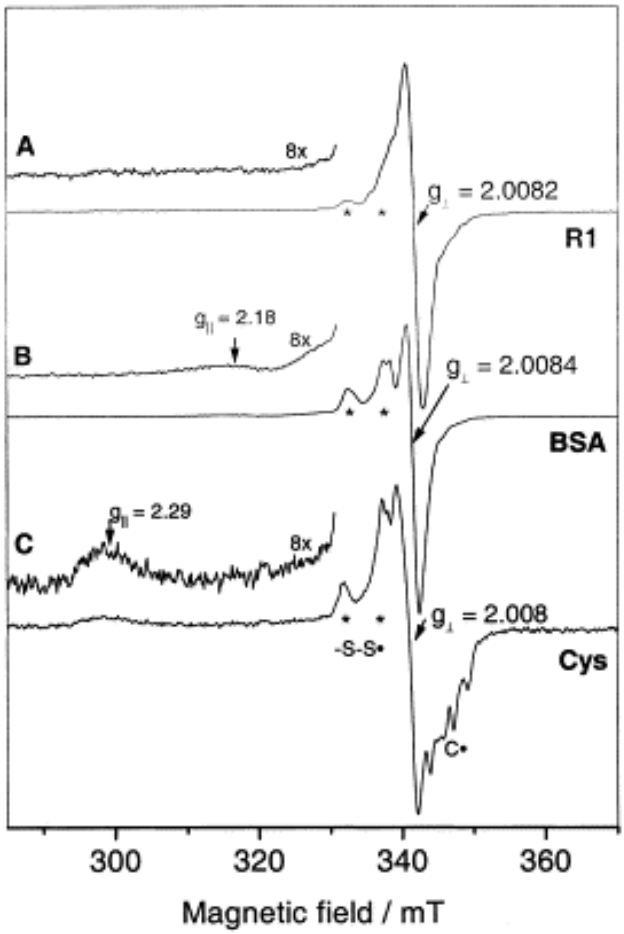

Figure 3.1 First derivative X-band EPR spectra of cysteinyl radicals. A) RNR protein of *E. coli* (500μM); B) BSA (4 mM); and C) cysteine (300 mM). This figure has been reproduced with permission.[236]

3.1.3 Proposed Spectroscopic Detection

Sulfur K-edge XAS is proposed as an alternative spectroscopic method for investigation and characterization of cysteinyl radicals. Figure 3.2 shows the possible electronic transitions that may be observed in a S K-edge XAS spectrum. Sulfide anion species having a filled valence shell will only result in direct ionization of the S 1s core electron, whereas thiolate species will have a near edge transition

corresponding to the $SC_{\sigma^*} \leftarrow$ S 1s transition. The thiyl radical in addition to the edge jump and near edge transition will exhibit a pre-edge feature that is due to a S 3p ← 1s transition. The energy and intensity of S K-edge XAS pre-edge features will provide information on the electronic structure and reactivity of biological sulfur-based radicals. Thus, XAS is a promising spectroscopic method in providing information on the nature of sulfur-based radicals and their chemical behaviour.

This chapter focuses on S K-edge XAS as a suitable spectroscopic method to detect cysteinyl radicals and investigates the sensitivity of S K-edge XAS to distinguish protein-based cysteinyl radicals in hydrophilic and hydrophobic protein environments.

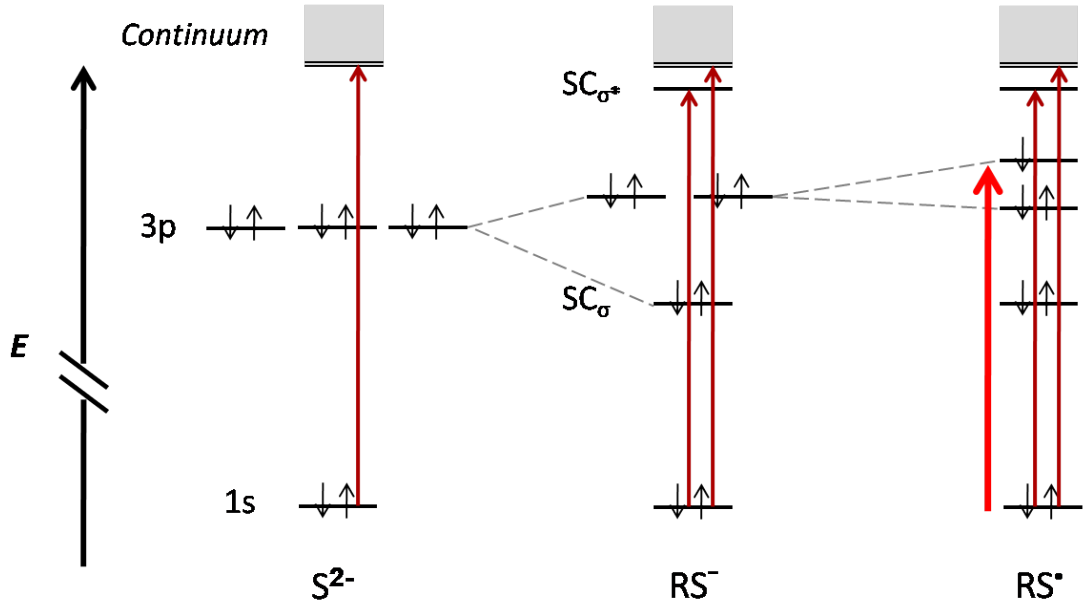

Figure 3.2 Qualitative valence molecular orbital diagram depicting electron excitation of sulfur species: sulfide anion, thiolate and thiyl radical.

3.1.4 *Pseudomonas aeruginosa* Azurin

In order to study sulfur-based radicals, isolated cysteinyl radicals were generated in *Pseudomonas aeruginosa* azurin (hereafter referred as azurin) using methods initially developed by Harry B. Gray and coworkers for the study of electron transfer in metalloproteins.[238] Gray's group has measured the kinetics of long-range electron transfer (~ 20 Å) reactions in metalloproteins labeled with inorganic photoinitiator complexes, coupled with laser excitation and transient spectroscopy.

Azurin is involved in the respiratory chain of the bacterium *P. aeruginosa* where it, together with cytochrome *c*551, transports electrons from the membrane bound *bc*1 complex to a soluble nitrite reductase in the periplasmic space of the bacterium. It has been widely studied as a prototypical electron transfer protein. Azurin is a small protein comprising of a single polypeptide chain, which contains 128 amino acid residues. The redox-active metal in the wild-type protein is a redox-active type 1 copper centre. Common to all such sites is the existence of three strongly-bound ligands: two histidines (His_{46} and His_{117}) and a cysteine (Cys_{112}), which form a roughly trigonal planar structure. In addition, azurin has two weakly interacting ligands that lie above and below the plane: the thioether sulfur of a methionine residue (Met_{121}) and the backbone carbonyl oxygen of a glycine (Gly_{45}).[16] This metal binding site can also ligate a series of other metals, such as Co^{2+}, Ni^{2+} and Zn^{2+}.[239,240] β-strands extend from the metal binding ligands forming a β sheet allowing azurin to be flexible for mutagenesis.

Azurin was chosen as an initial model protein because it is robust and can be easily expressed in *E. coli*. Also, there are different electronic environments present within the protein (Figure 3.3). This combination of properties makes azurin an attractive system in which to examine cysteinyl radicals.

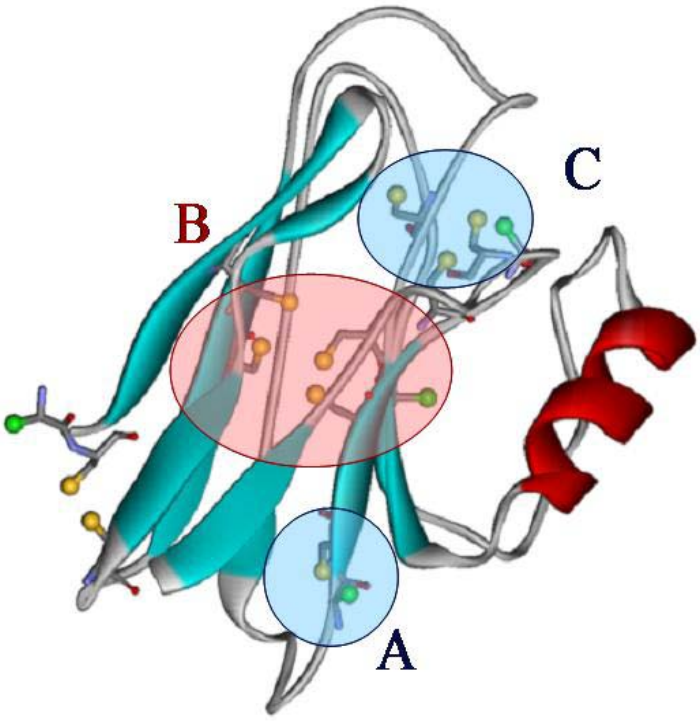

Figure 3.3 Azurin model system highlighting the different electronic environments. A is hydrophilic, B is hydrophobic and C is metal binding region.

3.1.5 Cysteines of Interest in Two Distinct Regions of Azurin

The structure of azurin contains two regions of interest, one hydrophilic and the other hydrophobic. In the hydrophilic region, the residue at position 108 is of interest for the cysteine radical study with an introduced surface histidine at position 107. The surface histidine is necessary for the attachment of the photoinitiator

complex as explained in Section 3.3.2. A mutant of azurin W48F/Y72F/H83Q/Q107H/Y108C (named Y108C for simplicity hereafter) was used by Gray and coworkers to study Cu^{1+} to Ru^{3+} electron transfer through the protein matrix. This mutant plasmid was kindly provided by Dr. Wehbi (past member of Gray's group) to study the cysteinyl radical in the highly solvent accessible region. Mutations in positions 48 and 72 were made from redox-active amino acids to redox-inactive residues. Previous studies done by Gray's group conclude that these mutations are necessary to prevent side electron transfer reactions from occurring. The mutation at position 83 is to ensure that no other surface histidine is available for the photoinitiator complex to attach other than to the introduced histidine at position 107.

In the hydrophobic region, the residue at position 48 is of interest for the cysteinyl radical study with the available surface histidine at position 83 for the photoinitiator attachment. A mutant plasmid W48C/Y72F/Y108F (named W48C hereafter) was also provided by Dr. Wehbi to investigate the formation of cysteinyl radicals in the hydrophobic core. Again, mutations at positions 72 and 108 are necessary to prevent side electron transfer reactions from occurring. Both Y108C and W48C mutants of azurin are used to test XAS as a spectroscopic method to detect cysteinyl radicals and to probe XAS sensitivity to distinguish the cysteinyl radicals in two extreme protein environments.

For quantitative analysis with S K-edge XAS, a mono cysteine protein model is necessary. Thus, mutants Y108C and W48C were further simplified by replacing all other sulfur containing amino acids such as cysteines (except the cysteine of

interest) and methionines. The mono Cys mutant azurin were named Y108C^{m} and W48C^{m} with single redox active cysteine in hydrophilic and hydrophobic region, respectively.

3.2 Experimental

3.2.1 Multi Site-directed Mutagenesis

Using Y108C and W48C as a template for Y108C^{m} and W48C^{m}, respectively, nine additional mutations were made which are listed on Table 3.1. Polymerase chain reaction was the preferred method of choice in generating the Y108C^{m} and W48C^{m} mutant plasmids. The Y108C^{m} and W48C^{m} mutant plasmids were generated by Anthony Lin, (past member of Kennepohl group) prior to my joining the lab.

Table 3.1 Additional mutations in Y108C^{m} and W48C^{m}.

Mutation Number	Mutation Location
1	Cys3Ala
2	Cys26Ile
3	Cys112Ser
4	Met13Gln
5	Met44Gln
6	Met56Gln
7	Met64Gln
8	Met109Gln
9	Met121Gln

3.2.2 Sequencing

To determine that the mutations were made correctly, the plasmids for the relevant mutants were over-expressed in XL1 Blue *E. coli* and plasmid DNA was isolated and purified using QIAprep Spin Miniprep Kit (Qiagen) with the procedures outlined in the QIAprep Miniprep handbook. Purified plasmid DNA concentration was determined using A_{260} and purity was confirmed using the ratio of A_{260}/A_{280}. Purified plasmid DNA (10 µL) with known concentration was submitted for sequencing to the Nucleic Acid Protein Service Unit (NAPS) at the University of British Columbia. This method produced a trace showing the sequence of DNA bases in the plasmid fragment of interest. By comparing the DNA sequence with the template sequence the exact composition of the resulting protein was confirmed. Y108C, W48C, $Y108C^m$ and $W48C^m$ were all submitted for DNA sequencing and once it was confirmed that all of these had correct sequences, protein expression was conducted. Raw output of these sequencing runs can be found in Appendix A.

3.2.3 Protein Expression and Purification

Protein expression depends on transforming the appropriate plasmid into *E. coli* to produce protein. The commonly used cell strain for protein expression is BL21(DE3).

BL21(DE3) *E.coli* cells were thawed from -80^{o}C to 0^{o}C by placing in ice. Aliquots of 50 µL of thawed cells were transferred into a pre-chilled, sterile* 1.5 mL Eppendorf tube and the remainder of the cells were refrozen at -80^{o}C. To the thawed cells, 1 µL of sequenced plasmid (concentration 30-60 ng) were added and gently mixed. The mixture was incubated at 0^{o}C for 30 minutes. This mixture was then warmed to 42^{o}C for 45 seconds followed by 5 minutes at 0^{o}C. 250 µL of SOC medium was added to the mixture then it was placed on a shaker for 1 hour at 225 rpm at 37^{o}C. Afterwards, 50 µL of the mixture was transferred on to a LB-agar plate containing ampicillin. The plates were incubated overnight at 37^{o}C at which time colonies of bacteria were visible. The plate was then stored at 4^{o}C until it was needed for the protein expression step.

To express the protein on a sufficient scale, the recombinant cells were cultured on a 9 L scale. First, using a sterile toothpick two colonies were inoculated from the agar plate into 10 mL of sterile terrific broth (TB, Invitrogen) containing 60 µg/mL ampicillin. This was placed in a shaker and allowed to grow for 7 hours at 37^{o}C, 225 rpm. After 7 hours, 1.5 mL of this starter culture was added to 6 x 4L Erlenmeyer flasks each containing 1.5 L sterile TB with 60 µg/mL of ampicillin. The remainder of the starter culture was used to prepare stock culture that was stored for later use. Starter culture (0.8 mL) and sterile 100% glycerol (0.2 mL) was placed

* All equipment and biological media were sterilized by autoclaving. The sterilized media was cooled before adding ampicillin.

into a sterile microcentrifuge tube and stored at -80^{o}C. The 4L flasks were placed in a shaker at 37^{o}C, 200 rpm for 12 hours at which point they had reached an optical density (OD) at 600 nm of 1.2. Then, to induce protein expression, isopropyl-β-thiogalacto-pyranoside (IPTG) (0.4 M, 1.5 mL) was added to each flask and incubated in the shaker at 37^{o}C, 200 rpm for an additional 3 hours. The cells were then harvested by centrifuging the cultures at 4,000 rpm at 4^{o}C for 20 minutes. Cell pellets were stored at -20^{o}C until ready for protein extraction step.

Osmotic shock was used as the method of choice for extraction of Y108C and W48C protein expressed in the periplasm. The cell pellets were then resuspended in a one-tenth volume of high osmolarity sucrose solution (0.3M Tris pH 8.1 with 1mM EDTA and 20% w/v sucrose). For 9 L cell cultures that were grown, 900 mL of sucrose solution was used. The suspensions were transferred to centrifuge tubes and placed on a shaker at room temperature for 30 min in order to swell the cells. The suspension was then centrifuged at 8,000 rpm at 4^{o}C for 15 min. The swelled pellet was then resuspended in cold (4^{o}C) 900 mL of 0.5 M $MgSO_4$ followed by shaking at 4^{o}C for 1 hour with the effect of lysing the cells so that the contents of periplasm can be released. The lysed cell remains were removed by centrifugation at 10,000 rpm at 4^{o}C for 20 min. To the supernatant containing the azurin protein, 250 mM sodium acetate buffer, pH 4.5 was added to give a final concentration of 25 mM sodium acetate, pH 4.5 and this solution was left to incubate at room temperature for 20 min. A white precipitant formed at this point which was attributed to DNA. Following the acetate precipitation, the periplasmic extrudate was centrifuged at 8,000 rpm for 15 min. The supernatant was saved and the white

pellet was discarded. $ZnSO_4$ (100 mM) was added to the supernatant to give a final concentration of 10 mM $ZnSO_4$. This solution was left to sit overnight at 4^0C to allow for metal incorporation.

Following the metal incorporation into azurin, the protein solution was concentrated by Amicon filtration over a 10,000 MWCO membrane (YM-10 Millipore). The concentrated protein solution was then washed several times with 25 mM sodium acetate pH 4.5 buffer until the effluent absorption at 260 nm was close to zero (small bits of DNA having washed through). The concentrated azurin was collected and stored in the acetate buffer at 4^oC until the purification step.

The preferred method for purification of crude azurin sample is purification with cationic exchange resin (HiTrap^{TM}SP HP, GE Healthcare). The resin consists of a surface sulfonate, thus it has an affinity for positively charged species. Given the pI of azurin is 5.4 and the protein solution was in acidic media (pH 4.5), the azurin would have a positive net charge which bound tightly to the SP column. The bound protein was eluted with a gradient between buffer A (25 mM sodium acetate buffer, pH 4.5) and buffer B (300 mM sodium acetate buffer, pH 4.5). First, the protein solution was applied to the SP column in 5 mg batches. Once the protein was loaded to the column, the loaded column was washed with 20 mL of buffer A to remove any unbound protein. This was then followed by a single elution step of the azurin protein with 85% buffer A, 15% buffer B. After the azurin had been eluted, the remaining protein impurities were eluted from the column with 100% buffer B.

To confirm the purity of the eluted azurin, the collected azurin fraction was analysed with SDS-PAGE. The eluted azurin sample (~ 50 μM, 5 μL) was mixed with 5 μL of denaturing buffer (consisting of 0.5 M Tris, pH 6.8, 10% w/v SDS, 10% v/v β-mercaptoethanol, 0.5% w/v bromophenol blue, and 20% v/v glycerol). This mixture was loaded on to the gel along with 10 μL of molecular weight marker in a separate lane. The gel was then developed by standard techniques and stained to show bands of approximate molecular weight.

3.2.4 Synthesis of Rhenium Complex

In order to generate controlled cysteinyl radicals in azurin, a photoinitiator complex (Figure 3.4) was synthesized and attached to the azurin. Synthesis of the photoinitiator complex was based on previously published experimental procedures.[241,242] First, 0.4 g of 5,6-dimethyl-1,10-phenanthroline (dmphen, from Aldrich) was dissolved in 15 mL of toluene in a 25 mL round bottom flask equipped with stir bar. Then, 0.5 g of rhenium pentacarbonyl chloride ($Re(CO)_5Cl$, from Aldrich) was added to the flask and this mixture was heated to 60^{o}C. In order to exclude water vapour, the flask was equipped with a reflux condenser. The mixture was allowed to stir for 5 hours at 60^{o}C. During this time, the solution changed colour from white to dark yellow with the formation of a yellow precipitate. The yellow precipitate is $Re(CO)_3$(dmphen)Cl which is insoluble in toluene. The suspension was then filtered over a fine porosity glass fritted funnel to give a yellow solid which was then washed several times with toluene. To remove the halide in the complex, the solid was then dissolved in 30 mL of dichloromethane. To this solution,

trifluorosulfonic acid (also known as triflic acid, from Fluka) was added dropwise until the mixture became transparent. Triflic acid (HOTf) is used to protonate the coordinated chloride and promote dissociation from the Re centre. Hydrochloric acid bubbled off and the triflate substituted for Cl. The reaction was left to stir at room temperature for 4 hours. Then diethylether was added dropwise to this solution causing a yellow precipitate to form which was $Re(CO)_3$(dmphen)OTf. This yellow solid was collected by filtering through fine porosity filter and washed with ether. This solid was then added to 25 mL water in a beaker equipped with stir bar. Water underwent a ligand substitution reaction to displace the triflate. The solution was stirred for 2 hours at 60^{o}C then the solution was filtered over a medium porosity glass fritted funnel. The solution contained the $Re(CO)_3$(dmphen)$(H_2O)^+$. The solid was collected and the triflate displacement was repeated twice more. All the solutions were then collected and the water was removed by gentle boiling followed by cooling the mixture to room temperature. The [$Re(CO)_3$(dmphen)$(H_2O)^+$](OTf^-) precipitated as orange crystals. These crystals were stored until needed for rhenium labelling reactions. To confirm the identity of the crystals, the crystals were submitted for MALDI-TOF analysis at the Mass Spectrometry lab in UBC. The result indicated a m/z peak at 479.3 confirming $Re(CO)_3$(dmphen) structure.

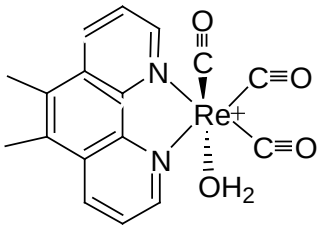

Figure 3.4 Re-photoinitiator complex

3.2.5 Re-labeling Reaction

Before labeling, the protein was equilibrated in 25 mM HEPES buffer, pH 7.2 (Sigma-Aldrich). The protein solution was then concentrated using Amicon Ultra-15 centrifugal filter with 10 kDa MWCO (Millipore) to ~3.5 mM. Meanwhile, 0.0084 g of $[Re(CO)_3(dmphen)(H_2O)^+](OTf^-)$ was dissolved in 6.5 mL of water by gentle heating and stirring over 2 hours to give a ~2 mM solution. The concentrated protein sample was divided in 5 aliquots of 100 µL each into a 2 mL Eppendorf tubes. To this, 1.3 mL of Re-complex solution was added. These tubes were incubated at 37^oC in the dark for 7 days. At the end of this time, the labeled samples were concentrated with Amicon centrifugal filter. The Re-labeled azurin was then exchanged into 25 mM sodium acetate buffer, pH 4.5 using the PD-10 gel filteration column (Pharmacia). The collected protein was again concentrated by Amicon centrifugal filter and allowed to stand in the dark at 4^oC for 3 days. Acetate buffer allowed the rhenium that might be mislabeled at glutamates or aspartates residues to be pulled off. Then, the Re-labeled azurin was centrifuged to remove the rhenium precipitate that did not bind and was prepared for the protein purification step. Using PD-10 column equilibrated the protein in 20 mM sodium phosphate, 750 mM sodium chloride, pH 7.2.

3.2.6 Purification of Labeled Azurins

Re-labeled azurin purification was necessary to remove proteins that are not labeled at the single surface histidine. To accomplish this, a HiTrap^{TM} Chelating HP column (GE Healthcare) was employed. The column uses a surface composed of

histidines which can be charged with Cu^{2+} from a $CuSO_4$ solution that was injected prior to loading the protein. The resin bound Cu^{2+} can bind tightly to a single exposed histidine residue. Thus if the azurin was not labeled with the rhenium then the surface histidine would be available to bind to the resin bound Cu^{2+} and the labeled protein will pass through the column. The protein was applied to the column in 5 mg batches and eluted with 20 mM sodium phosphate, 750 mM sodium chloride, pH 7.2. To remove the tightly bound unlabeled protein, the column was washed with a solution containing 20 mM sodium phosphate and 750 mM ammonium chloride, pH 7.2. The unlabeled protein fraction was recovered and reused for labelling reactions. Both Re-Y108C and Re-W48C were submitted for MALDI-TOF analysis to ensure that proteins were labeled.

3.2.7 The Flash/Quench/Freeze Methodology

The following procedure was used to generate the cysteinyl radicals in Re-W48C and Re-Y108C. The purified Re-labeled protein was reduced in volume to 150 µL to give final concentration of ~7-8 mM. The concentrated protein solution was incubated with a small amount of oxidative quencher, $[Co(NH_3)_5Cl]Cl_2$ for 5 min at room temperature in the dark. The solution was then carefully removed from the remaining solid by pipette and transferred to a microcentrifuge tube. To this 100 µL of 100% glycerol was added to give final concentration of 40% glycerol (v/v) in the sample. Glycerol is a good glassing agent which is a prerequisite for solution sample in soft XAS data collection. The protein solution was then degassed using a Schlenk line and purged with Ar gas. This pump/purge procedure was repeated

several times to ensure complete removal of oxygen. In an Ar-filled inert atmosphere glovebag, the sample was then transferred to an XAS cell sealed with a polypropylene window on the front. The XAS cell containing the protein sample was exposed to a Xe arc lamp for 10 seconds and then frozen in liquid nitrogen. This allows for trapping of photogenerated cysteinyl radicals.

3.2.8 XAS Data Acquisition

S K-edge XAS data were collected at the Stanford Synchrotron Radiation Lightsource (SSRL) on beamline 6-2 under ring conditions of 3 GeV and 60-100 mA. The setup used a 54-pole wiggler beamline operating in high-field (10 kG) mode with a Ni-coated harmonic rejection mirror and a fully tuned Si(111) double-crystal monochromator. Energy calibrations were carried out using an external standard of sodium thiosulfate ($Na_2S_2O_3$) with the first pre-edge feature being calibrated at 2472.02 eV. Signals were detected with a N_2 fluorescence (Lytle) detector at the temperature of liquid He. For each sample two sweeps were taken and the experiment was repeated twice to ensure reproducibility.

3.2.9 XAS Data Processing and Analysis

SixPACK software was used for XAS data processing.[220] Pre and post-data calibration scans were compared, and the energy scale of the data was adjusted by taking the first pre-edge feature of $Na_2S_2O_3$ and setting this to 2472.02 eV. Background subtraction and normalization were performed simultaneously using a linear pre-edge and post-edge function.

The commercially available PeakFit software package[243] was used to fit the pre-edge and near-edge feature with single pseudo-Voigt line shape (Equation 3.1). This line shape is appropriate as the experimental features are expected to be a Lorentzian transition and a Gaussian line shape is imposed by the beam line optics. A fixed 1:1 ratio of Lorentzian:Gaussian shapes were used for pre-edge and near-edge features. The ionization edge feature was fitted with a cumulative Gaussian/Lorentzian function (Equation 3.2). The spectra were fitted over the energy region from 2467 eV to 2476 eV.

Equation 3.1 Voigt Area Function

$$y = \frac{a_0 \int_{-\infty}^{\infty} \frac{\exp(-t^2)}{a_3^2 + \left(\frac{x - a_1}{a_2} - t\right)^2} dt}{\int_{-\infty}^{\infty} \frac{\exp(-t^2)}{a_3^2 + t^2} dt}$$

a_0 = area
a_1 = centre
a_2 = width (>0)
a_3 = shape (≥0)

Equation 3.2 Cumulative Gaussian/Lorentzian Function

$$y = a_4 \times \frac{a_0}{2}\left[1 + erf\left(\frac{x - a_1}{\sqrt{a_2}}\right)\right] + (1 - a_4) \times \frac{a_0}{\pi}\left[\tan^{-1}\left(\frac{x - a_1}{a_3}\right) + \frac{\pi}{2}\right]$$

a_0 = amplitude
a_1 = inflection point
a_2 = Gaussian width
a_3 = Lorentzian width
a_4 = shape

3.3 Results and Discussion

3.3.1 Re-labeled Azurin mutants

Mutants Y108C and W48C were successfully expressed in *E. coli* and purified. The purity of the mutant azurin proteins were confirmed by the SDS gels that showed only a single band of approximate weight of 14 kDa (Figure 3.5).

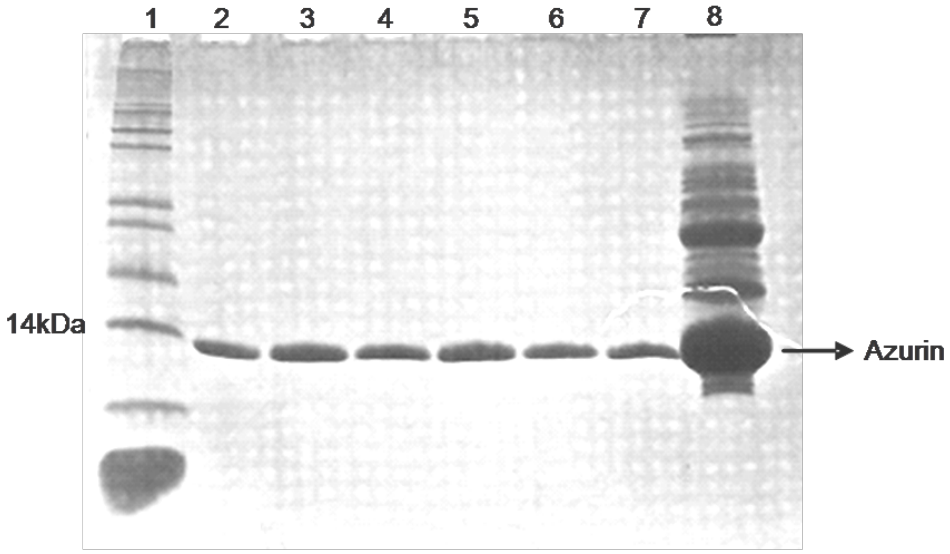

Figure 3.5 SDS-PAGE Gel. Lane 1 is protein ladder, lanes 2-7 are purified fractions of Y108C, and lane 8 is Y108C isolated by osmotic shock.

Y108C^{m} and W48C^{m} however, were not successfully expressed. Several attempts were made to express these mutants under different conditions such as various temperatures, ODs at which the expression was induced, and the IPTG concentrations. Table 3.2 lists the conditions that were tried. Of these conditions, protein expression of Y108C^{m} and W48C^{m} at 28^{o}C and 0.8 OD with 0.8 mM IPTG concentration showed the most promising results, but the expression level was not

enough to proceed further. Therefore, only Y108C and W48C were expressed and purified for incorporating Re-complex.

Table 3.2 Protein expression conditions attempted for $Y108C^{m}$ and $W48C^{m}$. The highlighted condition produced observable protein expression level.

Temperature (^{o}C)	Optical Density	IPTG Concentration (mM)
22	0.8	0.4
22	0.8	0.8
22	1.0	0.4
22	1.0	0.8
22	1.2	0.4
22	1.2	0.8
28	0.8	0.4
28	0.8	0.8
28	1.0	0.4
28	1.0	0.8
28	1.2	0.4
28	1.2	0.8
33	0.8	0.4
33	0.8	0.8
33	1.0	0.4
33	1.0	0.8
33	1.2	0.4
33	1.2	0.8
37	0.8	0.4
37	0.8	0.8
37	1.0	0.4
37	1.0	0.8
37	1.2	0.4
37	1.2	0.8

Histidine acts as an ideal ligand for coordination compounds. Thus, a single surface histidine on each azurin mutant binds to a Re-complex. Surface histidine at position 83 is exploited for the attachment of the Re-complex in W48C, and for Y108C the introduced surface histidine at position 107 is used. The histidine attaches to the $Re(CO)_3$(dmphen) unit by displacing water from the labeling reagent, $[Re(CO)_3(dmphen)(H_2O)^+](OTf^-)$. In order to determine if a single Re-complex is attached to the mutant azurin, the Re-labeled azurin was submitted for MALDI-TOF (spectrum found in Appendix B). The results are shown in Table 3.3 along with an unlabeled sample. The difference in the labeled and unlabeled protein is Δm/z 479 which is the molecular weight of $Re(CO)_3$(dmphen). This indicates that a single rhenium is attached in both Y108C and W48C.

Table 3.3 Mass spectral results for the labeled and unlabeled azurin mutants.

Azurin mutant	Unlabeled	Labeled
W48C	13 828.8	14 308.4
Y108C	13 824.7	14 304.5

3.3.2 Generation of Cysteinyl Radicals

One of the most efficient methods of quickly inducing a change in redox states is the so-called flash/quench technique.[244] This method is based on irradiation of a molecule, in this case a Re-complex, to generate a reactive excited state. The excited state can then interact with an exogenous electron acceptor $[Co(NH_3)_5Cl]^{2+}$ to generate a highly reactive redox Re(II). The exogenous electron

acceptor is referred to as an oxidative quencher. After the flash/quench, the photo-oxidized Re-complex will react with an electron donor in the system. Since the Re-complex is conveniently attached near a Cys residue (~10 Å), Cys can donate an electron to Re(II) and form a cysteinyl radical. A representation of this experiment is shown in Figure 3.6.

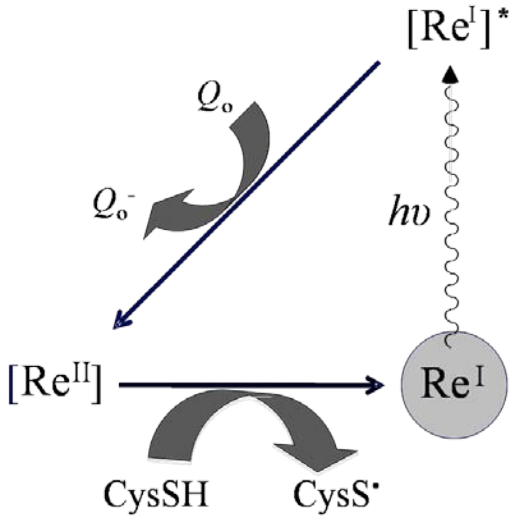

Figure 3.6 Simplified flash/quench reaction between Re-complex and the nearby Cys with oxidative quencher (Q_o).

3.3.3 Characterization of Cysteinyl Radicals by Sulfur K-edge XAS

A small but noticeable pre-edge feature was present in the S K-edge XAS spectra of the W48C radical and Y108C radical. The pre-edge feature arises from transitions to empty or partially empty valence orbitals. The XAS spectra of W48C and W48C radical (Figure 3.7) showed an intense near-edge transition at 2473.6 eV that corresponds to the $SC_{\sigma^*} \leftarrow$ S 1s transition and the W48C radical showed a pre-

edge feature at 2469.3 eV which corresponds to the S 3p ← 1s transition due to the presence of a hole in the S 3p orbital. The presence of such a pre-edge feature is characteristic of species that exhibit a radical character on the sulfur atom. Similarly, the XAS spectrum of Y108C radical (Figure 3.8) showed a pre-edge feature at 2470.9 eV in addition to the near-edge feature. The 1.6 eV shift in energy of the pre-edge feature for Y108C radical is due to the cysteinyl radical being in a hydrophilic environment that is susceptible to interact with the H_2O. This interaction with H_2O results in hydrogen bonding (H-bonding) which may play an important role in tuning the electronic structure and reactivity of the cysteinyl radical. H-bonding is likely to increase the energy of the 3p orbital in which an unpaired electron resides hence increasing the pre-edge transition energy. Also, the dielectric constant of the local protein environment of the Cys radical in Y108C can cause the observed energy change. The cysteine in W48C, on the other hand, is buried in the protein environment, thus it is well protected from H_2O and therefore H-bonding is not in effect.

The effect of H-bonding is also observed in the pre-edge features that result from metal ligated thiolate.[245] Solomon and coworkers have studied a series of P450 model complexes with increased H-bonding using S K-edge XAS. In addition to the increase in energy of the pre-edge transition, a decrease in intensity is observed in complexes of H-bonding. This decrease in intensity of the pre-edge feature is also evident in Y108C radical compared to the W48C radical. The intensity of the pre-edge feature (peak area) is quantitatively estimated from fits to the experimental spectra (Figure 3.9). The intensity of the pre-edge feature for the

Y108C radical and W48C are 0.23 and 0.31, respectively. However, the pre-edge intensity of the radical is dependent on the radical yield which cannot be quantified in this model protein system. In order to estimate the radical yield, a mono Cys protein system is required. Thus, the intensity is coincidently lower for the cysteinyl radical in the hydrophilic region. However, the observed energy difference of the pre-edge feature of Y108C radical compared to the W48C radical suggests that the combined effects of hydrogen bonding and the dielectric constant of the local protein environment are likely to play a role.

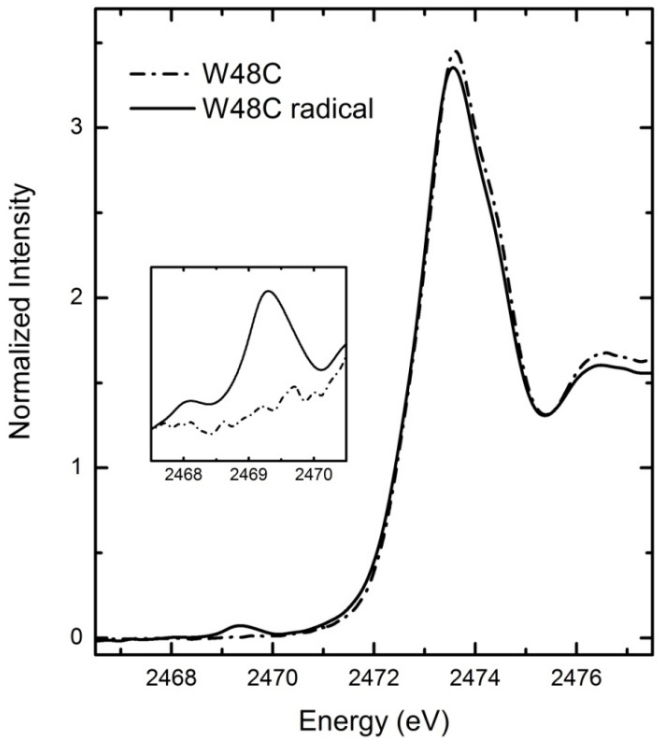

Figure 3.7 S K-edge XAS spectra of W48C and W48C radical with pre-edge feature expanded (inset).

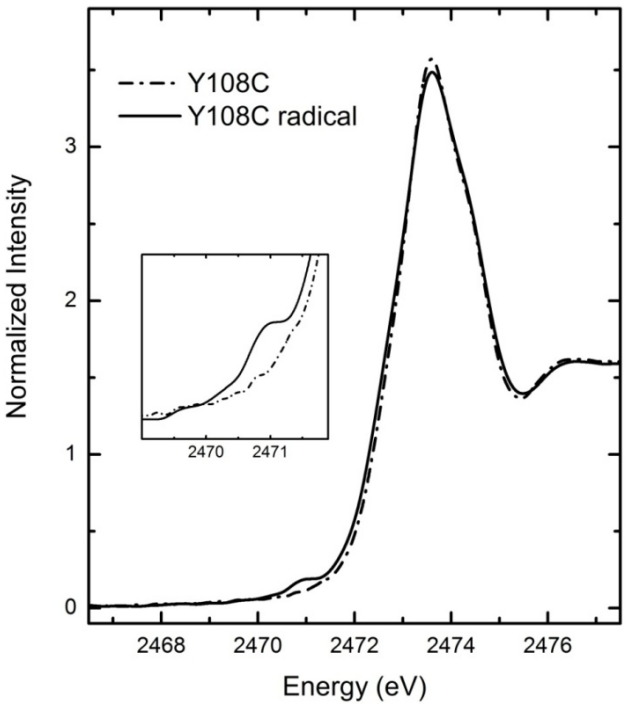

Figure 3.8 S K-edge XAS spectra of Y108C and Y108C radical with pre-edge feature expanded (inset).

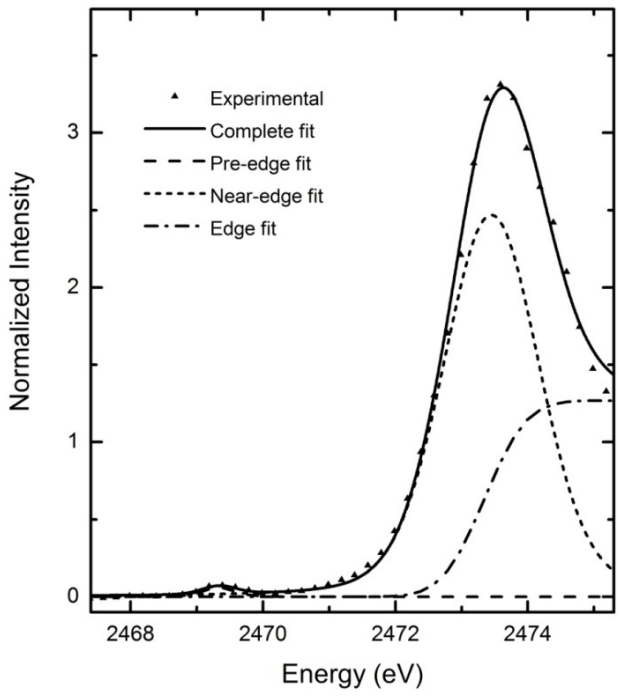

Figure 3.9 S K-edge XAS experimental data and fit for W48C radical.

3.4 Conclusions

Although protein-based cysteinyl radicals are implicated in various biological functions, direct detection has been challenging. EPR is the predominant spectroscopic method in studying unpaired electron, but it is difficult to detect cysteinyl radicals due to the large spin-orbit coupling of sulfur that results in signal broadening. My work in generating controlled cysteinyl radical in azurin has been successful in investigating with sulfur K-edge XAS. The transition of the 1s electron into the partially filled 3p orbital results in a pre-edge feature, that is well separated from the near-edge feature. Thus, S K-edge XAS has been shown to be a promising spectroscopic method in investigating sulfur-based radicals. In addition, S K-edge XAS is sensitive in differentiating the cysteinyl radical in different protein environments. A cysteinyl radical in a hydrophilic environment is able to H-bond, which can affect the reactivity of this radical and is evident in the pre-edge feature energy.

CHAPTER 4: PHOTOCHEMISTRY OF METHIONINE, METHIONINE SULFOXIDE, AND METHIONINE SULFONE

4.1 Introduction

4.1.1 Methionine Oxidation

Formal oxidation of methionine is generally considered to involve two oxo transfer steps, producing methionine sulfoxide (MetSO) in the first oxidation step and methionine sulfone ($MetSO_2$) in the subsequent step (Scheme 4.1). While the first oxidation product MetSO can be physiologically reduced back to Met by methionine sulfoxide reductase (Msr), a further oxidation to $MetSO_2$ is considered to be biologically irreversible, as highlighted in chapter 1.[246] Oxidative damage resulting in Met oxidation in proteins has been linked to several diseases such as age-related cataracts and Alzheimer's disease.[174,247]

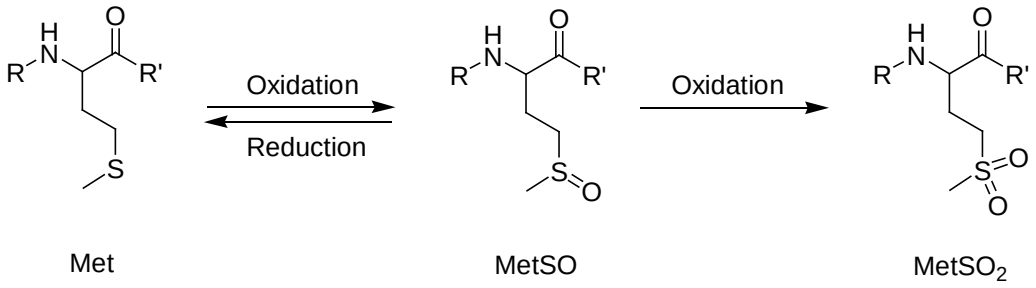

Scheme 4.1 Oxidation and reduction of methionine residues in proteins.

4.1.2 Age-related Cataracts

Cataracts are an eye disease that typically progresses slowly to cause vision loss and is potentially blinding if untreated; it is a leading cause of blindness in the world.[202] Age-related, or senile cataracts, are the most common type of cataracts. The term “cataract” has been used to mean any opacity or loss of transparency of the lens. Lens opacities are the earliest visible changes in cataractogenesis. The lens, the biconvex crystalline structure behind the iris, serves to transmit, filter and focus light upon the retina. To serve this function, the eye lens has to provide transparency and a high refractive index. The transparency and high refractive index of the lens are due to the high concentration of structural proteins called crystallins.[248] Crystallins are known to constitute about 90% of water soluble proteins of the lens and can be separated into three distinct families, the α-, β-, and γ-crystallin, on the basis of their oligomeric size. In addition to its structural role, α-crystallins has been shown to function as a molecular chaperone, helping to prevent formation of large light-scattering aggregates from denatured crystallins.[205]

To maintain transparency, the crystallins must remain stable for the duration of the host’s lifetime without being denatured. However, with age, crystallins undergo a wide variety of irreversible covalent modifications, caused by proteolysis, deamidation, extensive oxidation and cross-linking.[249] Such undesired post-translational modification of the crystallins is believed to decrease their solubility in the lens, which leads to cataract formation. Oxidation of α-crystallin has been demonstrated to cause a significant reduction in its chaperone activity, which suggests that oxidation may have important consequences for protein aggregation in

the lens.[206] One of the major post-translational modifications of α-crystallin is oxidation of Met to MetSO and $MetSO_2$. Met oxidation in both bovine and human α-crystallin occurs *in vivo*.[247,249] Several factors have been attributed to cataract formation. Of these, UV light exposure has been proposed to be involved in age-related cataract formation.[250] In general, very little UV-C (< 280 nm) radiation reaches the earth's surface because of atmospheric absorption in the ozone layer. However, UV-B (280-320 nm) and UV-A (320-400 nm) can reach the eye, and the human cornea filters out all radiation below 290 nm. UV-B radiation is generally absorbed by the cornea and aqueous humor before reaching the lens,[251] yet UV-B exposure over extended periods has been shown to cause damage to the lens that can lead to cataract formation.[252-254] The higher wavelength UV-A can pass through the cornea to be absorbed by the lens, thus it has also been proposed to cause damage to the lens leading to cataract formation. [255,256] However, the mechanism of light-induced cataract formation is still not clear, in particular the light-induced oxidation of Met residues.

4.1.3 Photooxidation of Thioether

Efforts have been made in studying the mechanism of sensitized photooxidation of functionalized thioethers.[257,258] Under such conditions, the mechanism of photooxidation is believed to involve the formation of singlet oxygen ($^1O_2$), as shown in Scheme 4.2. $^1O_2$ produced on energy transfer from the sensitizer reacts efficiently with dialkyl sulfides to yield persulfoxide intermediates. The persulfoxide acts as an oxygen atom transfer agent to form the sulfoxide[259,260] and

sulfone[261] or can undergo fragmentation, however, the mechanisms of these formations are not clear. An alternative mechanism involves photosensitized electron transfer (ET) oxidation (Scheme 4.3), where a sulfide radical cation forms upon ET to the excited sensitizer, which is then regenerated by a reaction with oxygen to yield the superoxide anion.[261] Recombination of the sulfide radical cation and the superoxide anion yields the persulfoxide intermediate which then can react with another thioether to form sulfoxide.

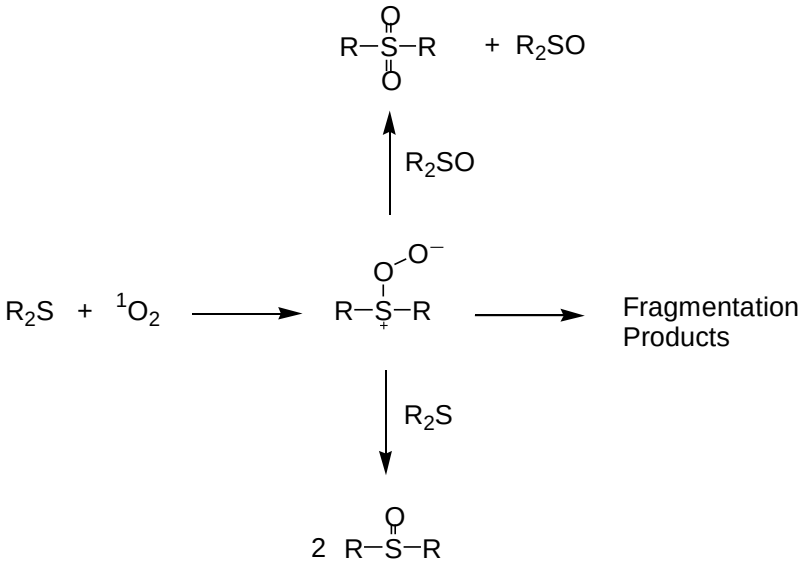

Scheme 4.2 Proposed mechanism of photooxidation of thioether involves the formation of singlet oxygen.[259]

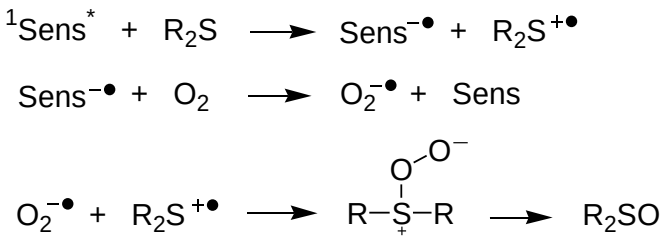

Scheme 4.3 Alternative mechanism of photooxidation of thioether involves formation of sulfide radical cation.[261]

The photochemistry of methionine and its related species methionine sulfoxide and sulfone have not been explored in the absence of sensitizer. Thus, this chapter provides new insights to factors that affect the photochemically activated Met and MetSO redox process in the presence and absence of oxygen.

4.2 Experimental

4.2.1 Materials

L-Methionine (purity 98.0%) and L-methionine sulfoxide (purity 99.0%) were purchased from Sigma-Aldrich. L-Methionine sulfone (99.0%) was purchased from MP Biomedicals. These compounds were checked for contamination using ESI and NMR before use. Sulfur-free Kapton tape was purchased from Creative Global Services and checked for sulfur contamination using sulfur K-edge XAS before use.

4.2.2 Sample Preparation

Solid samples of Met, MetSO, and $MetSO_2$ were finely ground, placed on Kapton tape, and mounted across the window of an Al plate. Solution samples of Met, MetSO and $MetSO_2$ were prepared at a concentration of 10 mM in distilled water with 50% glycerol as a glassing agent to reduce diffraction produced by ice crystals in XAS. For aerobic photochemical experiments, samples were exposed to irradiation from a 75 W Xe arc lamp for 0-3 hours at room temperature followed by analysis using XAS. Anaerobic photochemical experiments were performed in a He filled glovebag, and XAS data were collected in situ (Figure 4.1).[262] An open-flow liquid He cooler from Cryo Industries allowed data to be obtained at ~ 20 K. For ^{1}H

NMR analysis, ground samples were irradiated on a clean Petri dish and then dissolved in D_2O for spectroscopic analysis. ^1H NMR spectra were collected on a Bruker Avance 400 MHz spectrometer at ambient temperature. All of the photochemistry was performed in the solid state or in 10 mM aqueous solutions, with qualitatively identical results.

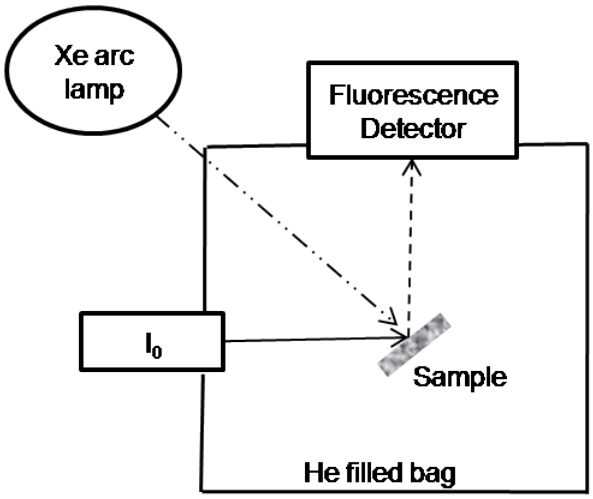

Figure 4.1 Sample compartment for *in situ* anaerobic photochemistry setup at SSRL beamline 6-2, where I_0 is the incident X-ray beam.

4.2.3 XAS Data Acquisition

XAS data were collected at the SSRL on beamline 6-2 under conditions described in section 3.2.8.

4.2.4 Data Processing and Analysis

SixPACK software was used for XAS data processing.[220] Pre- and post-data calibration scans were compared, and the energy scale of the data was adjusted by

taking the first pre-edge feature of $Na_2S_2O_3$ and setting this to 2472.02 eV. Background subtraction and normalization were performed simultaneously using a linear pre-edge and post-edge function.

SixPACK software was also used for principal component analysis (PCA), target transformation, and linear least-squares fitting. PCA was used to determine the smallest number of principal components (PCs) required to sufficiently describe the composite data set. During target transformation, SPOIL value ranges as defined by Malinowski[263] were interpreted as follows: acceptable (<3), moderately acceptable (3-6), and unacceptable (>6). Linear least-squares fitting of reference spectra was used to evaluate component spectra over the energy range from 2465 to 2490 eV.

4.3 Results and Discussion

4.3.1 Met Photochemistry

Photoirradiation of Met by Xe arc lamp under aerobic conditions produces rapid photodegradation of the thioether. The changes can be observed in the S K-edge XAS spectra as a function of irradiation time, (Figure 4.2). The intense main feature of Met at ~2473.5 eV corresponds to the thioether CS $\sigma^* \leftarrow$ S 1s transition.[264] Upon irradiation, this feature decays with formation of new, intense features at 2476.3 eV and 2479.9 eV. These new features correspond to the formation of MetSO and $MetSO_2$ as seen in Figure 4.3 of S K-edge XAS spectra of clearly resolved features for MetSO (2476.3 eV), and $MetSO_2$ (2479.9 eV). At longer

irradiation times, further changes are observed, including the appearance of higher-energy features at 2481.0 eV and 2482.5 eV. These more highly oxidized species were presumed to result from fragmentation via carbon-sulfur bond cleavage. The feature at 2481.0 eV was consistent with the formation of sulfenate species, given its similarity to the pre-edge feature of methane sulfenate ($CH_3SO_3^-$) in Figure 4.3. Similarly, the feature at 2482.5 eV corresponds to the highly oxidized form of sulfur; sulfate (SO_4^{2-}). Liebster and co-workers in their work on radiation induced Met degradation have identified the fragmentation products of Met to be homocysteic acid and homoserine.[265] The formation of homoserine is proposed to result in sulfate species. Thus it is likely that the feature at 2481.0 eV is due to the fragmentation of Met resulting in homocysteic acid and the feature at 2482.5 eV to be a sulfate.

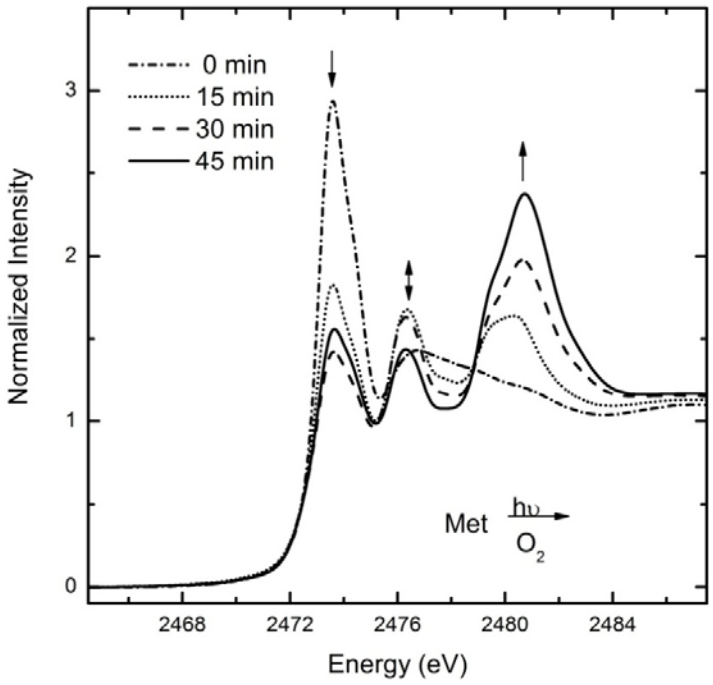

Figure 4.2 S K-edge XAS spectra with photoirradiation of Met by Xe arc lamp under aerobic conditions.

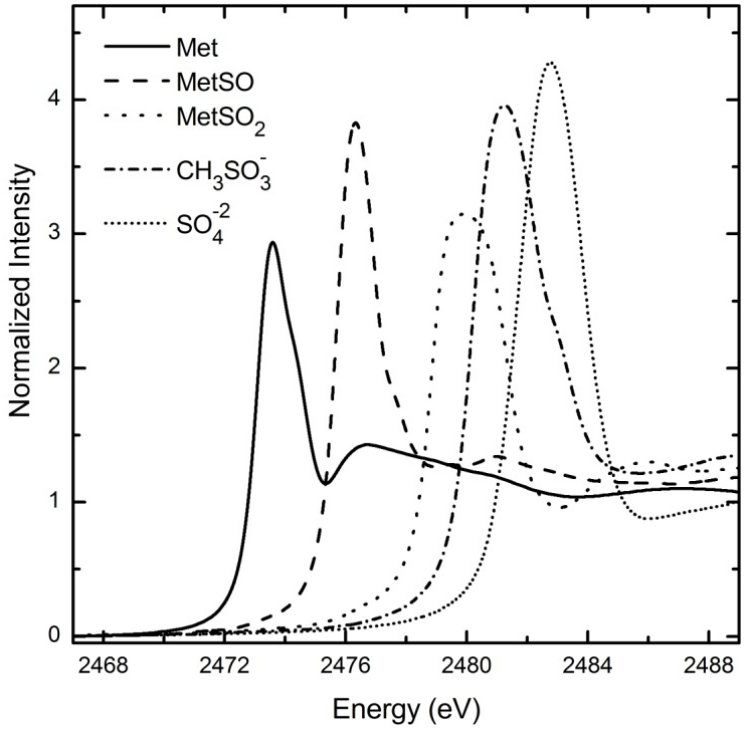

Figure 4.3 S K-edge XAS spectra of Met, MetSO, $MetSO_2$, $CH_3SO_3^-$, and SO_4^{-2}.

Under anaerobic conditions, Met photoirradiation by Xe arc lamp does not produce MetSO or $MetSO_2$ (Figure 4.4), presumably because of the lack of an oxygen source. However, careful investigation of the time-resolved XAS spectra indicates the formation of a small pre-edge feature at low energy ~ 2470.0 eV (Figure 4.4 inset). The formation of this pre-edge feature is concomitant with a small decrease in the CS $\sigma^* \leftarrow$ S 1s feature of Met, which eventually achieves an apparent photo-steady state (Figure 4.5). My work with azurin cysteinyl radicals (see Chapter 3) and other related work[266] suggests that such low-energy pre-edge features are consistent with the formation of sulfur-centred radical species. Therefore, this feature is tentatively assigned to the formation of the one-electron-photooxidized

species $MetS^{\bullet+}$. Evidence for the Met radical cation has been previously observed in pulse radiolysis reaction of N-acetyl-L-methionine amide.[167] Formation of a photo-steady state during XAS data collection can easily result from concomitant X-ray photoreduction of the cation radical to generate Met, as shown in Scheme 4.4.

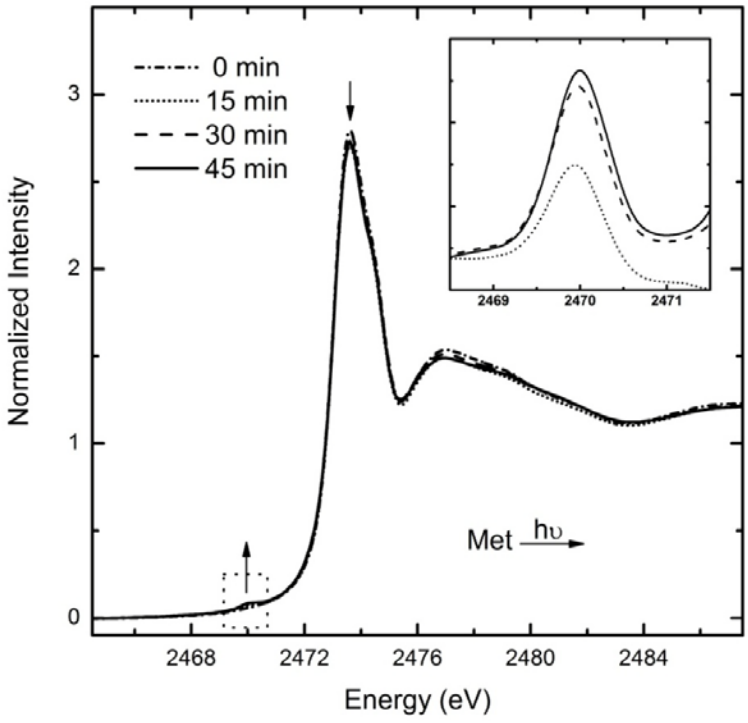

Figure 4.4 S K-edge XAS spectra with *in situ* photoirradiation of Met by Xe arc lamp under anaerobic condition. Inset shows the difference spectra of the low-energy.

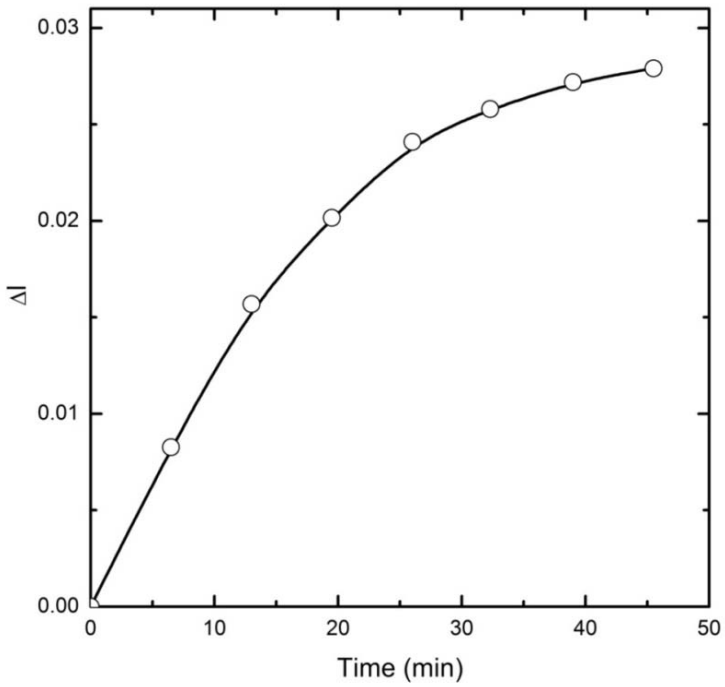

Figure 4.5 Kinetic profile of the weak pre-edge feature from *in situ* photoirradiation of Met by Xe arc lamp under anaerobic conditions.

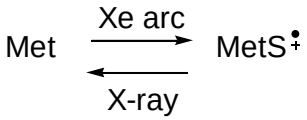

Scheme 4.4 Met photooxidation by Xe arc lamp and photoreduction by X-ray beam.

The mechanism of aerobic photooxidation of Met is generally believed to involve photoexcitation of dioxygen to its highly energetic singlet excited state followed by reaction with the thioether. The presence of sensitizer may enhance the production of $^1O_2$ as well as provide alternative or concurrent pathways in which the Met radical cation is generated (Scheme 4.3). My work on the anaerobic Met photochemistry suggests that a third option must be considered in which direct one-

electron photoexcitation of Met occurs in the absence of an exogenous sensitizer. Given the small absorption coefficient for Met in the visible region (Figure 4.6), this is rather unexpected. However, high-resolution electronic spectroscopy reveals weak low-lying absorption bands at 262 and 285 nm assigned as singlet to triplet transitions.[267,268] I postulate that these triplet excited states are sufficiently high in energy (~4 eV) to make them efficient reductants, thus yielding the cation radical. Reactivity through this triplet-excited-state channel may also point to an additional pathway for O_2 photoactivity. The formation of a $^3Met^*$ species should allow for a rapid spin-allowed reaction with ground-state $^3O_2$. The two new pathways that are proposed here have not been explored and provide an alternative mechanism for Met oxidation.

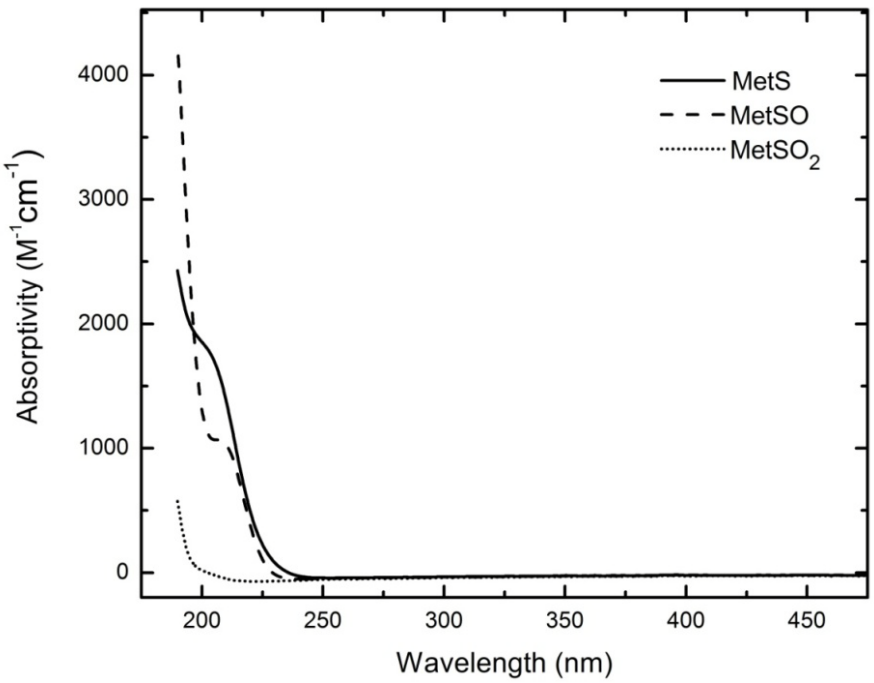

Figure 4.6 UV-Vis spectra of Met, MetSO, and $MetSO_2$.

4.3.2 MetSO Photochemistry

The MetSO photoirradiation by Xe arc lamp under aerobic conditions is shown in Figure 4.7. As with Met photoirradiation, formation of $MetSO_2$ is observed at relatively short times. At longer irradiation times, more highly oxidized species of sulfenate and sulfate that are likely due to fragmentation products are observed. However, MetSO photoirradiation also results in the formation of a new feature at lower energy, indicative of photoreductive processes. An intense feature at 2473.5 eV, corresponding to the spectrum of the parent thioether Met is observed during photoirradiation.

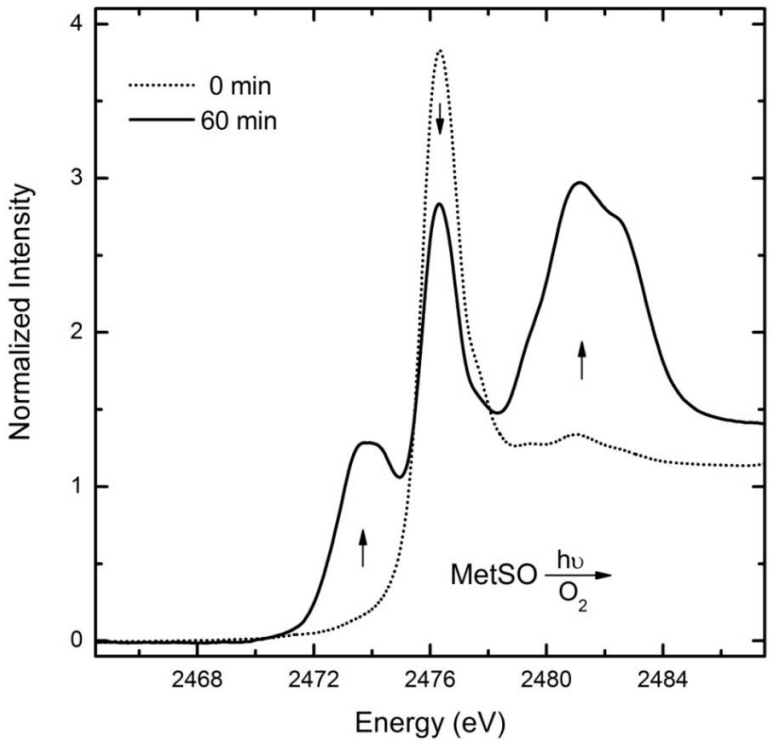

Figure 4.7 S K-edge XAS spectra with photoirradiation of MetSO by Xe arc lamp under aerobic conditions.

The MetSO photoirradiation by Xe arc lamp in the absence of O_2 shows no evidence of oxidation products (Figure 4.8). However, the lower-energy feature at 2473.5 eV is still observed with a simultaneous decrease in the intensity of the MetSO feature. Photoreduction is also observed as a result of photodamage from the X-ray beam during data collection, but the rate of formation is markedly smaller than the observed irradiation from the Xe arc lamp, (Figure 4.9). To confirm that the feature at 2473.5 eV is identical to that of Met, ^{1}H NMR analysis was performed on the photoirradiated MetSO by Xe arc lamp (Figure 4.10). The signal from the methyl group protons (S-CH_3,δ = 2.04) is useful in identifying the formation of Met in the photoirradiated MetSO.

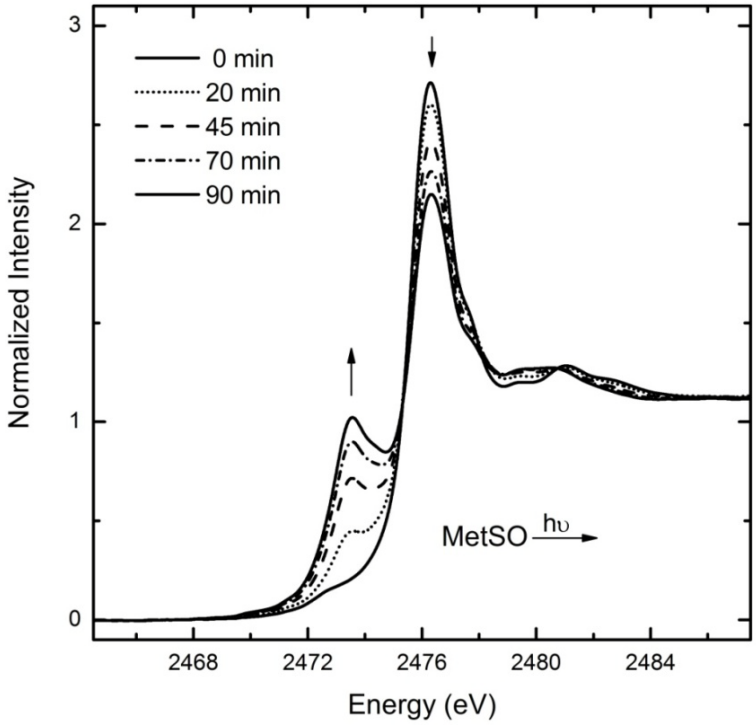

Figure 4.8 S K-edge XAS spectra with *in situ* photoirradiation of MetSO with Xe arc lamp under anaerobic conditions.

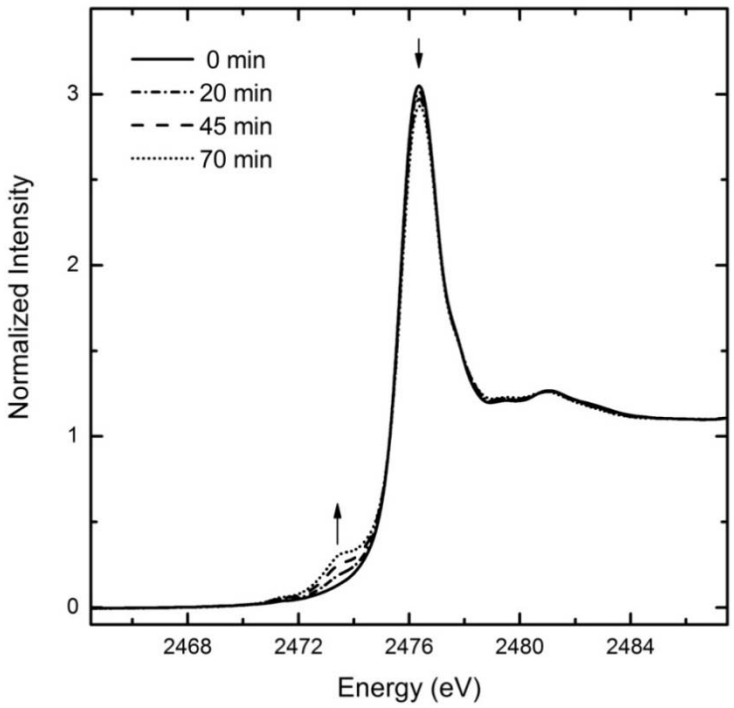

Figure 4.9 S K-edge XAS spectra with X-ray photoreduction of MetSO during data collection.

A more quantitative analysis of the photoreductive process was obtained through principal component analysis (PCA) and target transformation to identify the number and types of components, respectively. From the PCA, it was identified that the first two PCA components of the XAS spectra of irradiated MetSO accounted for over 99% of the total variance (Table 4.1). The first two components reproduce all of the features of the spectra, confirming that anaerobic irradiation of MetSO yields only one product. Based on the PCA results, target transformation was performed using two components in order to identify the two species. According to the calculated SPOIL values (Table 4.2) and by visual inspection of the target transforms, the species were identified as MetSO and Met. Linear least-squares

fitting of Met and MetSO in fractional contributions of 0.46 and 0.54, respectively yielded a reasonable fit to the MetSO irradiated data under anaerobic condition (Figure 4.11).

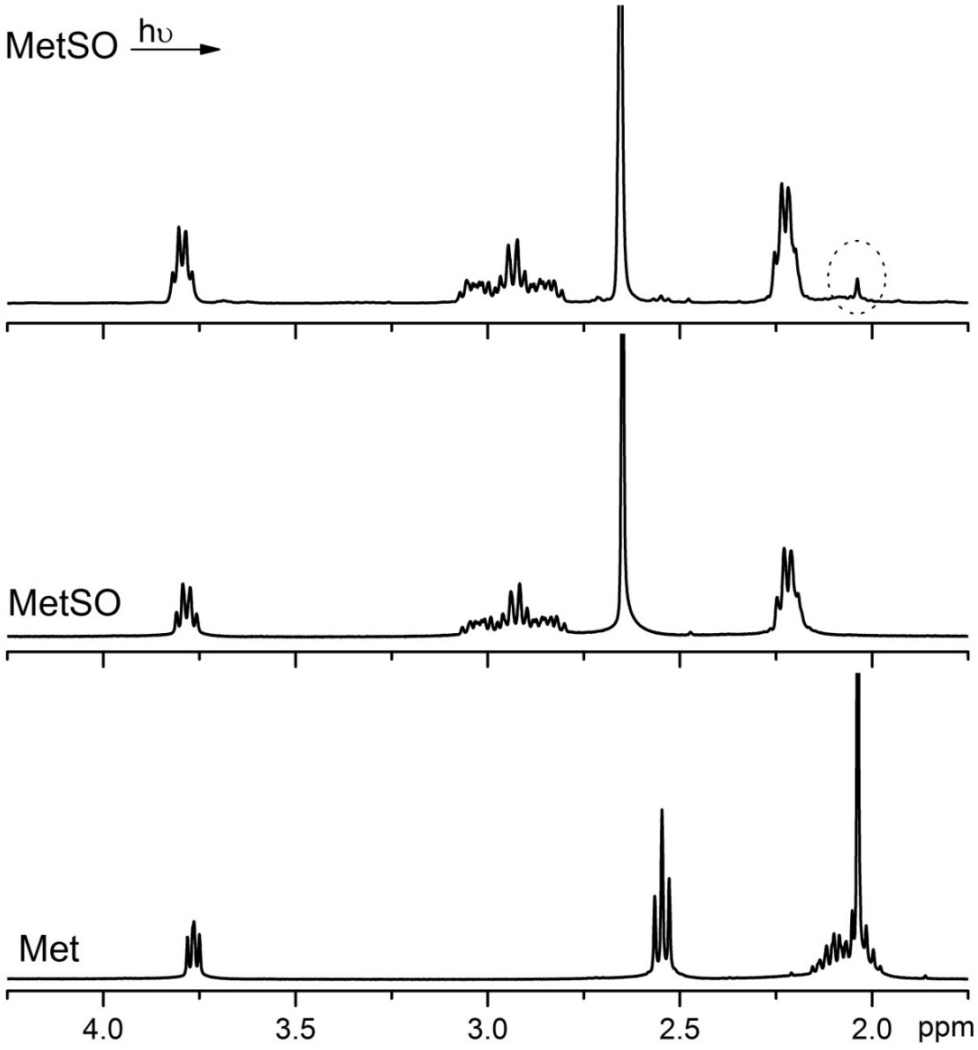

Figure 4.10 ^{1}H NMR spectra of MetSO photoirradiation with Xe arc lamp products under anaerobic conditions after 15 minutes.

Table 4.1 Results from principle component analysis of *in situ* photoirradiation of MetSO by Xe arc lamp under anaerobic conditions. The highlighted portion shows the minimum number of components needed for >99% cumulative variance.

Component	Eigenvalue	Cumulative Variance
1	52.378	0.924
2	3.975	0.994
3	0.159	0.997
4	0.050	0.998
5	0.025	0.998
6	0.014	0.999
7	0.012	0.999
8	0.010	0.999
9	0.009	0.999
10	0.008	1.0

Table 4.2 Results of PCA target transformation performed in SixPACK

Target (Standard)	SPOIL
Cysteine	7.12
Methionine	3.09
Methionine Sulfoxide	2.26
Methionine Sulfone	14.57

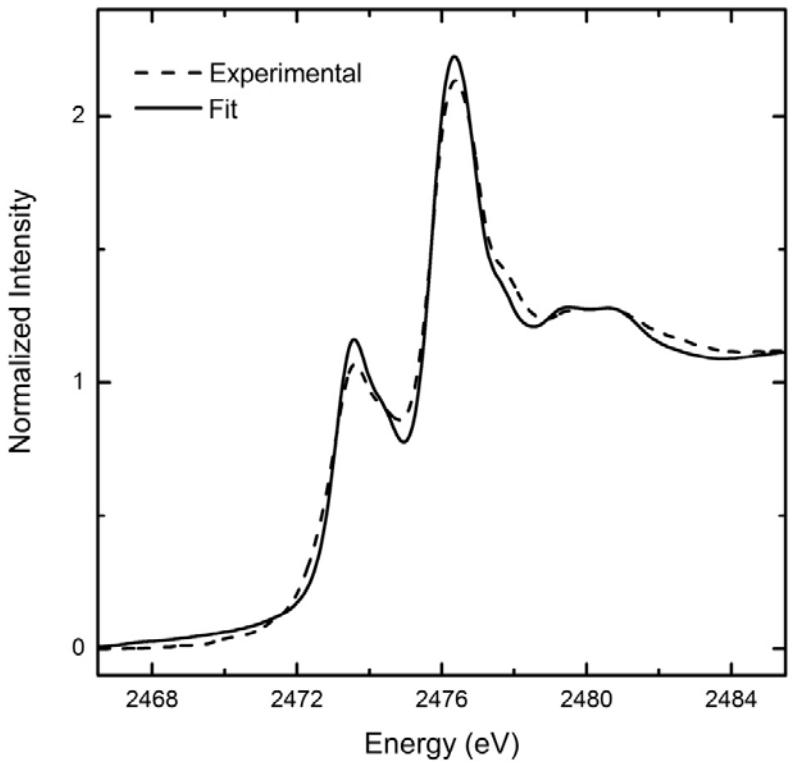

Figure 4.11 Linear least-squares fit of *in situ* MetSO photoirradiation by Xe arc lamp under anaerobic conditions after 90 minutes.

Harvey and Lang[269] have reported a similar photoreduction of DMSO to DMS. They attributed disproportionation as a likely source of DMS; however, the observation of MetSO irradiation by Xe arc lamp under anaerobic conditions is inconsistent with this interpretation as no $MetSO_2$ was observed, whereas Met was still produced. To ensure that the photochemistry of DMSO is similar to MetSO, DMSO was irradiated by Xe arc lamp under anaerobic conditions and analysed by XAS, (Figure 4.12). The formation of the photoreduced species, DMS was observed with concomitant decrease in DMSO feature showing that DMSO photoreduction is indeed proceeding in a similar manner to MetSO.

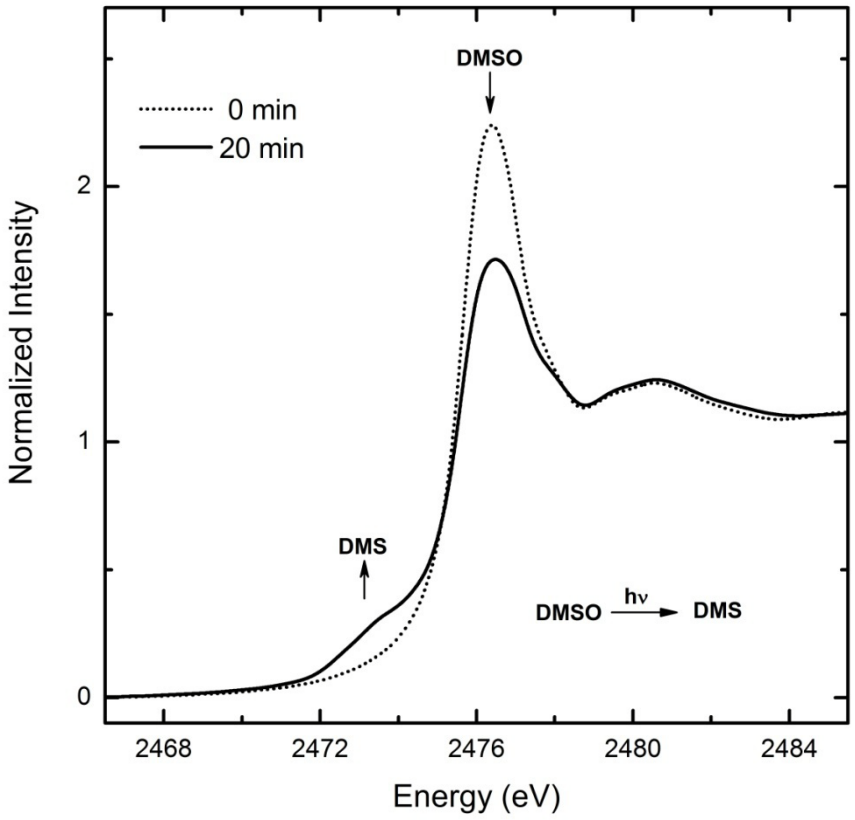

Figure 4.12 S K-edge XAS spectra with *in situ* photoirradiation of DMSO by Xe arc lamp under anaerobic conditions.

4.3.3 $MetSO_2$ Photochemistry

Photoirradiation of $MetSO_2$ by Xe arc lamp is both oxidatively and reductively inert under aerobic and anaerobic conditions (Figure 4.13). A small background reaction was observed and the products were identified as resulting from MetSO contamination undergoing photoreduction. The lack of highly oxidized species such as sulfenate and sulfate due to fragmentation suggests that $MetSO_2$ is highly stable. Also, the fragmentation products such as sulfenate and sulfate that are observed in

Met and MetSO photoirradiation are likely to go through the persulfoxide intermediate postulated by Foote and co-workers.[259]

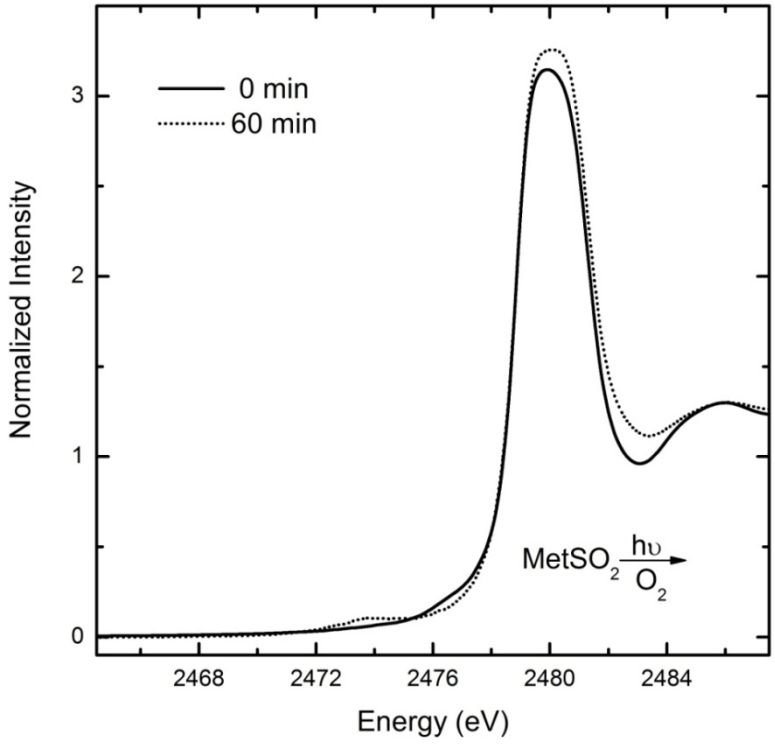

Figure 4.13 S K-edge XAS spectra with photoirradiation of $MetSO_2$ by Xe arc lamp under aerobic conditions.

4.4 Conclusions

Photochemical redox processes of Met are particularly relevant in cataracts, whose formation is correlated with long-term UV irradiation of the crystalline lens.[250] Physiologically irreversible oxidation of Met to $MetSO_2$ should lead in many cases to the loss of function and, therefore, to pathophysiological situations. Evidence of

$MetSO_2$ has been reported in age-related cataracts. Also, Met oxidation to MetSO in combination with insufficient reduction capacity to Met has similar consequences. There is significant literature on the photoredox properties of Met in the presence of sensitizers in order to enhance $^1O_2$ production. My work shows the photochemistry of Met in the absence of such sensitizers which give rise to two new pathways. First, a direct one-electron oxidation of Met to give a sulfur-centered radical cation that can react with oxygen to give the oxidized species, MetSO and $MetSO_2$. Second, formation of $^3Met^*$ can go through a spin allowed reaction with molecular oxygen to produce MetSO and $MetSO_2$. The human eye is potentially vulnerable to solar radiation derived photodamage, although there are several mechanisms that protect the eye from such damage.[270] Since the maximum absorption of the lowest-energy singlet to triplet transition in Met (285 nm) extends into the 300-400 nm range, it may be possible that, over long time frames, this overlap may cause photodamage. The photoreduction of MetSO back to Met also suggests that in the absence of O_2, oxidative damage involving MetSO may potentially be repaired. $MetSO_2$ is a photochemical dead-end product, thus the formation of sulfone may ultimately be the most detrimental product of photooxidation.

CHAPTER 5: METAL-INDUCED METHIONINE OXIDATION IN AMYLOID-BETA PEPTIDE

5.1 Introduction

5.1.1 Alzheimer's Disease

Alzheimer's disease (AD) is a neurodegenerative disease characterized by a progressive decline in memory, impairment of cognitive function and behavioural deterioration.[271] Currently, there are two types of AD recognized: early-onset and late-onset AD. Early-onset AD is diagnosed before the age of 65 and genetic factors have been identified in its development.[272] Late-onset AD is the most common type of the disease, affecting about 95% of all those with AD. It affects people over the age of 65 and advancing age is the major risk factor.[273] The pathological hallmarks in both forms of AD are extracellular amyloid plaques and intracellular neurofibrillary tangles.[168-170] The main component in the plaques is a peptide called amyloid-β (Aβ) and the tangles are made of hyperphosphorylated tau protein. How these features interrelate and which one is of primary importance is still unclear. However, one of the most prevalent hypotheses is the *amyloid cascade hypothesis* postulated by Hardy and Higgins in 1992.[274] It proposes that the fibrillisation of amyloid-β peptide as amyloid deposits is critically responsible for the neurodegeneration that occurs in AD. This prominent hypothesis has guided most of the AD research and provided the framework for the development of therapies used to treat AD.

5.1.2 Amyloid-beta (Aβ) Peptide

Aβ peptide is found ubiquitously in human cells, but its natural function is not yet well understood. It is generated by sequential proteolytic cleavage of the much larger amyloid precursor protein (APP), a transmembrane protein of unknown function with single membrane-spanning domain. APP can be processed by α, β, and γ-secretases; Aβ is generated by successive action of the β and γ-secretases, (Figure 5.1). β-Secretase cleaves to form the N-terminal end of the Aβ, while γ-secretase produces the C-terminal end. γ-Secretase cleaves within the transmembrane region of APP and the cleavage site determines the length of Aβ peptide. γ-Secretase cleaves to give $A\beta_{1-40}$ and $A\beta_{1-42}$ which are 40 and 42 amino acids in length, respectively. The two additional amino acids in $A\beta_{1-42}$ are isoleucine and alanine (Figure 5.2) which are hydrophobic amino acids, which therefore has a higher propensity for aggregation. Aβ peptides consist of a largely hydrophilic N-terminal domain (residues 1-28) and a hydrophobic C-terminal domain (residues 29-40/42).

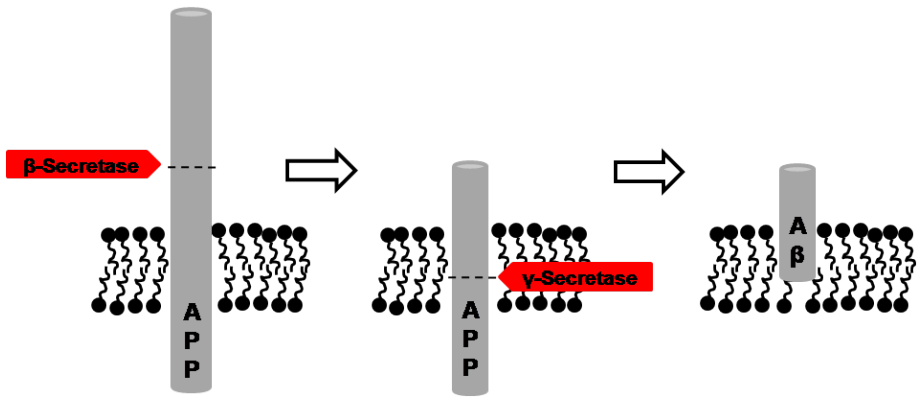

Figure 5.1 Processing of the amyloid precursor protein (APP) to yield amyloid-β (Aβ) peptide.

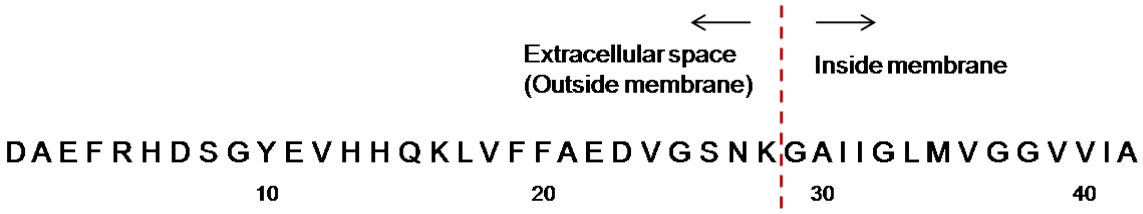

Figure 5.2 Amino acid sequence of $A\beta_{1-42}$. Note that the peptide contains a single methionine residue at position 35.

Aβ has been found in three biochemical forms in the brain: membrane associated, soluble and aggregated. In healthy individuals, the vast majority of Aβ is membrane associated, but in individuals with AD the aggregated and soluble fractions increase markedly.[275,276] The aggregated Aβ is found in a fibrillar form: long and insoluble fibres bound together forming the amyloid plaques. The soluble Aβ is in the oligomeric form and recent evidence suggest it to be toxic.[277,278] The role of fibrillar and oligomeric Aβ in the pathogenesis of AD remains unclear, however it is believed that polymerised Aβ, from small oligomers to large fibrils, is detrimental.[279] Since the aggregated and soluble forms of Aβ occur particularly in AD patients, steps in the process from the membrane associated Aβ to the plaques are key events.

5.1.3 Metal Ion Involvement in Alzheimer's Disease

The brain tightly regulates metal ion concentrations as a part of normal physiological processes. However, the metal ion concentration in the brain increases as a result of normal aging.[280,281] Various lines of evidence have implicated metal ions, in particular Cu, Zn, and Fe in the pathogenesis of AD.[282,283]

There is evidence that normal enzyme-assisted homeostasis of these metal ions is drastically altered in AD brains.[284] With increasing age, these homeostatic mechanisms become less efficient and increases in metal ion concentrations are observed.

Copper(II) is concentrated in Aβ plaques and is found in high concentrations up to 400 μM, almost double the normal brain extracellular concentration.[285,286] It is thought that the Cu in the AD brain is miscompartmentalised rather than universally elevated as studies from bulk tissue indicate that total Cu concentration in an AD brain is comparable to the age matched controls.[278,287]

Similarly, zinc(II) is concentrated in Aβ plaques and can be found as high as approximately 1 mM.[288] There is evidence for elevated Zn levels in AD tissues compared to control tissues in various brain regions and Zn levels in bulk tissues are more difficult to quantify.[285,289] The third transition metal found localized in amyloid plaques is iron(III) in as high concentrations as 900 μM.[288]

The roles of metal ions in the aggregation of Aβ peptides and in ROS production are two key events that have been of particular interest in the pathophysiology of AD. Aβ is a metalloprotein that displays high affinity binding of Cu^{2+}, Zn^{2+}, and Fe^{3+}.[290] The metal binding site is found to be in the N-terminal region of the peptide and the process of Aβ misfolding and aggregation leading to plaques is greatly influenced by the aforementioned metal ions. Zn^{2+} has been indicated to have a primary role in inducing precipitation of Aβ along with its capability to build up protease-resistant Aβ aggregates.[291] *In vitro* studies indicate

that Zn^{2+} rapidly precipitates soluble Aβ into amyloid aggregates[292], and it is believed that the aggregation is promoted by intermolecular His(N_τ)-Zn^{2+}-His(N_τ).[293]

Like Zn^{2+}, Cu^{2+} acts as a potent mediator of Aβ aggregation under conditions of mild acidosis.[294] Fe^{3+} also induces Aβ aggregation[295], however, it does it to a lesser degree than does Cu^{2+}.[294] Transition metals such as Cu^{2+} and Fe^{3+} are capable of mediating the oxidative stress mechanism of Aβ toxicity. Aβ dissolved in Cu^{2+} or Fe^{3+} containing media is toxic to neurons, while Aβ in the absence of redox-active metals is not toxic.[296,297] There is good evidence that AβCu^{2+} or AβFe^{3+} complexes produce ROS, such as H_2O_2 which mediates toxicity.[298,299] Furthermore, the addition of the H_2O_2 scavenging enzyme catalase to the cell cultures inhibits Aβ toxicity, which suggests that Aβ neurotoxicity is mediated by ROS generation.[298,300] Co-incubation of Aβ with metal chelators has also shown to attenuate toxicity.[300]

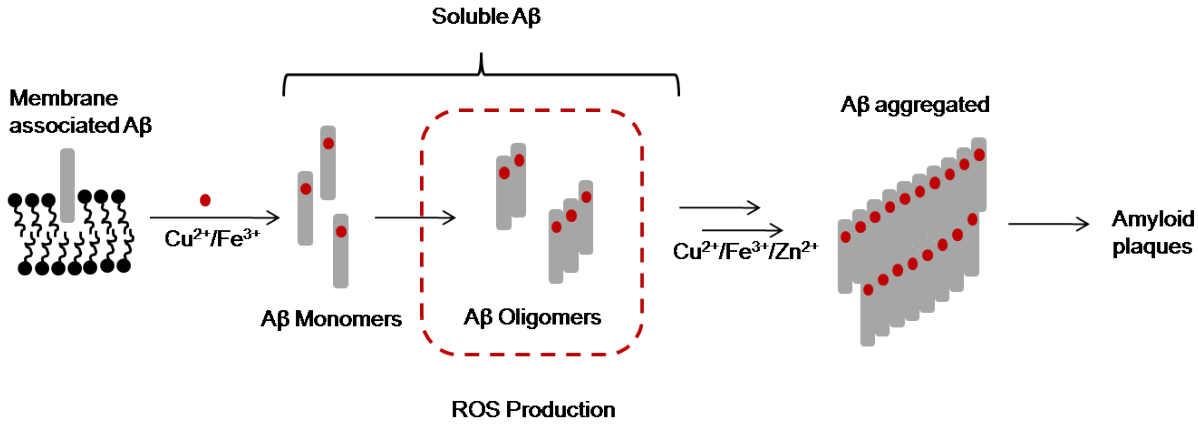

Figure 5.3 Schematic view of the amyloid cascade hypothesis.[301]

The production of H_2O_2 is correlated to the early aggregation process,[302] (Figure 5.3), which supports the amyloid cascade hypothesis that the early stages of aggregation are the toxic forms.[303] The exact mechanism of ROS production is not known, but it is thought to occur through the reduction of Cu^{2+} and Fe^{3+}, using O_2 and biological reducing agents.[298,299,304] A proposed reaction pathway for the sequence of electron transfers that converts O_2 into H_2O_2 is described in Scheme 5.1.[282,301,304] An electron is initially transferred from Aβ peptide to reduce the metal ion forming a positively charged particle, $A\beta^{+\bullet}$. The reduced metal ion then reacts with O_2 to form $O_2^{\bullet-}$ which is then converted to H_2O_2. After electron donation to O_2, the radicalized Aβ peptide-metal complex might be restored by electron transfer from biological reducing agents such as Vitamin C, dopamine, and catecholamines.[304] The generated H_2O_2 may degrade forming a highly reactive $^{\bullet}OH$ via Fenton chemistry or a Haber-Weiss reaction as outlined in Equation 5.1 and Equation 5.2, respectively.[305,306] The biological implications of the ROS produced by Aβ result in protein oxidation, lipid peroxidation, cellular dysfunction and subsequent neuronal death.[307]

Equation 5.1 Fenton chemistry.

$$M^{n+} + H_2O_2 \longrightarrow M^{(n+1)+} + OH^{\bullet} + OH^{-}$$

Equation 5.2 Haber-Weiss reaction.

$$O_2^{-} + H_2O_2 \longrightarrow OH^{\bullet} + OH^{-} + O_2$$

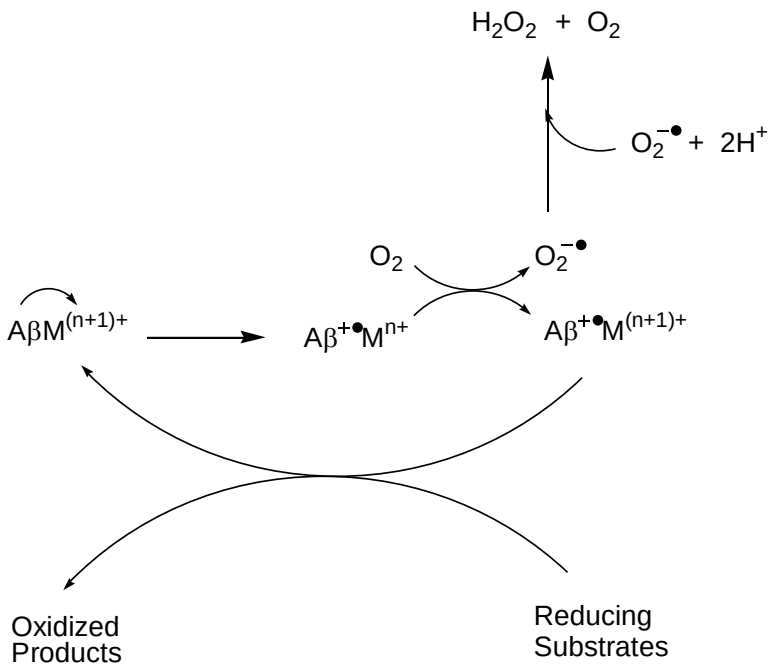

Scheme 5.1 Proposed mechanism of H_2O_2 production by Aβ bound to redox active metal.[304]

5.1.4 The Role of Met_{35} in Aβ

Special attention has been paid to the role of Met_{35}, which has been shown to play a critical role in the oxidative stress and neurotoxicity properties exhibited by Aβ. The generation of ROS by Aβ requires the reduction of metal ions Cu^{2+} or Fe^{3+}, thus inducing oxidation of another moiety. The most likely candidate for oxidation is the sulfur atom of Met_{35}.[308] Met_{35} may serve as a source of electrons for the reduction of molecular oxygen to H_2O_2.[309-311] Consistent with this hypothesis is the evidence of oxidized Met_{35} that is found in post-mortem AD plaques.[175,312] Additional evidence includes the mutation of the methionine to valine or norleucine,

which greatly reduces the rate of H_2O_2 generation[313] even in the presence of other reducing agents.[312]

The redox potentials for Met oxidation and Cu^{2+} reduction result in a thermodynamically unfavourable electron transfer process.[165] The peak potential for the Met_{35} oxidation to its radical cation has been reported to exceed 1.5V vs SHE in aqueous solution.[314] The originally proposed redox potential for $A\beta Cu^{2+}$ was 0.75V vs SHE.[298] Recently this redox potential was redetermined to be substantially less positive 0.28V vs SHE,[315] rendering the redox reaction even less favourable. However, stabilization of the sulfur radical cation by amide moieties and the C-terminal carboxylate ion in Met peptides has been reported.[167,310,316] The neighbouring group participation in the oxidation of thioethers not only stabilizes, but may also render the oxidation potential of thioethers less positive, which will be easier to oxidize.[317] For Aβ, modeling studies indicate that the amide carbonyl group of isoleucine at position 31 is in close proximity to the sulfur of Met_{35} and is proposed to stabilize the corresponding sulfur radical cation by bond formation.[318] The oxidation of Met_{35} causes rearrangement of the helical conformation present within the membrane-spanning region of Aβ.[174] This rearrangement caused by the Met_{35} oxidation is proposed to be a cause for the elevation of soluble Aβ in Alzheimer's disease,[300] as the oxidized Aβ becomes less strongly associated with the membrane.

To date there have been many inconsistencies in the literature regarding Met_{35} oxidation. Mass spectrometry has shown that Cu^{2+} ions are able to oxygenate Aβ with the most likely candidate being the sulfur atom of Met_{35}.[308,319] However,

recent mass spectrometry results have shown no indication of Met_{35} oxidation.[315] Most of the research in identifying Met oxidation involves use of H_2O_2, which is known to oxidize Met, but a direct observation of metal-induced oxidation of Met_{35} is lacking. Thus, this chapter focuses on the work of metal-induced oxidation of Met only in the presence of redox active metals. Since Sulfur K-edge XAS is an element specific technique, it is an ideal spectroscopic tool to investigate the oxidation of a single sulfur containing amino acid, Met_{35} in Aβ in the presence of metal ions such as Cu^{2+} and Fe^{3+}. The aim of this study is to test if the sulfur atoms in Met_{35} in Aβ or Met in N-acetyl-L-methionine amide are altered in any way in the presence of redox active Cu^{2+} and Fe^{3+} in the absence of exogenous reducing agents and H_2O_2.

5.2 Experimental

5.2.1 Materials

Synthetic $A\beta_{1-40}$ peptide was obtained from Bachem (Torrance, CA, USA). $A\beta_{1-16}$ was synthesised on a CS Bio Co peptide synthesizer using standard Fmoc chemistries and subsequently purified by high performance liquid chromatography (HPLC) as previously described.[320] The synthesis and purification was carried out by Dr. Jinhe Pan (past graduate student from Dr. Straus' lab in UBC). The purified products were confirmed by mass spectral analysis. Both $A\beta_{1-40}$ and $A\beta_{1-16}$ were stored at -20^{o}C until use. Water of ultrahigh quality (TraceSELECT® Ultra) was purchased from Sigma-Aldrich. $CuCl_2$, $FeCl_3$, and phosphate buffered saline (PBS) tablets were also purchased from Sigma-Aldrich. N-acetyl-L-methionine amide (purity 99%) was purchased from Bachem.

5.2.2 Sample Preparation

$A\beta_{1-40}$ (1 mg) was dissolved in 200 µL of 50 mM PBS buffer, pH 6.5 with 40% glycerol (v/v). Inclusion of glycerol as a cryoprotectant for biological samples is an accepted method for soft XAS data collection. To this peptide solution, metal solution ($CuCl_2$ or $FeCl_3$) was added so that the peptide to metal ratio was 1:1. The final concentration of $A\beta_{1-40}$ in the peptide-metal mixture was approximated to 1 mM. The stock metal solutions were also made in 50 mM PBS buffer, pH 6.5 with 40% glycerol (v/v).

N-acetyl-L-methionine amide (ac-Met-NH_2) samples were prepared in similar manner to $A\beta_{1-40}$, but with higher concentrations of approximately 5 mM. Metal solutions were also added to ac-Met-NH_2 solutions so that ratio of ac-Met-NH_2 to metal was 1:1. Additional samples were also prepared with ac-Met-NH_2 which included the presence of $A\beta_{1-16}$ to mimic the metal binding mode of Aβ peptide. For samples with H_2O_2, 3% H_2O_2 (v/v) was added to metal solutions or was directly added to $A\beta_{1-40}$ or ac-Met-NH_2 solutions.

All the reactions were carried out in the absence of light to avoid photochemical reactions and were incubated at 37^oC for a period of 1-2 hours. The buffer and metal solutions were tested for any sulfur contamination with S K-edge XAS prior to addition to the samples.

5.2.3 XAS Data Acquisition

XAS data were collected at SSRL on beamline 6-2 under conditions described in section 3.2.8.

5.2.4 Data Processing and Analysis

Complete XAS data reduction and analysis is described in section 2.3.1.

5.3 Results and Discussion

5.3.1 Copper(II)-Induced Oxidation

Cu^{2+}-induced oxidation of Met was investigated by repeating the experiments from previously published evidence.[308] This required the $A\beta_{1-40}$ to be incubated with Cu^{2+} in the presence of H_2O_2. The sulfur contribution in $A\beta_{1-40}$ came from a single sulfur atom from Met_{35}, thus the pre-edge feature at 2473.5 eV in the S K-edge XAS spectrum $A\beta_{1-40}$ was due to the sulfur of Met_{35}, (Figure 5.4). In agreement with the literature findings, this sulfur atom in the Cu^{2+}/H_2O_2 system was modified to give a pre-edge feature at 2476.3 eV, corresponding to methionine sulfoxide (MetSO). Since H_2O_2 has strong oxidizing properties and is known to oxidize Met to MetSO, a reaction of $A\beta_{1-40}$ only in the presence of H_2O_2 without Cu^{2+} was also performed. As expected, the same pre-edge feature at 2476.3 eV was observed, suggesting direct peroxide oxidation of Met_{35} to MetSO (Figure 5.4). Since H_2O_2 alone was sufficient to oxidize Met_{35}, this brings into question the role that Cu^{2+} plays in the oxidation of Met_{35} in the Cu^{2+}/H_2O_2system. It seems that H_2O_2 is at least partly responsible for

the observed Met oxidation of Aβ peptide in the Cu^{2+}/H_2O_2 system. Furthermore, to investigate whether $A\beta_{1-40}$ Met_{35} oxidation was unique to the peptide, similar reactions using N-acetyl-L-methionine amide (ac-Met-NH_2) were performed. Both, in the Cu^{2+}/H_2O_2 system and in H_2O_2, ac-Met-NH_2 was oxidized to MetSO indicating that the observed oxidation of Met in $A\beta_{1-40}$ was not specific to the peptide alone, but to Met in general.

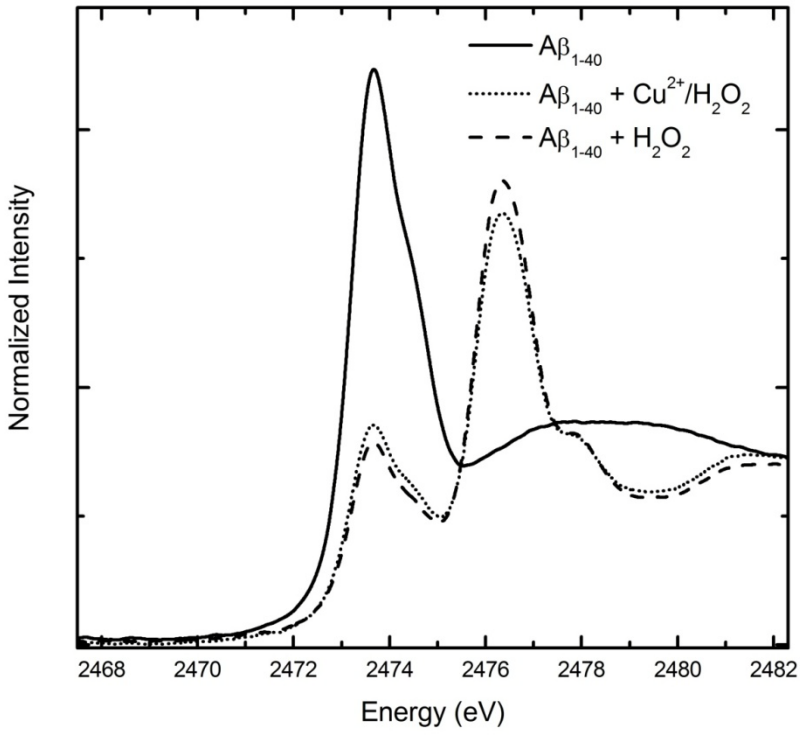

Figure 5.4 S K-edge XAS spectra of $A\beta_{1-40}$ peptide before and after incubation with Cu^{2+}/H_2O_2 or H_2O_2.

To investigate whether Cu^{2+} alone can induce oxidation of Met_{35}, a reaction involving $A\beta_{1-40}$ in the presence of Cu^{2+} only was used. Figure 5.5 shows evidence of Met_{35} oxidation to MetSO in $A\beta_{1-40}$ in the presence of Cu^{2+} under aerobic

conditions. Met is thought to be a possible electron source for the reduction of bound Cu^{2+}, which would then result in Cu^{1+} and $MetS^{\bullet+}$. The generated $MetS^{\bullet+}$ can react with O_2 to form MetSO (see section 4.1.3). Another possibility of Met oxidation might be that the reduced Cu^{1+} is able to transfer an electron to O_2 generating $O_2^{\bullet-}$ (see Scheme 5.1), which can then undergo fast reactions with $MetS^{\bullet+}$ producing the observed MetSO.

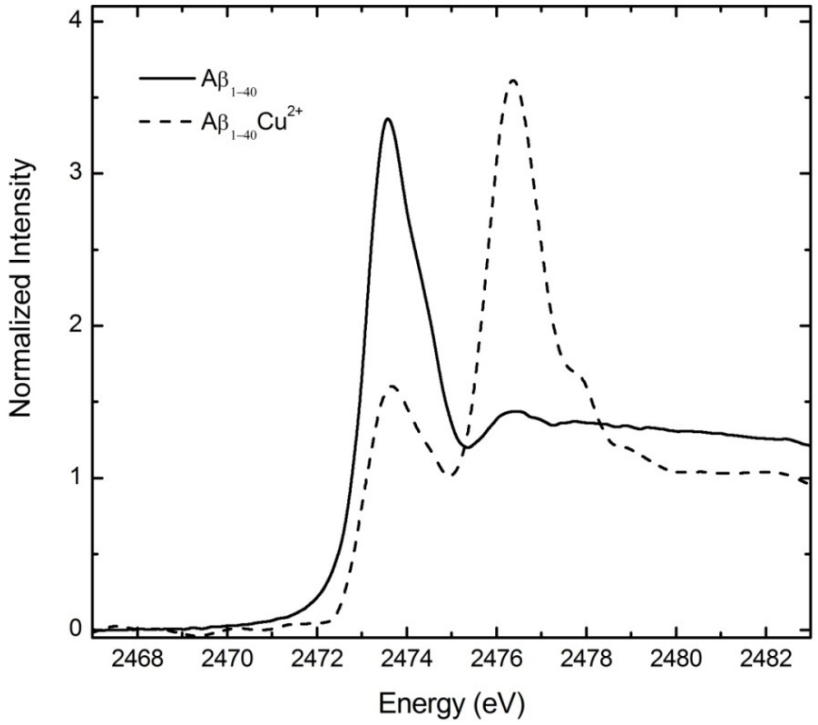

Figure 5.5 S K-edge XAS spectra of $A\beta_{1-40}$ peptide before and after incubation with Cu^{2+}.

In order to substantiate that this Cu^{2+}-induced oxidation is unique to Aβ peptide, ac-Met-NH_2 was also subjected to a reaction with Cu^{2+}. This reaction however, failed to produce the pre-edge feature at 2476.3 eV that corresponds to

the formation of MetSO, which suggests that perhaps binding of Cu^{2+} to the Aβ peptide is necessary for the observed Met_{35} oxidation in Aβ. Thus, to mimic the metal binding mode in $Aβ_{1-40}$, a shorter fragment of the peptide, $Aβ_{1-16}$ was used since the metal binding region is thought to be in the N-terminal region. Therefore, a reaction with ac-Met-NH_2 in the presence of $Aβ_{1-16}$ bound to Cu^{2+} was tested and this also failed to produce the MetSO oxidized peak, (Figure 5.6). The absence of MetSO formation in ac-Met-NH_2 with $Aβ_{1-16}Cu^{2+}$ was consistent with finding that Cu^{2+} was not reduced with the addition of methionine to $Aβ_{1-16}$ or $Aβ_{1-20}$.[321,322] It seems as though the Cu^{2+}-induced oxidation of Met is only observable in the full-length Aβ peptide, which might be due to reduction of the bound Cu^{2+}.

The lack of MetSO production in $Aβ_{1-16}Cu^{2+}$ with ac-Met-NH_2 also suggests that H_2O_2 might not have been produced, as it had been shown earlier that the presence of H_2O_2 alone can oxidize Met. Recent findings suggest that, in the absence of reducing substrates, production of H_2O_2 is not observed in the $Aβ_{1-40}Cu^{2+}$ and $Aβ_{1-16}Cu^{2+}$. However, the reduction of the bound Cu^{2+} persists in $Aβ_{1-40}$ while $Aβ_{1-16}$ with an exogenous Met source still failed to reduce the bound Cu^{2+}.[322] This is consistent with the production of MetSO in full-length Aβ, which suggests that the bound Cu^{2+} must be reduced to Cu^{+} but the source of the electron may not be Met_{35}. Once Cu^{+} is formed, it may then generate $O_2^{\bullet-}$ via electron transfer to O_2. The $O_2^{\bullet-}$ being highly reactive and is good oxidizing agent, it can react with Met_{35} to generate the observed MetSO. Furthermore, the lack of MetSO formation in $Aβ_{1-16}Cu^{2+}$ suggests that ac-Met-NH_2 does not provide the electron for the Cu^{2+} reaction, thus it is unable to generate $O_2^{\bullet-}$ which can then react with ac-Met-NH_2. As a result, the

source of the electron for Cu^{2+} must come from the Aβ peptide since external reducing substrates were not available in the reaction. This also suggests that the electron source might be the missing residues 17-40 which lack in $A\beta_{1-16}$.

Another possibility is that Met_{35} still might be the electron source for the Cu^{2+} reduction but Met might be too remote from the metal centre for direct electron transfer.[238] Thus, it requires intermediate residues between the Met and the metal centre to mediate electron transfer though the peptide from Met to the metal centre. This possibility has been proposed from computational studies which suggest that phenylalanine at position 20 might play such role.[323]

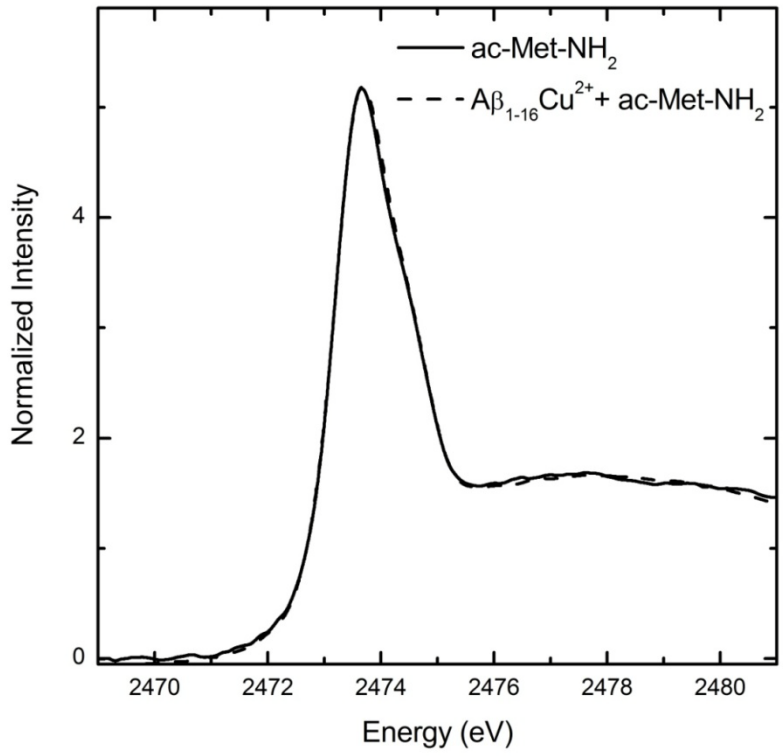

Figure 5.6 S K-edge XAS spectra of N-acetyl-methionine amide (ac-Met-NH_2) before and after incubation with $A\beta_{1-16}Cu^{2+}$.

5.3.2 Iron(III)-Induced Oxidation

The result of $A\beta_{1-40}$ in a Fe^{3+}/H_2O_2 system is shown in Figure 5.7 along with $A\beta_{1-40}$ with H_2O_2. As expected, Met_{35} is oxidized to MetSO as evidenced by the pre-edge feature at 2476.3 eV, and H_2O_2 is the oxidizing agent that is responsible for the Met_{35} oxidation. The result was the same when the source of Met is changed to ac-Met-NH_2. In the absence of H_2O_2, the Fe^{3+} did not oxidize Met_{35} in $A\beta_{1-40}$, (Figure 5.8). This was a little surprising since Cu^{2+} alone caused an oxidation of Met_{35}, but Fe^{3+} failed to do so. This raises questions of whether Fe^{3+} was binding to Aβ: if so, is the binding mode similar to that of Cu^{2+}? There is limited evidence in the literature regarding Fe^{3+} interaction with Aβ. Most of the research has been focused on Cu^{2+} and the assumption is that since both Cu^{2+} and Fe^{3+} are redox-active, they should have similar redox chemistry with Aβ. This assumption has not been investigated to this point. The differences in the oxidation of Met_{35} may be attributed to whether the Fe^{3+} binds to the Aβ or not and whether the binding modes are similar between the Cu^{2+} and Fe^{3+}. In order to get a complete understanding of these differences the metal-binding regions must be probed which may give insight into this. This will be pursued in Chapter 6.

ac-Met-NH_2 was subjected to the same reaction as Aβ, which failed to produce any oxidized Met in Fe^{3+} solutions under aerobic conditions. Furthermore, Aβ was also mimicked by using the shorter fragment of the peptide $A\beta_{1-16}$. The Fe^{3+} bound to $A\beta_{1-16}$ still failed to oxidize ac-Met-NH_2.

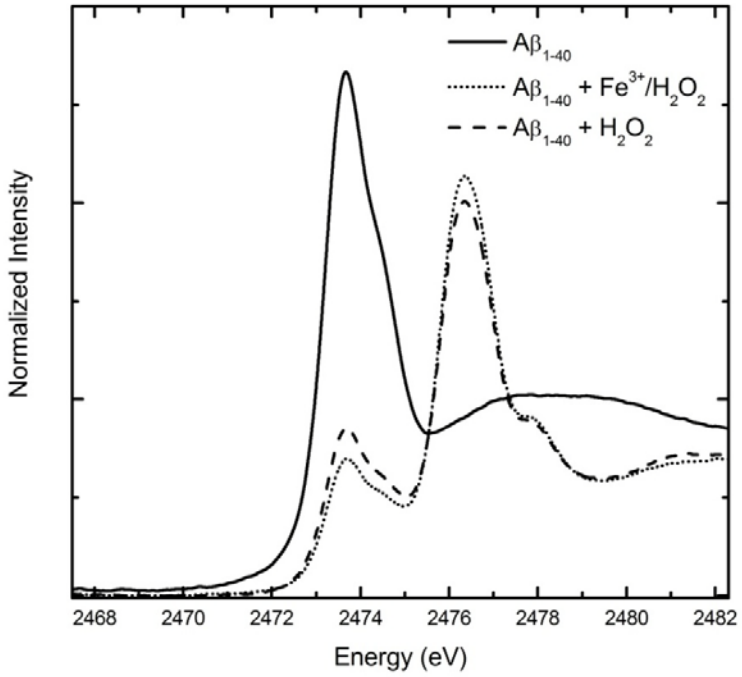

Figure 5.7 S K-edge XAS spectra of $A\beta_{1-40}$ peptide before and after incubation with Fe^{3+}/H_2O_2 or H_2O_2.

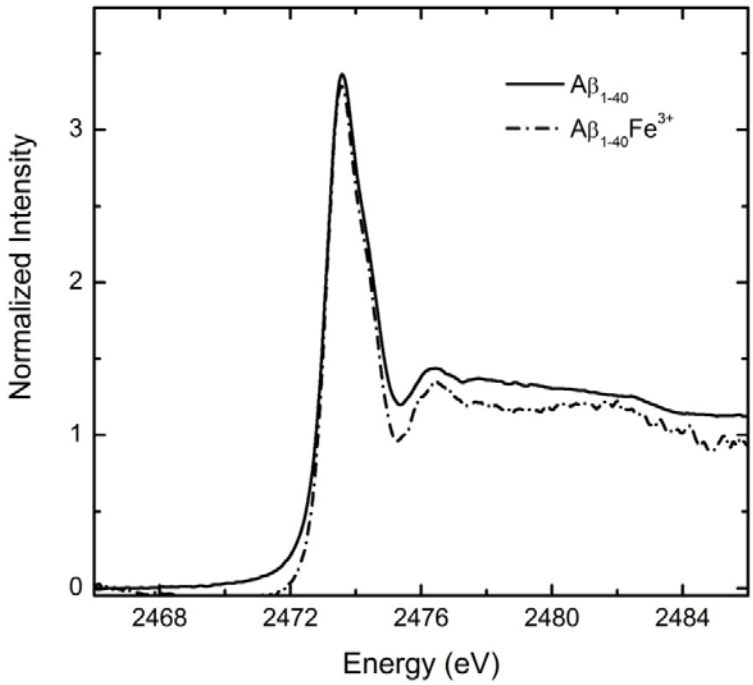

Figure 5.8 S K-edge XAS spectra of $A\beta_{1-40}$ peptide before and after incubation with Fe^{3+}.

5.4 Conclusions

Much of the research to date has focused on the redox chemistry of Cu^{2+} in Aβ peptide and has produced inconsistent findings in regards to the role of Met_{35} and the oxidation state of Met_{35}. The inconsistencies are likely largely due to the use of H_2O_2 to observe the metal-induced oxidation and the lack of direct detection methods to observe the changes in the Met_{35} residue. Sulfur K-edge XAS is an ideal spectroscopic tool to detect the changes in the Met residue since Aβ peptide has a single sulfur atom in the entire peptide in Met_{35}. The full-length peptide in the presence of Cu^{2+} contained an oxidized species in Met_{35}. When Cu^{2+} was bound to the $A\beta_{1\text{-}40}$, there was evidence of MetSO formation, which is consistent with the finding of post-mortem AD plaques. Mimicking the metal binding region of Aβ and adding an exogenous Met is not sufficient to oxidize the Met, which suggests that the observed Met oxidation is unique to the full-length peptide. Surprisingly, Fe^{3+} does not oxidize the Met residue in the full-length peptide. Until now the redox chemistry of Fe^{3+} has been thought to be similar to Cu^{2+}. Here I report that the Aβ peptide redox chemistry is different between the two metal ions. The next step in understanding the difference in the effect of the two metals on Aβ peptide is to investigate whether the two metals bind in similar fashion.

CHAPTER 6: STRUCTURAL CHARACTERIZATION OF THE COPPER(II) AND IRON(III) COORDINATION TO THE AMYLOID-BETA PEPTIDE

6.1 Introduction

6.1.1 Experimental Techniques

Metal ions such as Zn^{2+}, Cu^{2+}, and Fe^{3+} bind to the N-terminal region of Aβ peptide. Crystal structure analysis using X-ray diffraction is, in many cases, the most effective method available for obtaining high-resolution structural information about metalloproteins. Neither $A\beta_{1-40}$ nor $A\beta_{1-42}$ crystallize due to peptide aggregation in the presence of metal, so crystallographic data are not available. Thus, many alternative structural methods have been used during the last decade to try to characterize the structure of the metal binding site in Aβ complexes, including EPR,[324,325] NMR,[325,326] Raman spectroscopy,[175,293] and XAS.[327-329] XAS, provides structural information about the absorber atomic environment through the study of the oscillations of the absorption coefficient that originates from the atoms surrounding it. This interference spectrum (EXAFS) contains detailed information about scatterer-absorber relative positions, from which the nature and geometric arrangement of the amino acids that are coordinated to the metal can be inferred with good accuracy.

6.1.2 Aβ-Cu Complexes

The coordination chemistry of Cu^{2+} has been studied in the past few years with truncated $A\beta_{1-16}$ and $A\beta_{1-28}$ and with native $A\beta_{1-40}$ and $A\beta_{1-42}$ peptides; however, no real consensus has been reached regarding the identity of the coordinating ligands. Earlier EXAFS measurements of $A\beta Cu^{2+}$ led to a model in which the Cu^{2+} ion binds to Aβ in a five-coordinate square-pyramidal ligand environment.[327] This coordination environment involves ligation of three imidazoles from the His at positions 6, 13, and 14, an oxygen atom donor from Tyr at position 10 and an axial water molecule. However, other EXAFS studies have been used as evidence for either a distorted six-coordinate[329] or four-coordinate[330] Cu^{2+} binding site in Aβ peptide. The six-coordinate model[329] involves the three imidazoles of His_6, His_{13} and His_{14} as well as a carboxylate oxygen from either glutamic acid (Glu_{11}) or aspartic acid (Asp_1) in an approximately equatorial planar arrangement, with the axial ligands consisting of a water molecule and the other carboxylate oxygen also from Glu_{11} or Asp_1. The four-coordinate model[330] proposes involvement of two His residues and two nitrogen and/or oxygen ligands. Both the six-coordinate and four-coordinate models agree on the absence of Tyr from the coordination environment. Furthermore, other spectroscopic data such as EPR[324] and theoretical work have also yielded conflicting conclusions with regards to the identity of the ligands as well as the coordination number.[325,331] Recent pH-dependence studies of Cu^{2+} coordination to Aβ peptide revealed that two complexes, distinguishable by conventional 9 GHz EPR, are present near physiological pH.[332] These complexes are called component I (lower pH values) and component II (higher pH values), both

of which having a five-coordinate geometry and the absence of Tyr as a coordinating ligand. There is still significant controversy regarding the physiologically-relevant form of Cu^{2+}-bound Aβ peptide.

6.1.3 Aβ-Zn Complexes

In the case of the Aβ-Zn^{2+} complex, the situation appears to be even more complicated and several coordination modes have been proposed. NMR investigations suggests an intermolecular dimer of Aβ, with Zn^{2+} binding involving several His and the peptide N-terminus.[326] Further support for this unusual binding mode was obtained from an XAS study of $Aβ_{13-21}$ bound to Zn^{2+} in which pairs of peptides appear to be cross-linked by a Zn^{2+} bridge binding two His residues, one from each of the peptides.[333] Further NMR studies propose intrapeptide coordination involving three His residues (His_6, His_{13}, and His_{14}) and the N-terminus.[334,335] Opposing this viewpoint, another Zn K-edge XAS study suggests a four His residue coordination mode.[328] Given that a fourth His residue is lacking in the Aβ peptide sequence, this proposal would require a Zn^{2+} bridged interpeptide coordination.

6.1.4 Aβ-Fe Complexes

The redox-active metal ion Fe^{3+} is found in AD plaques, suggesting that it might mediate ROS generation. Thus, answers to fundamental questions regarding the coordination environment and reactivity of Fe^{3+} when bound to Aβ peptide are essential; however, much of the investigation on the metal binding of Aβ peptide has

been focused on Cu^{2+} and Zn^{2+}. It is generally assumed that Fe^{3+} has a similar binding mode as Cu^{2+} and has similar reactivity as a result. Recent evidence of Fe^{3+} binding to Aβ peptide comes from electrospray ionization mass spectrometry (ESI-MS),[336] however, this study did not reveal any details on the coordination environment of Fe^{3+}.

In order to get a better understanding of the differences of the metal-induced Met_{35} oxidation that was observed with Cu^{2+} and Fe^{3+} in the full-length peptide Aβ (Chapter 5), the metal binding site of Cu^{2+} and Fe^{3+} must be investigated. Thus, this chapter looks at the metal binding site of Cu^{2+} and Fe^{3+} in the full-length Aβ peptide as well as the truncated $Aβ_{1-16}$.

6.2 Experimental

6.2.1 Materials

Materials used for this study are described in section 5.2.1.

6.2.2 Sample Preparation

$Aβ_{1-40}$ (1 mg) was dissolved in 200 µL of 50 mM PBS buffer, 75 mM NaCl, pH 6.5 with 40% glycerol (v/v) as a cryoprotectant. To this peptide solution, the metal solution ($CuCl_2$ or $FeCl_3$) was added so that the peptide to metal ratio was 1:1. The final concentration of $Aβ_{1-40}$ in the peptide-metal mixture was ~1 mM. The stock metal solutions were also made in 50 mM PBS buffer, 75 mM NaCl, pH 6.5 with 40% glycerol (v/v). Immediately after preparation, the samples were injected into XAS

cells sealed with a polypropylene window on the front, and rapidly frozen in liquid nitrogen. $A\beta_{1-16}$ samples were prepared in similar manner to $A\beta_{1-40}$, but the final peptide concentration was ~3 mM.

6.2.3 XAS Data Acquisition

Fe K-edge XAS and Cu K-edge XAS data were collected at the SSRL on beamline 7-3 under ring conditions of 80-100 mA at 3.0 GeV. This setup used a 20-pole, 2 Tesla wiggler, 0.8 mrad beam and a Si (220) double-crystal monochromator. The beamline is equipped with harmonic rejection mirrors which can efficiently minimise higher harmonic contamination. The incident X-ray intensity (I_0), sample absorption (I_1), and Fe or Cu reference (I_2) were measured as transmittance in three consecutive N_2-filled ionisation chambers and fluorescence data were collected using a 30-element Ge detector array. The fluorescence signal was windowed at K-alpha emission of the element, either Cu or Fe depending on the sample. For each sample, 10 to 15 sweeps were taken and all data were measured to k = 15 $Å^{-1}$. All samples were maintained at 15 ± 3 K throughout data collection by using a continuous-flow liquid helium cryostat. Photoreduction of Cu^{2+} or Fe^{3+} by the X-ray beam was monitored by comparing edge spectra (XANES) for consecutive sweeps. All the experiments were repeated to ensure reproducibility.

6.2.4 Data Processing and Analysis

ATHENA software[221] was used for Cu and Fe K-edge XANES data reduction. For energy calibration, the lowest-energy maximum of the first derivative of the

reference spectra was assigned, for the Cu K-edge was set to 8979 eV and for Fe K-edge set to 7112 eV. Data scans were averaged and background subtraction and normalization were performed simultaneously using a linear pre-edge and post-edge function.

The averaged energy calibrated data were used for EXAFS analysis. The EXAFS oscillations $\chi(k)$ were extracted using an automated background subtraction AUTOBK algorithm[337] implemented in the ATHENA software. The EXAFS oscillations $\chi(k)$ were quantitatively analyzed by the ARTEMIS software, using *ab initio* theoretical amplitude, phase, and mean-free path factors calculated by FEFF6. FEFF is an automated program for *ab initio* multiple scattering (MS) calculations of EXAFS. The atomic coordinates (x, y, z) for the theoretical model were generated by a software program based on MATLab that has been developed by Dr. Mario Jaime-Delgado (past graduate student in Kennepohl lab). The atomic coordinates were used in the FEFF6 input file to generate the multiple scattering paths.

6.2.5 Model Building and Fitting Strategy

To get reliable information from EXAFS data, a crucial point of analysis is the choice of the initial trial geometry around the absorber. Lacking crystallographic data for Aβ peptides, the only indication about possible metal ligands comes from the knowledge of the peptide amino acid sequence. Also, previous spectroscopic evidence of ligand coordination is helpful in building a theoretical model.

Initial fits of the EXAFS data were performed with only a single scattering (SS) shell. This simple scattering model gives reasonable fits, but cannot account for scattering waves corresponding to longer distances and is insufficient for developing an accurate representation of metal-binding. More detailed models, including multiple scattering, were investigated with many of the suggested models from the literature.[324,325,327,329,332] In both, Cu^{2+} and Fe^{3+} EXAFS, the starting models were remodelled accordingly to give good fit in the R-space.

Constrained and restrained refinement procedures[338] were followed, in which the His imidazole and the Tyr phenyl rings are treated as rigid bodies. Constrained and restrained refinement minimizes the number of free parameters in the least-squares refinement to increase the degree of determinacy of the model. Light scatterers such as nitrogen and oxygen atoms are difficult to distinguish based solely on their individual contribution to the EXAFS signal; however, when these atoms are tightly anchored to a large and well ordered structure such as an imidazole or a phenyl ring, they can be unambiguously identified due to the multiple scattering contributions, in general.

The structural parameters refined during constrained/restrained refinements included the distance r_i of ligands and the Debye-Waller factors σ_i^2 for each ligand. The Debye-Waller factors for atoms at similar distances for a given ligand type were grouped together. In addition to the Debye-Waller factor for the atoms directly coordinated to the metal, only the Debye-Waller factor for the second and third shell atoms of the rigid ligands were selected for refinement. The remaining terms were fixed at a value of 0.010 $Å^2$. The coordination number N_i for each type of atom was

kept fixed. In addition to the structural parameters, the photoelectron energy threshold (ΔE_0), which was treated as a single overall parameter for the multiple shell fits, was varied to correct for the simple estimate of E_0 made in ATHENA. The amplitude reduction factor S_0^2 was allowed to be adjusted around the starting value 0.9. The $\chi(k)$ data were weighted by k^3 and windowed between $2 < k < 12$ Å^{-1} using a Kaiser-Bessel window with dk = 2.0 Å^{-1} to minimize spectral ringing. The fits were carried out in $\chi(r)$ in the region of $1 < r < 5$ Å using a Kaiser-Bessel window with dr = 0.2 Å. All SS contributions of atoms ≤ 5 Å and all MS contributions > 10% and l ≤ 4 (triple scattering paths with four legs) were included in fits.

Best fits to the experimental data were determined by selecting the model that gave both chemically reasonable refinement parameters and the lowest R-factor automatically calculated by ARTEMIS.

6.3 Results and Discussion

6.3.1 AβCu^{2+} Complexes

The Cu K-edge XAS data obtained for the Cu^{2+} bound $A\beta_{1-40}$ and $A\beta_{1-16}$ are shown in Figure 6.1 along with Cu^{2+} in 50 mM PBS buffer. In both peptides, the pre-edge is characterized by a weak transition at 8979.7 eV that corresponds to the electric quadrupole allowed Cu 3d ← 1s transition (labeled a in Figure 6.1) and a shoulder in the pre-edge region at 8986.8 eV that corresponds to a Cu 4p ← 1s transition with a metal-ligand charge-transfer shakedown (labeled b in Figure 6.1).[339] The corresponding normal Cu 4p ← 1s transition is not resolvable from the edge.

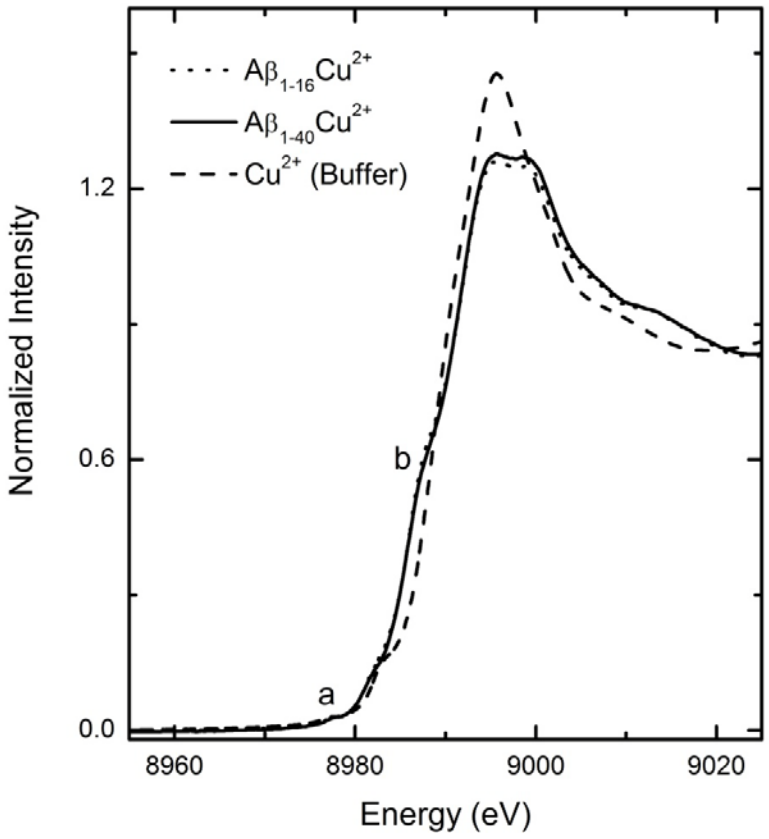

Figure 6.1 The XANES region of the Cu K-edge XAS of $A\beta Cu^{2+}$. The pre-edge transition of 3d ← 1s is marked a and b represents the 4p ← 1s + shakedown transition.

Figures 6.2A and B show the EXAFS region of $A\beta_{1\text{-}16}Cu^{2+}$ and $A\beta_{1\text{-}40}Cu^{2+}$, respectively. The similarity in the XANES and EXAFS regions between $A\beta_{1\text{-}40}$ and $A\beta_{1\text{-}16}$ suggests that geometry of the Cu^{2+} coordination does not change significantly. In both peptides, initial fits of the EXAFS data with only a single-scattering (SS) shell including N/O scatterers suggest a coordination number (CN) of 5 for Cu^{2+}. Fourier-transformed EXAFS data in R-space (Figures 6.2C and D) shows strong outer-sphere scattering between r = 2 and 4 Å, which is characteristic of MS contributions between the Cu centre and rigid ligands such as imidazole rings from

His residues. Using a MS analysis, the number of imidazole ligands was determined to be three in the coordination environment. Addition of more or fewer imidazole ligands yielded poorer fits to the data. This preference of Cu^{2+} binding to nitrogen of imidazole is in accordance with the principle of hard/soft acids and bases.

For the remaining two ligands, various models were tested. Based on the previous spectroscopic evidence, the candidates included the phenolate group from the Tyr residue and a water molecule or carboxylate group of glutamic acid (Glu) or aspartic acid (Asp). A model involving three imidazoles of His and two oxygen of the carboxylate group either from Glu or Asp residue gave a good fit for the Cu^{2+} coordinated in $A\beta_{1\text{-}40}$ and $A\beta_{1\text{-}16}$ (Figure 6.2, Table 6.1).

Available His residues in Aβ peptide are His_6, His_{13} and His_{14} account for the three N(His) contributions in the EXAFS fit. The two oxygen atoms are presumed to be from the N-terminal Asp_1.[340,341] However, Asp at position 7 and Glu at position 3 and 11 are also potential carboxylate donors. The strongest argument for Asp_1 as the coordinating ligand comes from the finding that the mutation of Asp_1 to asparagine (Asn) affects the EPR spectrum.[340] Use of oxygen from phenolate and a water molecule yielded a poorer fit to the data; this is also consistent with UV-Vis spectroscopic data. Cu^{2+}-phenolate containing complexes exhibit a characteristic intense charge transfer band around 400 – 500 nm, but such a band has never been observed in this system.[320,342,343] In addition, NMR[320,325] and EPR[325,332,344] studies are in agreement with Tyr not being involved in the coordination geometry. Furthermore, the pK_a of Tyr_{10} has been determined[320] to be identical to that of a free Tyr residue (pKa ~ 10.1), which suggests that Cu^{2+} is not bound to the Tyr residue.

Copper binding is in competition with protonation, which means that Cu^{2+} binds to N/O ligands with a low pK_a, which favours a carboxylate group of Asp (pKa ~ 3.8) and His (pKa ~ 6.5). Also, the involvement of a water molecule as a ligand was rejected based on the EPR study of ^{17}O-labeled H_2O.[344] Thus the most likely model is that of Cu^{2+} bound to three His and the carboxylate group of Asp. A schematic picture of the molecular arrangement is shown in Figure 6.3.

Table 6.1 EXAFS parameters for $A\beta_{1-16}Cu^{2+}$ and $A\beta_{1-40}Cu^{2+}$.

Sample	Coordinating Ligand	N	R (Å)	σ^2 ($Å^2$)	ΔE_0 (eV)	S_0^2	R-factor
*$\mathbf{A\beta Cu^{2+}}$	N (His)	3	1.95	0.0039	0.93	0.88	0.0177
	O (Glu/Asp)	2	1.99	0.0051			
$\mathbf{A\beta Cu^{2+}}$	N (His)	2	1.94	0.0031	1.21	0.94	0.0416
	N/O	2	2.04	0.0040			
$\mathbf{A\beta Cu^{2+}}$	N (His)	3	1.95	0.0039	1.02	0.89	0.0279
	O (Glu/Asp)	2	1.99	0.0050			
	O (H_2O)	1	2.03	0.0054			
Cu^{2+} (buffer)	O (H_2O)	4	1.97	0.0032	1.98	0.90	0.0091
	O (H_2O)	2	2.36	0.0081			

* Since $A\beta_{1-16}Cu^{2+}$ and $A\beta_{1-40}Cu^{2+}$ data are superimposable, their fits yielded the same EXAFS parameters.
N = path degeneracy, R = distance in Å, σ^2 = Debye-Waller factor, S_0^2 = amplitude reduction parameter, ΔE_0 = internal reference energy. The R-factor indicates quality of fit and is calculated in R-space.
For $A\beta Cu^{2+}$ (k^3, Δk = 2 – 12 $Å^{-1}$, Δr = 1 – 5 Å), for Cu^{2+} in buffer (k^3, Δk = 2 – 12 $Å^{-1}$, Δr = 1 - 2.5 Å).

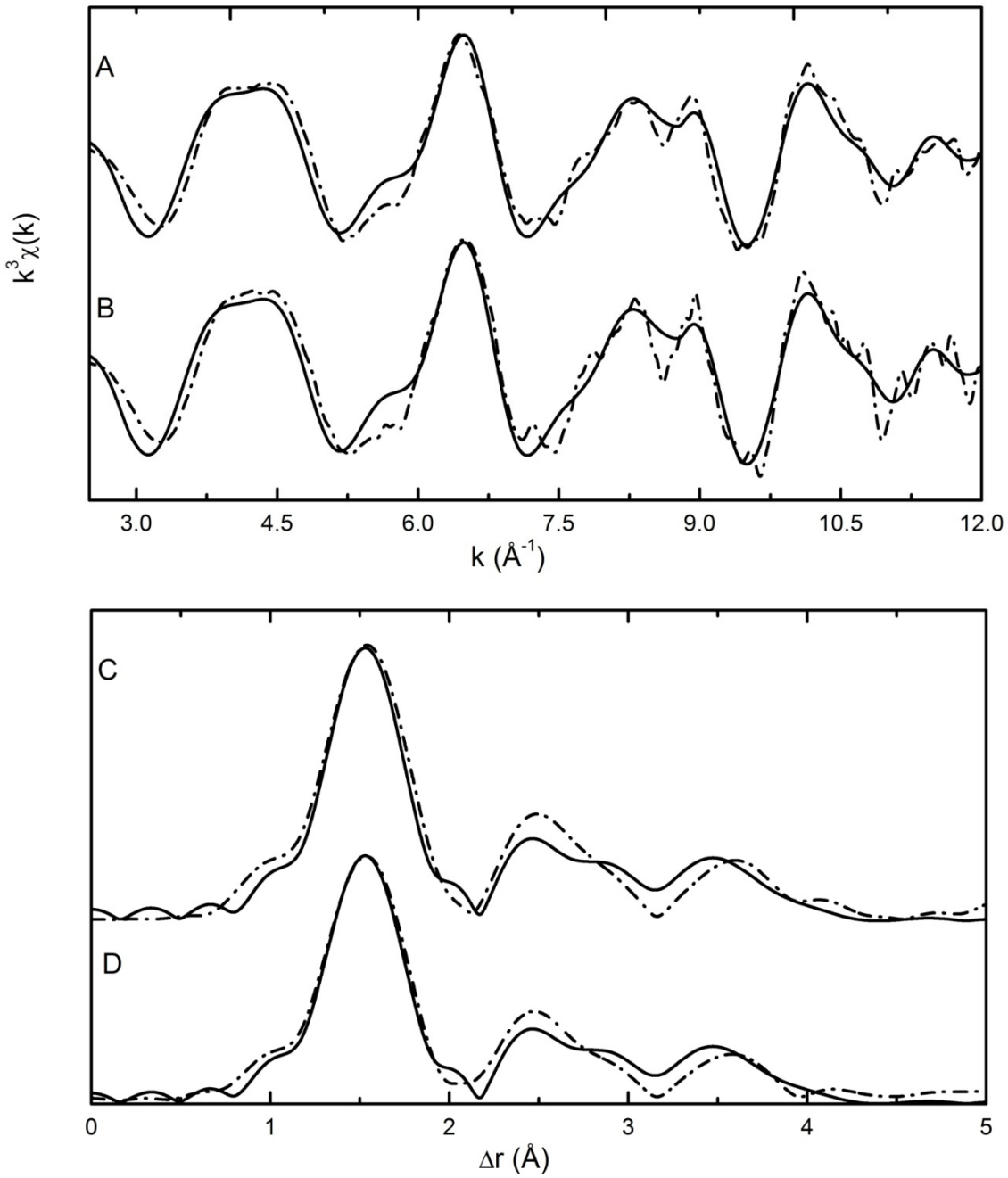

Figure 6.2 EXAFS of $A\beta_{1\text{-}16}Cu^{2+}$and $A\beta_{1\text{-}40}Cu^{2+}$. A) and B) are k^3 weighted $\chi(k)$ of $A\beta_{1\text{-}16}Cu^{2+}$ and $A\beta_{1\text{-}40}Cu^{2+}$, respectively. C) and D) are corresponding Fourier-transformed (FT) of $A\beta_{1\text{-}16}Cu^{2+}$ and $A\beta_{1\text{-}40}Cu^{2+}$. Experimental data are shown by dashed lines and simulations to the data by solid lines.

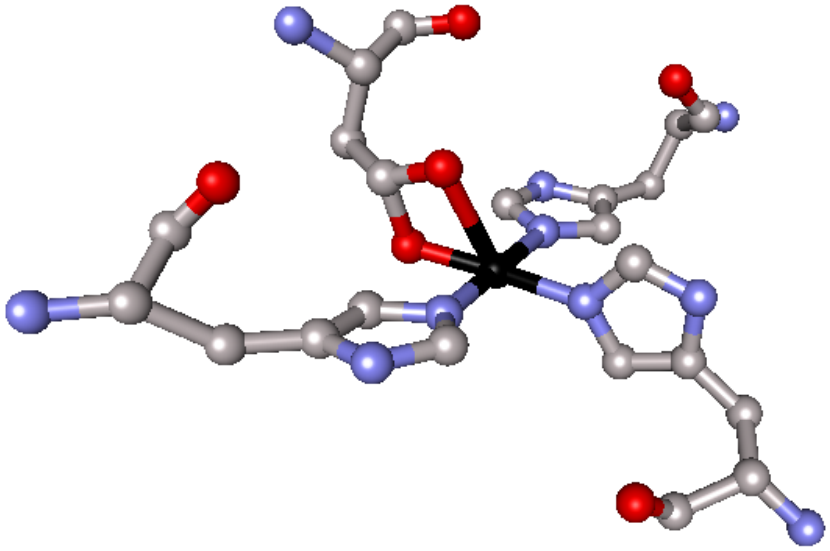

Figure 6.3 Schematic picture of the molecular arrangement around the Cu^{2+} in Aβ. Atom colours are as follows: copper (Cu) *black*; oxygen (O) *red*; nitrogen (N) *blue*; carbon (C) *gray*.

Previous EXAFS studies indicate a four-coordinate[330] and a six-coordinate[329] Cu^{2+} binding to Aβ peptide. The four-coordinate model suggests Cu^{2+} coordinated to two imidazole of His residue and two nitrogen/oxygen ligands, while the six-coordinate model is similar to the proposed five-coordinate model (Figure 6.3) with an additional water molecule. The corresponding four-coordinate and six-coordinate model fits are shown in Figure 6.4 and EXAFS parameters in Table 6.1. These models yield poorer fits to the data, thus strengthening the conclusion that the five-coordinate model is most reasonable for Cu^{2+} binding in Aβ peptide at pH 6.5.

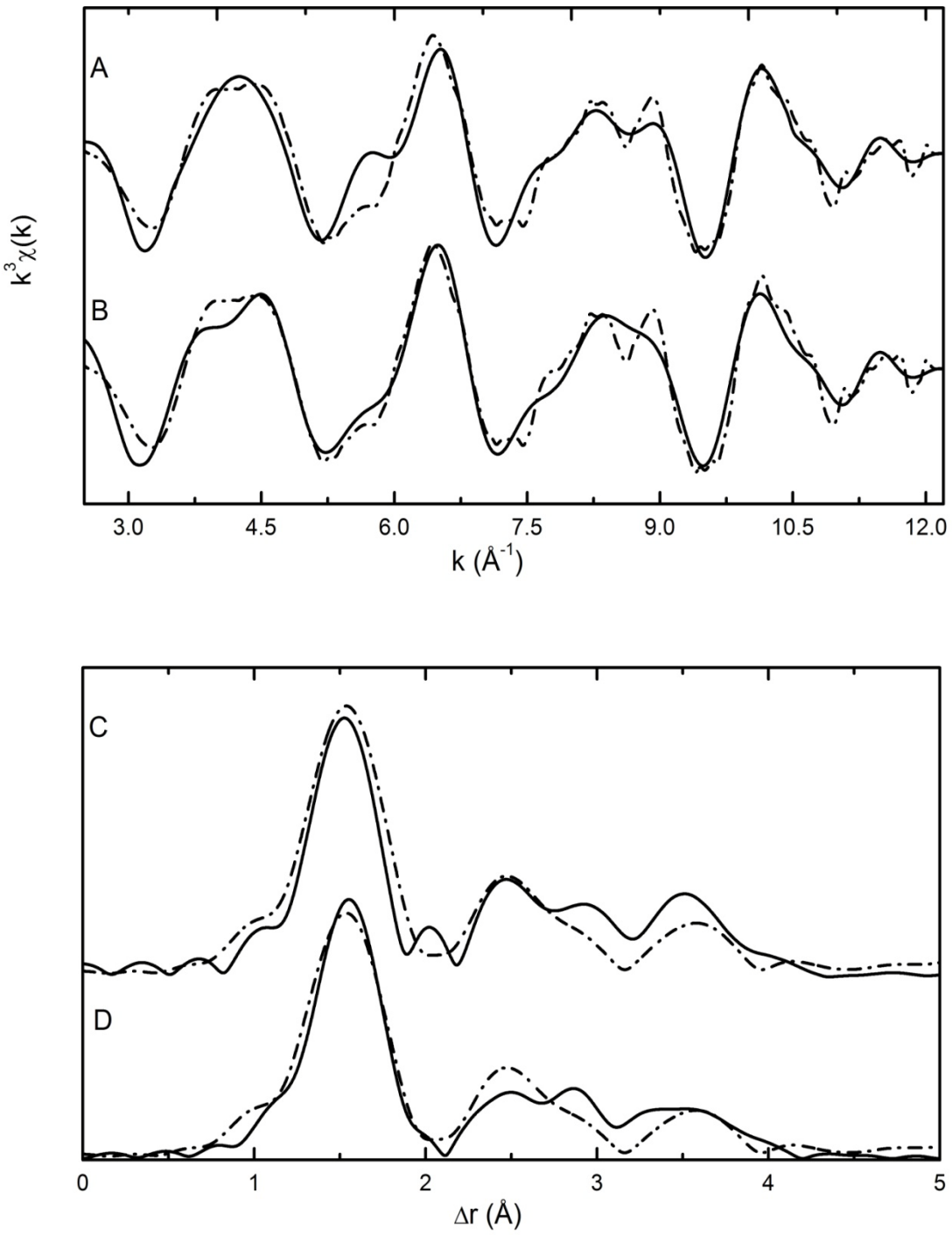

Figure 6.4 Four-coordinate and six-coordinate fits of $A\beta_{1\text{-}40}Cu^{2+}$. A) and B) are k^3 weighted $\chi(k)$ of $A\beta_{1\text{-}40}$ with four-coordinate and six-coordinate Cu^{2+} fits, respectively. C) and D) are corresponding fits in R-space. Experimental data are shown by dashed lines and simulations to the data by solid lines.

The inconsistency with previous EXAFS studies is likely due to the dynamic nature of Aβ and the existence of multiple forms at physiological pH.[332,342] All previous EXAFS studies were done at pH 7.2 to 7.4, thus the available data are for mixtures of two forms of $A\beta Cu^{2+}$. According to EPR[332] and potentiometric studies,[320,340,342] at pH 6.5, only component 1 is present, thus a single species should be observed. Furthermore, only one EXAFS study[327] proposed Tyr as a coordinating ligand, however, a high R-factor of 32% for this simulation is reported even though they were calculated in k-space, which includes high frequency noise components.

For completeness, the parameters of the best fit of the Cu^{2+} buffer sample is reported in Table 6.1 and a single-scattering (SS) fit is shown in Figure 6.5. In the absence of peptide, Cu^{2+} is in a six-coordinate geometry with oxygen atoms, probably from water molecules. Also, multiple scattering features observed for the Cu^{2+} bound Aβ peptide at 2 to 4 Å are not observed in the peptide-free Cu^{2+}. The EXAFS analysis of Cu^{2+} buffer sample corresponds with others.[345,346]

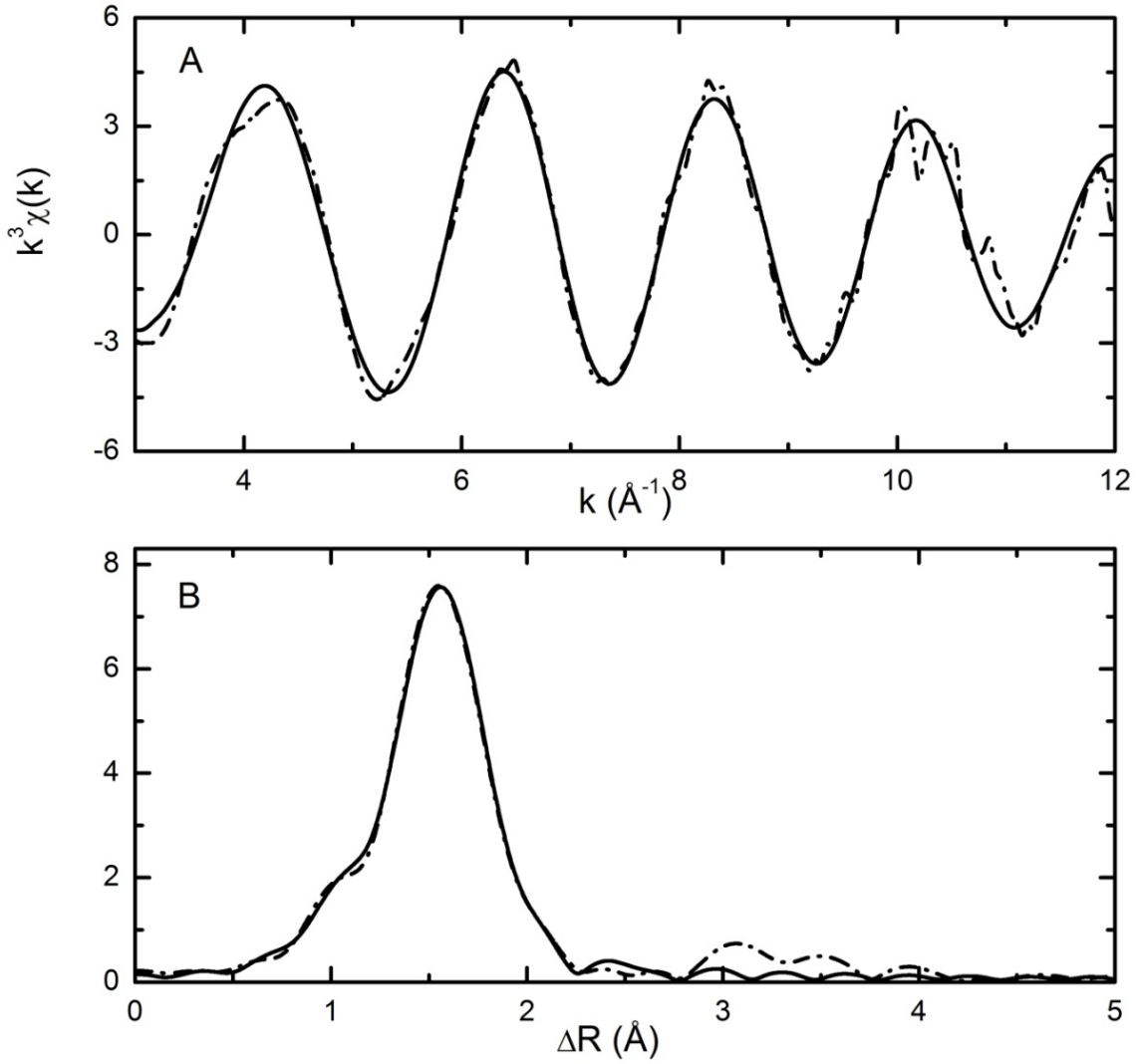

Figure 6.5 EXAFS of Cu^{2+} in buffer. A) is k^3 weighted $\chi(k)$ of Cu^{2+} in buffer and B) is the corresponding Fourier-transformed (FT) of Cu^{2+} in buffer Experimental data are shown by dashed lines and simulations to the data by solid lines.

6.3.2 AβFe^{3+} Complexes

The XANES region of Fe^{3+} bound $A\beta_{1-40}$ and $A\beta_{1-16}$ is depicted in Figure 6.6 along with the Fe^{3+} in 50 mM PBS buffer. In both the peptides and the Fe^{3+} in buffer, the pre-edge is characterized by a weak transition at 7114.5 eV that corresponds to

the electric quadrupole allowed transition Fe 3d ← 1s. This pre-edge feature is split by ~ 1 eV (inset of Figure 6.6). This pre-edge feature has shown to be sensitive to the geometry of the iron atom and the splitting of the pre-edge feature has been attributed to an octahedral geometry of the iron atom.[347]

The Fe K-edge EXAFS region of Fe^{3+} bound to $A\beta_{1-16}$ and $A\beta_{1-40}$ is shown in Figures 6.7A and B. As seen with Cu^{2+} coordination, the Fe^{3+} XANES and EXAFS spectra are similar for both the full-length and the truncated Aβ peptide. In both peptides, the single-scattering analysis has shown that Fe^{3+} is in a six-coordinate environment. Fourier-transformed EXAFS in R-space (Figures 6.7C and D) shows outer-sphere scattering between r = 2 and 4 Å, but these are not as prominent as the ones found for Cu^{2+}. Nevertheless, MS analysis suggests that two His residues are bound to the Fe^{3+} ion. The remaining four ligands are speculated to be carboxylate oxygen or a water molecule. Fe^{3+} preferentially binds to oxygen ligands, thus water molecules and carboxylate are the likely candidates. The octahedral geometry observed in EXAFS analysis is consistent with the observed splitting of the pre-edge feature in XANES confirming that Fe^{3+} is bound to Aβ in a six-coordinate environment. The schematic picture of the molecular arrangement of Fe^{3+} is shown in Figure 6.8. An EXAFS fit for a five-coordinate geometry in which Fe^{3+} is coordinated to two His residues and 3 nitrogen/oxygen ligands is also shown in Figure 6.9 and EXAFS parameters in Table 6.2. This further supports the proposed six-coordinate model.

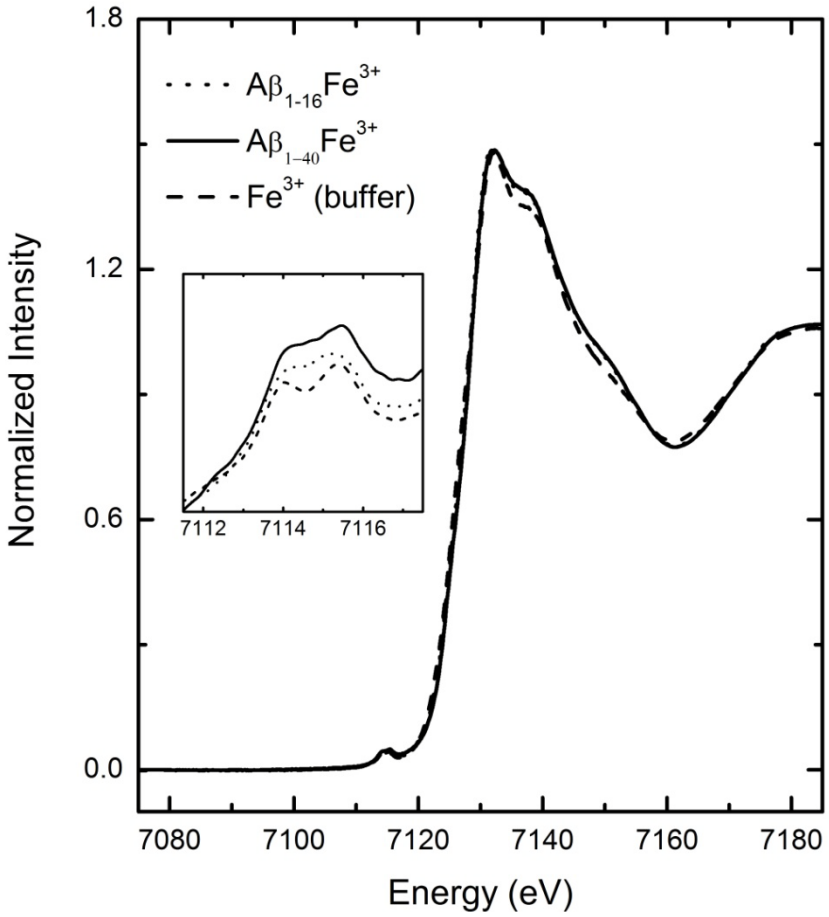

Figure 6.6 The XANES region of the Fe K-edge XAS of $A\beta Fe^{3+}$. Inset shows the Fe 3d ← 1s pre-edge features.

For completeness, the Fe K-edge XAS of Fe^{3+} in the absence of Aβ peptide was also subjected to EXAFS analysis, (Figure 6.10). For Fe^{3+} in buffer, the best fit parameters are compatible with an octahedral geometry and the EXAFS parameters are reported in Table 6.2.[347]

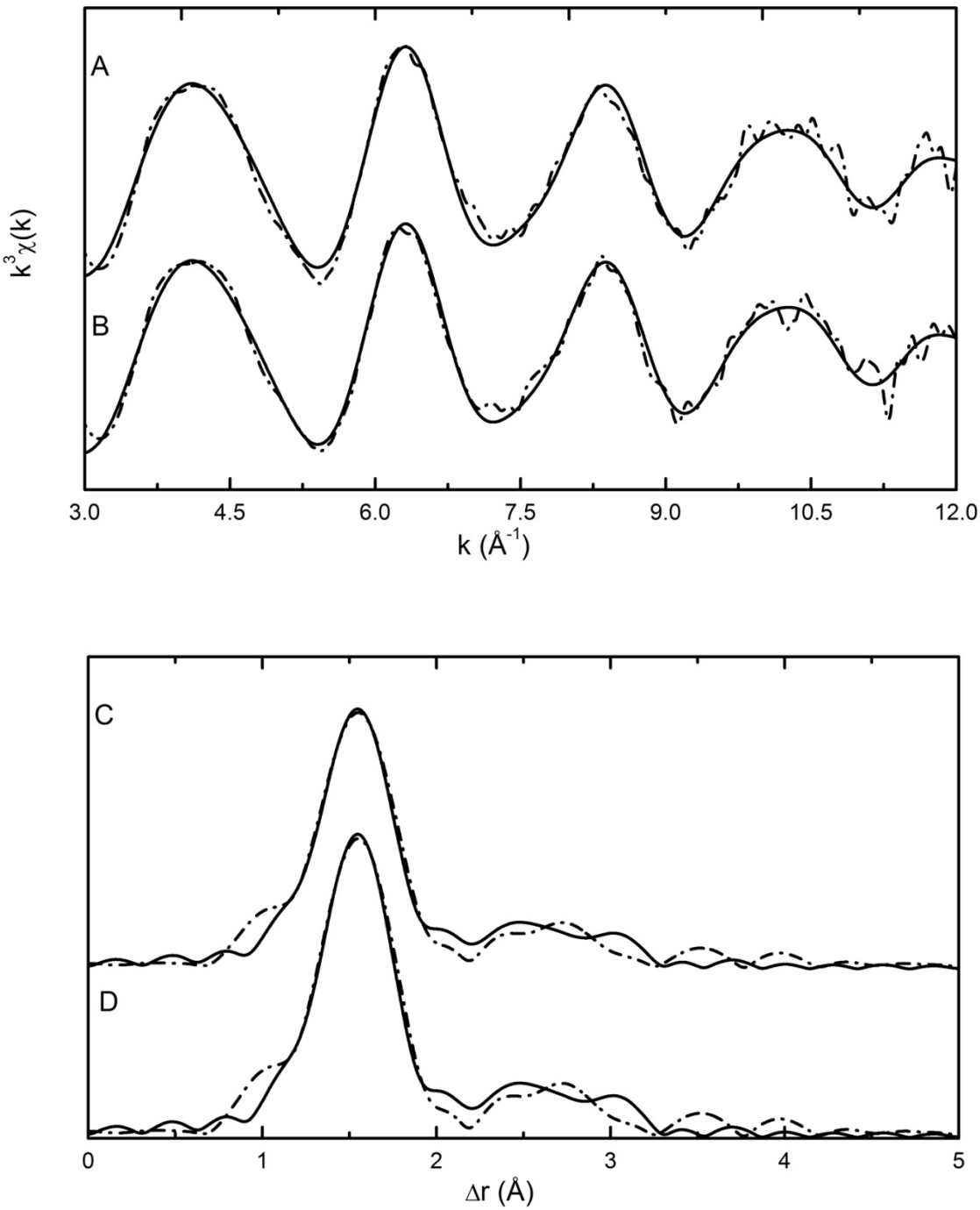

Figure 6.7 EXAFS of $A\beta_{1\text{-}16}Fe^{3+}$ and $A\beta_{1\text{-}40}Fe^{3+}$. A) and B) are k^3 weighted $\chi(k)$ of $A\beta_{1\text{-}16}Fe^{3+}$ and $A\beta_{1\text{-}40}Fe^{3+}$, respectively. C) and D) are corresponding Fourier transformed (FT) of $A\beta_{1\text{-}16}Fe^{3+}$ and $A\beta_{1\text{-}40}Fe^{3+}$. Experimental data are shown by dashed lines and simulations to the data by solid lines.

Table 6.2 EXAFS parameters for $A\beta_{1-16}Fe^{3+}$ and $A\beta_{1-40}Fe^{3+}$.

Sample	Coordinating Ligand	N	R (Å)	σ^2 ($Å^2$)	ΔE_0 (eV)	S_0^2	R-factor
***AβFe^{3+}**	N (His)	2	1.95	0.0021	- 1.37	0.92	0.0183
	N/O	4	2.04	0.0063			
AβFe^{3+}	N (His)	2	1.95	0.0021	-1.66	0.94	0.0205
	N/O	3	2.04	0.0062			
Fe^{3+} (buffer)	O (H_2O)	4	1.94	0.0031	1.22	0.78	0.0003
	O (H_2O)	2	2.07	0.0036			

* Since $A\beta_{1-16}Fe^{3+}$ and $A\beta_{1-40}Fe^{3+}$ data are superimposable, their fits yielded same EXAFS parameters.
N = path degeneracy, R = distance in Å, σ^2 = Debye-Waller factor, S_0^2 = amplitude reduction parameter, ΔE_0 = internal reference energy. The R-factor indicates quality of fit and is calculated in R-space.
For $A\beta Fe^{3+}$ (k^3, Δk = 2 – 12 $Å^{-1}$, Δr = 1 – 5 Å), for Fe^{3+} in buffer (k^3, Δk = 2 – 12 $Å^{-1}$, Δr = 1 - 2.5 Å).

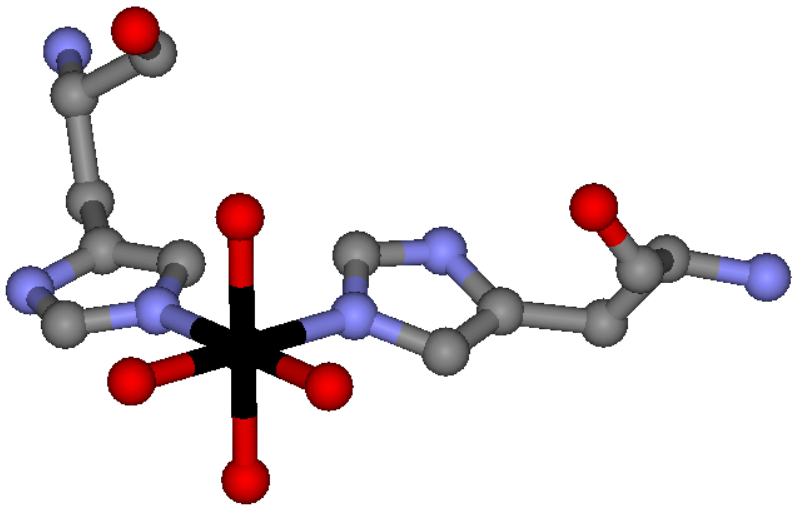

Figure 6.8 Schematic picture of the molecular arrangement around the Fe^{3+} in Aβ. Atom colours are as follows: iron (Fe) *black*; oxygen (O) *red*; nitrogen (N) *blue*; carbon (C) *gray*.

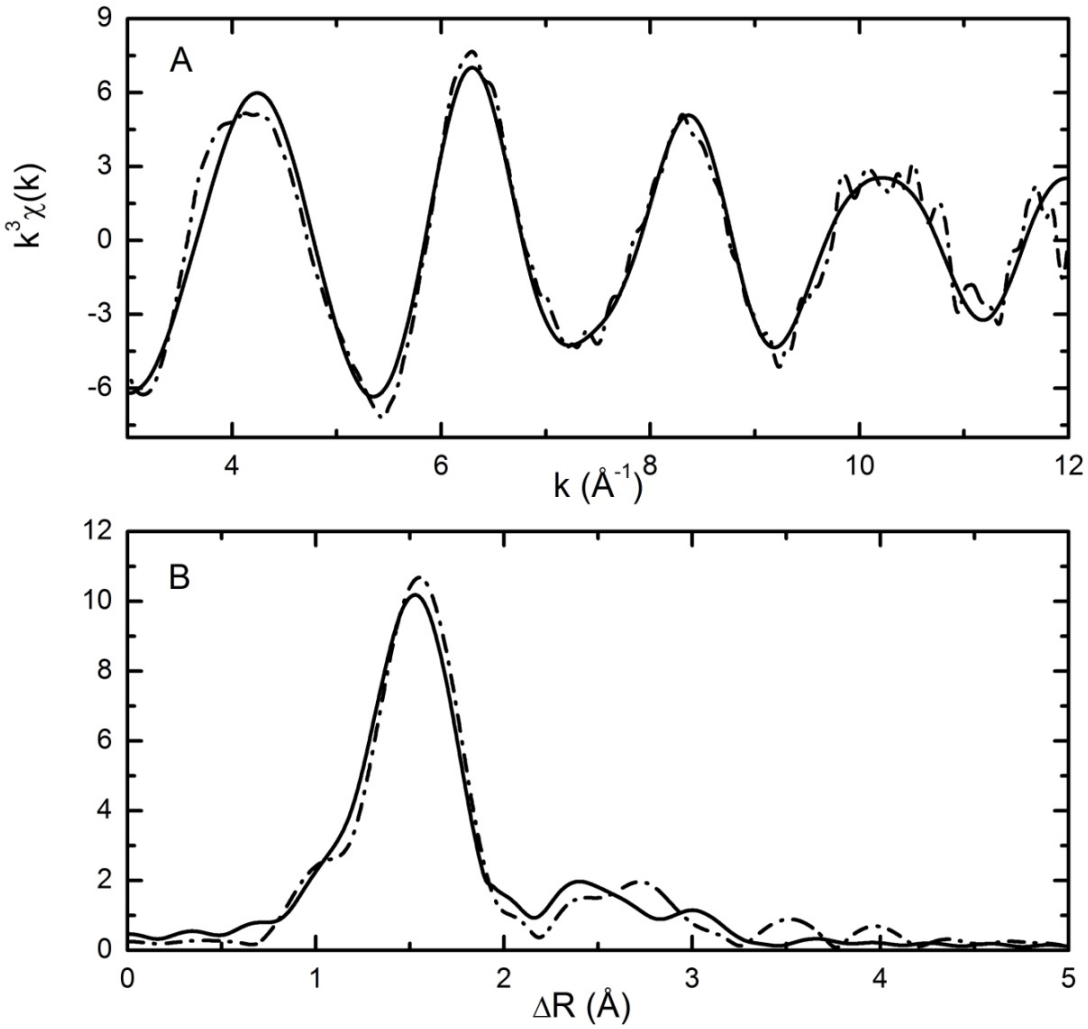

Figure 6.9 Five-coordinate fit of $A\beta_{1\text{-}40}Fe^{3+}$. A) k^3 weighted $\chi(k)$ of $A\beta_{1\text{-}40}$ with five-coordinate Fe^{3+} fit. B) is corresponding fit in R-space. Experimental data are shown by dashed lines and simulations to the data by solid lines.

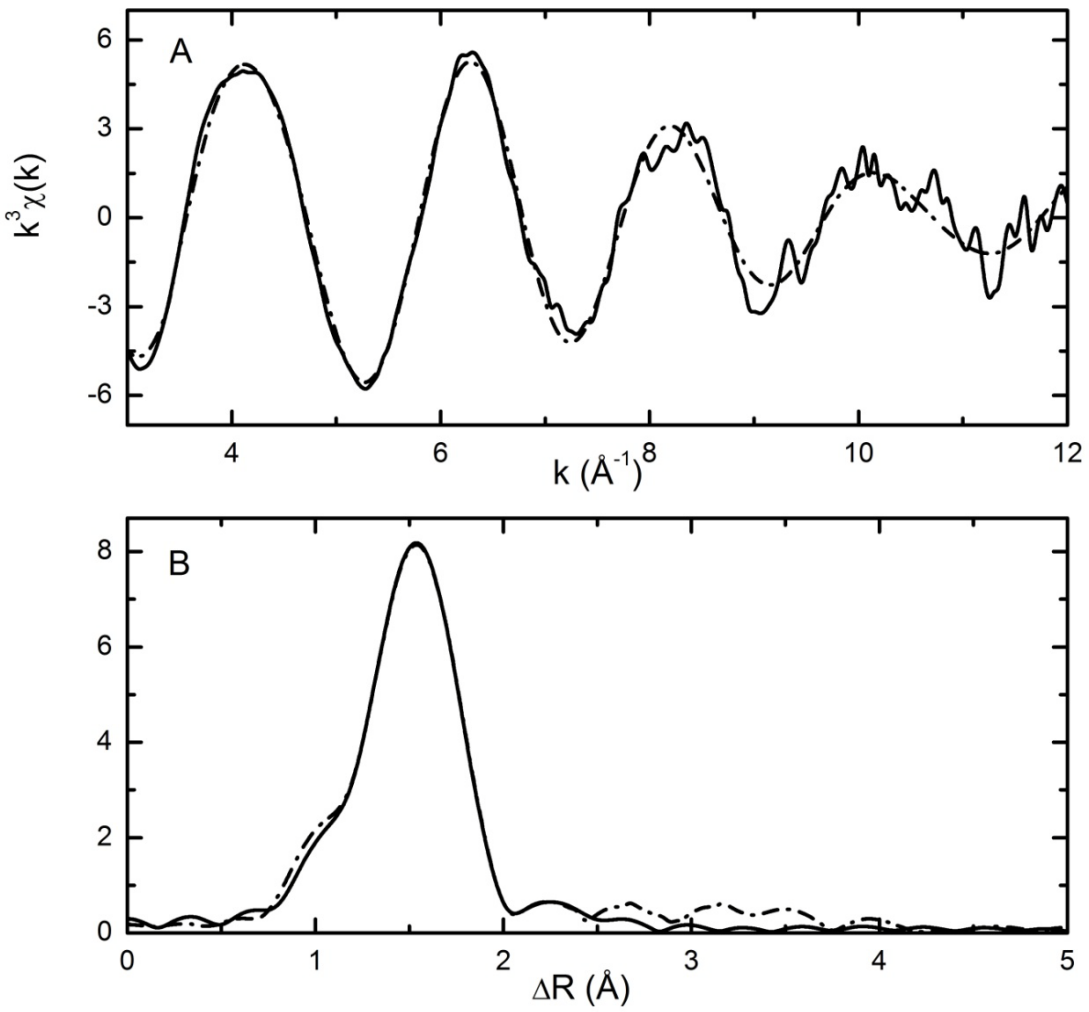

Figure 6.10 EXAFS of Fe^{3+} in buffer. A) is k^3 weighted $\chi(k)$ of Fe^{3+} in buffer and B) is the corresponding Fourier-transformed (FT) of Fe^{3+} in buffer Experimental data are shown by dashed lines and simulations to the data by solid lines.

6.4 Conclusions

The metal-binding affinity of Aβ peptide is an important parameter because it gives information about the biological significance of the metal binding. It is also important for therapeutic approaches in Alzheimer's disease based on the withdrawal of metal ions from Aβ, but not from essential metal proteins.[348]

Although several spectroscopic techniques have been used to understand the metal binding site of Aβ peptide, much of the attention has been focussed on the redox-active Cu^{2+} and redox-inactive Zn^{2+}. No consensus has been reached in regards to the coordination number or the identity of the ligands for Cu^{2+}. The lack of consensus is most likely due to the dynamic nature of Aβ, which is sensitive to pH. The previous spectroscopic studies were done at physiological pH, at which two Aβ binding modes exits, component I (low pH) and component II (high pH). The EXAFS analysis of the Cu^{2+} bound Aβ presented here was performed at pH 6.5, where component I is the predominant species. The Cu^{2+} bound to Aβ has a five-coordinate geometry with three His residues and carboxylate oxygen of Asp. This geometry is similar to the proposed six-coordinate geometry for $A\beta Cu^{2+}$ without the axial water molecule.[329]

Evidence of Fe^{3+} interaction with the Aβ in the literature is limited. It was assumed that since Fe^{3+} is a redox-active metal like Cu^{2+}, it would have a similar binding mode and redox-active chemistry to Cu^{2+}. Here I report that the coordination of Aβ differs between the two metals. While Cu^{2+} is shown to be in a five-coordinate geometry with a His-rich coordinating environment, Fe^{3+} is in a six-coordinate geometry with an oxygen-rich environment. This difference in binding may have some effect on the observed Met_{35} oxidation differences in Chapter 5. The lack of information on the Fe^{3+} bound Aβ peptide leads me to speculate on the identity of the remaining 4 N/O coordinating ligands. Furthermore, the essential coordinating ligands for Cu^{2+} and Fe^{3+} are in the N-terminal region of the peptide because the metal bound $A\beta_{1-16}$ and $A\beta_{1-40}$ produced superimposable EXAFS oscillations.

CHAPTER 7: CONCLUDING REMARKS AND FUTURE DIRECTIONS

Sulfur K-edge X-ray absorption spectroscopy has been used to investigate cysteine and methionine oxidation as it provides a direct spectroscopic evidence for the redox state of the sulfur atom in these amino acids. Through the findings from these specific projects in this thesis, a clear understanding was gained of the fundamental redox chemistries of Cys and Met and its implications in diseases such as age-related cataracts and Alzheimer's disease. Although cysteine oxidation to the cysteinyl radical has been implicated in various biological functions, the applicability of the predominant spectroscopic method, EPR is limited. These challenges of detecting sulfur-based radicals with EPR led to the development of S K-edge XAS as a spectroscopic tool to evaluate the sulfur-based radical species. My work has been successful in investigating cysteinyl radicals in a protein system with S K-edge XAS. The cysteinyl radical is characterized by a pre-edge feature that corresponds to the 3p ← 1s transition, which is well separated from the near-edge feature of the sulfur. S K-edge XAS has also shown to be a sensitive method to detect these cysteinyl radicals in hydrophobic and hydrophilic protein environments. The pre-edge feature of the cysteinyl radicals that were in a hydrophobic environment was found to be lower in energy than that of cysteinyl radicals that were in a hydrophilic environment probably due to the hydrogen bonding interactions.

The usefulness of S K-edge XAS can further be investigated in detecting thiyl peroxyl radical (RSOO•), which have been shown to be very reactive and to have an important role in biology. Thus, the generated cysteinyl radical in the hydrophobic and hydrophilic environments of azurin can be probed with O_2 to generate such radicals and see its interaction in these different environments. Furthermore, these cysteinyl radicals can also be probed with other biologically relevant small molecules such as NO, to understand the fundamental reactivity of these radicals and perhaps gain insight into the mechanism of S-nitrosylation.

My work in detecting cysteinyl radicals with S K-edge XAS provides a new approach to study the sulfur-based radicals. A future application of significant interest using this technique would be to investigate sulfur-based radical species implicated in a number of enzymatic systems, particularly ribonucleotide reductases (RNR), an enzyme that catalyzes the conversion of ribonucleotide to deoxyribonucleotide, an essential component for the biosynthesis of DNA. S K-edge XAS can provide a solution to the current difficulties in detecting proposed cysteinyl radicals that initiates the catalytic mechanism and potentially new insights into the proposed mechanism can be gained.

Through this thesis, XAS has been successfully used to address the Met oxidation and its implications in disease such as age-related cataracts and Alzheimer's disease. S K-edge XAS was also used to investigate the photochemistry of Met and its oxidized derivatives, MetSO and $MetSO_2$. Photoirradiation of Met under aerobic condition produces oxidized products MetSO and $MetSO_2$, while under anaerobic conditions, Met photoirradiation produces

$MetS^{\bullet+}$. The mechanism for aerobic photooxidation is believed to involve photoexcitation of O_2 to its singlet excited state. Indirect photooxidation of thioether using photosensitizer to generate thioether radical cation has been proposed as an alternative pathway. My work on the formation of $MetS^{\bullet+}$ in the absence of O_2 and without any sensitizer gives two new pathways. First, a direct one-electron oxidation of Met gives a sulfur-centered radical cation that can react with oxygen to give the oxidized species, MetSO and $MetSO_2$. Second, formation of $^3Met^*$ can go through a spin allowed reaction with molecular oxygen to produce MetSO and $MetSO_2$.

The photochemistry of MetSO is noteworthy as it reveals the reduction to Met. Photoirradiation of MetSO in presence of O_2 produces oxidized product $MetSO_2$ and reduced product Met, and in the absence of O_2 only produced Met. However, $MetSO_2$ is both oxidatively and reductively inert to photoirradiation**.** My photochemistry work with Met, MetSO and $MetSO_2$ offers significant insights into the mechanisms of photoredox processes that are relevant to the age-related cataract formation. My photochemistry data presented herein ultimately serves as a reference to the Met oxidations that occurs in α-crystallins, the predominant component in the cataracts. Thus, it is worthwhile to investigate the photooxidation of α-crystallin proteins using S K-edge XAS. XAS imaging can also be used to investigate the oxidation state of Met in cataract eye lens tissue samples.

Another interesting aspect that is worth investigating is the fate of the oxygen in the reduction of MetSO to Met. This can be accomplished with the use of ^{18}O-labeled MetSO. Doing a similar *in situ* XAS photochemistry with the ^{18}O-labeled

MetSO and monitoring the decrease of labeled oxygen can provide information on the destination of this cleaved oxygen from the photoirradiation.

Also with the development of *in situ* photochemistry XAS presented in Chapter 4, this new technique gives the potential to investigate the photochemistry of other sulfur compounds that are biologically relevant such as cysteine sulfenic acid, cysteine sulfinic acid, and cysteine sulfonic acid. Probing the fate of these compounds in aerobic and anaerobic conditions may provide some fundamental understanding of the reactivity of these compounds. These *in situ* investigations are not limited to these compounds, as they can also be used to study S-nitrosothiols. The cleavage of the S-NO bond can provide some useful insights into the mechanism of NO mediated cell signaling.

In addition to exploring the photochemistry of Met, I have also explored the metal-induced oxidation of Met, specifically in understanding the Met_{35} oxidation of amyloid-β (Aβ) peptide. My work shows that Met_{35} is oxidized to methionine sulfoxide in the presence of Cu^{2+} alone but Fe^{3+} failed to oxidize Met_{35}. This difference in the oxidation behaviour and the lack of evidence for Fe^{3+} binding to Aβ led me to probe the metal binding site of both Cu^{2+} and Fe^{3+}. Here I report that the coordination between the two metals is different. While Cu^{2+} is shown to be in a five-coordinate geometry with a His-rich coordinating environment, Fe^{3+} is in a six-coordinate geometry with an oxygen-rich environment. This difference in binding may have some effect to the observed Met_{35} oxidation differences.

In order to gain information regarding Met_{35} as a potential electron source for the Cu^{2+} reduction, the Met_{35} cation radical must be isolated. This requires a set-up in which freezing of the final $A\beta Cu^{2+}$ mixture is possible, as the Cu^{2+} solution is mixed with Aβ peptide solution. Other approaches that can be undertaken in understanding the Met oxidation in Aβ peptide includes X-ray imaging of amyloid plaques to identify the oxidized form of Met as well as identifying the metals deposited in these plaques.

Overall, the work in this thesis has shown that S K-edge XAS is a valuable tool for studying the oxidation of cysteine and methionine. I have shown S K-edge to be a promising tool in investigating sulfur-based radicals. Using S K-edge XAS, I have gained insight into the oxidation of Met and its implication in age-related cataract formation as well amyloid-β peptide oxidation in Alzheimer's disease.

REFERENCES

(1) Jao, S. C.; Ospina, S. M. E.; Berdis, A. J.; Starke, D. W.; Post, C. B.; Mieyal, J. J. *Biochemistry* **2006**, *45*, 4785-4796.
(2) Nelson, K. J.; Parsonage, D.; Hall, A.; Karplus, P. A.; Poole, L. B. *Biochemistry* **2008**, *47*, 12860-12868.
(3) Guan, K. L.; Dixon, J. E. *J. Biol. Chem.* **1991**, *266*, 17026-17030.
(4) Okudo, H.; Urade, R.; Moriyama, T.; Kito, M. *FEBS Lett.* **2000**, *465*, 145-147.
(5) Ascenzi, P.; Bocedi, A.; Visca, P.; Antonini, G.; Gradoni, L. *Biochem. Biophys. Res. Commun.* **2003**, *309*, 659-665.
(6) Shigehiro, S.; Nakasako, M.; Dohmae, N.; Tsujimura, M.; Tokoi, K.; Odaka, M.; Yohda, M.; Kamiya, N.; Endo, I. *Nat. Struct. Biol.* **1998**, *5*, 347-351.
(7) Beinert, H.; Kennedy, M. C.; Stout, C. D. *Chem. Rev.* **1996**, *96*, 2335-2373.
(8) Sono, M.; Roach, M. P.; Coulter, E. D.; Dawson, J. H. *Chem. Rev.* **1996**, *96*, 2841-2887.
(9) Netto, L. E. S.; de Oliveira, M. A.; Monteiro, G.; Demasi, A. P. D.; Cussiol, J. R. R.; Discola, K. F.; Demasi, M.; Silva, G. M.; Alves, S. V.; Faria, V. G.; Horta, B. B. *Comp. Biochem. Physiol. C Comp. Pharmacol.* **2007**, *146*, 180-193.
(10) Klug, A.; Schwabe, J. W. R. *FASEB J.* **1995**, *9*, 597-604.
(11) Levonen, A. L.; Landar, A.; Ramachandran, A.; Ceaser, E. K.; Dickinson, D. A.; Zanoni, G.; Morrow, J. D.; Darley-Usmar, V. M. *Biochem. J.* **2004**, *378*, 373-382.
(12) Powis, G.; Briehl, M.; Oblong, J. *Pharmacol. Ther.* **1995**, *68*, 149-173.
(13) Brosnan, J. T.; Brosnan, M. E. *J. Nutr.* **2006**, *136*, 1636S-1640S.
(14) Costa, H. S.; Santos, H.; Turner, D. L. *Eur. J. Biochem.* **1994**, *223*, 783-789.
(15) Blackledge, M. J.; Guerlesquin, F.; Marion, D. *Nat. Struct. Mol. Biol.* **1995**, *2*, 532-535.
(16) Olsson, M. H. M.; Ryde, U. *J. Biol. Inorg. Chem.* **1999**, *4*, 654-663.
(17) Guss, J. M.; Merritt, E. A.; Phizackerley, R. P.; Freeman, H. C. *J. Mol. Biol.* **1996**, *262*, 686-705.
(18) Levine, R. L.; Mosoni, L.; Berlett, B. S.; Stadtman, E. R. *Proc. Natl. Acad. Sci. U. S. A.* **1996**, *93*, 15036-15040.
(19) Vogt, W. *Free Radic. Biol. Med.* **1995**, *18*, 93-105.
(20) Gille, G.; Sigler, K. *Folia Microbiol.* **1995**, *40*, 131-152.
(21) Winterbourn, C. C. *Nat. Chem. Biol.* **2008**, *4*, 278-286.
(22) Klotz, L. O.; Kroncke, K. D.; Sies, H. *Photochem. Photobiol. Sci.* **2003**, *2*, 88-94.
(23) Turrens, J. F. *Biosci. Rep.* **1997**, *17*, 3-8.
(24) Kuppusamy, P.; Zweier, J. L. *J. Biol. Chem.* **1989**, *264*, 9880-9884.
(25) Babior, B. M. *Blood* **1999**, *93*, 1464-1476.
(26) Benson, S. W.; Nangia, P. S. *J. Am. Chem. Soc.* **1980**, *102*, 2843-2844.
(27) Dix, T. A.; Hess, K. M.; Medina, M. A.; Sullivan, R. W.; Tilly, S. L.; Webb, T. L. L. *Biochemistry* **1996**, *35*, 4578-4583.

(28) Bannister, J. V.; Bannister, W. H.; Rotilio, G. *CRC Crit. Rev. Biochem.* **1987**, *22*, 111-180.
(29) Winterbourn, C. C.; Hampton, M. B.; Livesey, J. H.; Kettle, A. J. *J. Biol. Chem.* **2006**, *281*, 39860-39869.
(30) Halliwell, B.; Gutteridge, J. M. C. *FEBS Lett.* **1992**, *307*, 108-112.
(31) Stuehr, D. J. *Biochim. Biophys. Acta* **1999**, *1411*, 217-230.
(32) Wink, D. A.; Mitchell, J. B. *Free Radic. Biol. Med.* **1998**, *25*, 434-456.
(33) Bertrand, G. *8th International Conference of Applied Chemistry* **1912**, *28*, 30.
(34) Valko, M.; Leibfritz, D.; Moncol, J.; Cronin, M. T. D.; Mazur, M.; Telser, J. *Int. J. Biochem. Cell Biol.* **2007**, *39*, 44-84.
(35) Droge, W. *Physiol. Rev.* **2002**, *82*, 47-95.
(36) Pacher, P.; Beckman, J. S.; Liaudet, L. *Physiol. Rev.* **2007**, *87*, 315-424.
(37) Halliwell, B. *Biochem. Soc. Trans.* **2007**, *35*, 1147-1150.
(38) Genestra, M. *Cell. Signal.* **2007**, *19*, 1807-1819.
(39) Beckman, K. B.; Ames, B. N. *J. Biol. Chem.* **1997**, *272*, 19633-19636.
(40) Marnett, L. J. *Toxicology* **2002**, *181*, 219-222.
(41) Berlett, B. S.; Stadtman, E. R. *J. Biol. Chem.* **1997**, *272*, 20313-20316.
(42) Halliwell, B. *Free Radic. Res.* **1999**, *31*, 261-272.
(43) Hayes, J. D.; McLellan, L. I. *Free Radic. Res.* **1999**, *31*, 273-300.
(44) Chaudiere, J.; Ferrari-Iliou, R. *Food Chem. Toxicol.* **1999**, *37*, 949-962.
(45) Nakamura, H.; Nakamura, K.; Yodoi, J. *Annu. Rev. Immunol.* **1997**, *15*, 351-369.
(46) Verdoucq, L.; Vignols, F.; Jacquot, J. P.; Chartier, Y.; Meyer, Y. *J. Biol. Chem.* **1999**, *274*, 19714-19722.
(47) Ritz, D.; Patel, H.; Doan, B.; Zheng, M.; Aslund, F.; Storz, G.; Beckwith, J. *J. Biol. Chem.* **2000**, *275*, 2505-2512.
(48) Rhee, S. G.; Jeong, W.; Chang, T. S.; Woo, H. A. *Kidney Int.* **2007**, *72*, S3-S8.
(49) Oien, D. B.; Moskovitz, J. In *Current Topics in Developmental Biology, Vol 80*, 2008; Vol. 80, pp 93-133.
(50) Valko, M.; Izakovic, M.; Mazur, M.; Rhodes, C. J.; Telser, J. *Mol. Cell. Biochem.* **2004**, *266*, 37-56.
(51) Willcox, J. K.; Ash, S. L.; Catignani, G. L. *Crit. Rev. Food Sci. Nutr.* **2004**, *44*, 275-295.
(52) Valko, M.; Rhodes, C. J.; Moncol, J.; Izakovic, M.; Mazur, M. *J. Clin. Pathol.* **2006**, *160*, 1-40.
(53) Valko, M.; Morris, H.; Cronin, M. T. D. *Curr. Med. Chem.* **2005**, *12*, 1161-1208.
(54) Goldberger, R. F.; Epstein, C. J.; Anfinsen, C. B. *J. Biol. Chem.* **1963**, *238*, 628-&.
(55) Bardwell, J. C. A.; Beckwith, J. *Cell* **1993**, *74*, 769-771.
(56) Missiakas, D.; Georgopoulos, C.; Raina, S. *EMBO J.* **1994**, *13*, 2013-2020.
(57) Shevchik, V. E.; Condemine, G.; Robertbaudouy, J. *EMBO J.* **1994**, *13*, 2007-2012.
(58) Horibe, T.; Gomi, M.; Iguchi, D.; Ito, H.; Kitamura, Y.; Masuoka, T.; Tsujimoto, I.; Kimura, T.; Kikuchi, M. *J. Biol. Chem.* **2004**, *279*, 4604-4611.

(59) Inaba, K.; Ito, K. *Biochim. Biophys. Acta, Mol. Cell Res.* **2008**, *1783*, 520-529.
(60) Frand, A. R.; Kaiser, C. A. *Mol. Cell* **1999**, *4*, 469-477.
(61) Frand, A. R.; Cuozzo, J. W.; Kaiser, C. A. *Trends Cell Biol.* **2000**, *10*, 203-210.
(62) Zapun, A.; Missiakas, D.; Raina, S.; Creighton, T. E. *Biochemistry* **1995**, *34*, 5075-5089.
(63) Brennan, J. P.; Bardswell, S. C.; Burgoyne, J. R.; Fuller, W.; Schroder, E.; Wait, R.; Begum, S.; Kentish, J. C.; Eaton, P. *J. Biol. Chem.* **2006**, *281*, 21827-21836.
(64) Yamawaki, H.; Berk, B. C. *Curr. Opin. Nephrol. Hypertens.* **2005**, *14*, 149-153.
(65) Mustacich, D.; Powis, G. *Biochem. J.* **2000**, *346*, 1-8.
(66) Schafer, F. Q.; Buettner, G. R. *Free Radic. Biol. Med.* **2001**, *30*, 1191-1212.
(67) Ballatori, N.; Krance, S. M.; Notenboom, S.; Shi, S. J.; Tieu, K.; Hammond, C. L. *Biol. Chem.* **2009**, *390*, 191-214.
(68) Dickinson, D. A.; Forman, H. J. *Biochem. Pharmacol.* **2002**, *64*, 1019-1026.
(69) Pai, E. F.; Schulz, G. E. *J. Biol. Chem.* **1983**, *258*, 1752-1757.
(70) Giustarini, D.; Dalle-Donne, I.; Colombo, R.; Petralia, S.; Giampaoletti, S.; Milzani, A.; Rossi, R. *Clin. Chem.* **2003**, *49*, 327-330.
(71) Giustarini, D.; Dalle-Donne, I.; Lorenzini, S.; Milzani, A.; Rossi, R. *J. Gerontol. A Biol. Sci. Med. Sci* **2006**, *61*, 1030-1038.
(72) Ghezzi, P.; Bonetto, V.; Fratelli, M. *Antioxid. Redox Signal.* **2005**, *7*, 964-972.
(73) Dalle-Donne, I.; Giustarini, D.; Colombo, R.; Milzani, A.; Rossi, R. *Free Radic. Biol. Med.* **2005**, *38*, 1501-1510.
(74) Dalle-Donne, I.; Milzani, A.; Gagliano, N.; Colombo, R.; Giustarini, D.; Rossi, R. *Antioxid. Redox Signal.* **2008**, *10*, 445-473.
(75) Chrestensen, C. A.; Starke, D. W.; Mieyal, J. J. *J. Biol. Chem.* **2000**, *275*, 26556-26565.
(76) Jung, C. H.; Thomas, J. A. *Arch. Biochem. Biophys.* **1996**, *335*, 61-72.
(77) Nordstrand, K.; Sandstrom, A.; Aslund, F.; Holmgren, A.; Otting, G.; Berndt, K. D. *J. Mol. Biol.* **2000**, *303*, 423-432.
(78) Srinivasan, U.; Mieyal, P. A.; Mieyal, J. J. *Biochemistry* **1997**, *36*, 3199-3206.
(79) Lundstrom-Ljung, J.; Vlamis-Gardikas, A.; Aslund, F.; Holmgren, A. *FEBS Lett.* **1999**, *443*, 85-88.
(80) Fernandes, A. P.; Holmgren, A. *Antioxid. Redox Signal.* **2004**, *6*, 63-74.
(81) Findlay, V. J.; Townsend, D. M.; Morris, T. E.; Fraser, J. P.; He, L.; Tew, K. D. *Cancer Res.* **2006**, *66*, 6800-6806.
(82) Holmgren, A.; Johansson, C.; Berndt, C.; Lonn, M. E.; Hudemann, C.; Lillig, C. H. *Biochem. Soc. Trans.* **2005**, *33*, 1375-1377.
(83) Wang, J.; Boja, E. S.; Tan, W. H.; Tekle, E.; Fales, H. M.; English, S.; Mieyal, J. J.; Chock, P. B. *J. Biol. Chem.* **2001**, *276*, 47763-47766.
(84) Dalle-Donne, I.; Giustarini, D.; Rossi, R.; Colombo, R.; Milzani, A. *Free Radic. Biol. Med.* **2003**, *34*, 23-32.
(85) Chai, Y. C.; Ashraf, S. S.; Rokutan, K.; Johnston, R. B.; Thomas, J. A. *Arch. Biochem. Biophys.* **1994**, *310*, 273-281.

(86) Dominici, S.; Valentini, M.; Maellaro, E.; Del Bello, B.; Paolicchi, A.; Lorenzini, E.; Tongiani, R.; Comporti, M.; Pompella, A. *Free Radic. Biol. Med.* **1999**, *27*, 623-635.
(87) Nulton-Persson, A. C.; Starke, D. W.; Mieyal, J. J.; Szweda, L. I. *Biochemistry* **2003**, *42*, 4235-4242.
(88) Finley, J. W.; Wheeler, E. L.; Witt, S. C. *J. Agric. Food Chem.* **1981**, *29*, 404-407.
(89) Giles, G. I.; Tasker, K. M.; Jacob, C. *Free Radic. Biol. Med.* **2001**, *31*, 1279-1283.
(90) Giles, G. I.; Tasker, K. M.; Collins, C.; Giles, N. M.; O'Rourke, E.; Jacob, C. *Biochem. J.* **2002**, *364*, 579-585.
(91) Giles, N. M.; Giles, G. I.; Jacob, C. *Biochem. Biophys. Res. Commun.* **2003**, *300*, 1-4.
(92) Carballal, S.; Radi, R.; Kirk, M. C.; Barnes, S.; Freeman, B. A.; Alvarez, B. *Biochemistry* **2003**, *42*, 9906-9914.
(93) Saurin, A. T.; Neubert, H.; Brennan, J. P.; Eaton, P. *Proc. Natl. Acad. Sci. U. S. A.* **2004**, *101*, 17982-17987.
(94) Nagy, P.; Ashby, M. T. *J. Am. Chem. Soc.* **2007**, *129*, 14082-14091.
(95) Hogg, P. J. *Trends Biochem. Sci.* **2003**, *28*, 210-214.
(96) Walsh, C. T. In *Posttranslational modifications of proteins: expanding nature's inventory*; Roberts and Company Publishers: Englewood, Colorado, 2006, pp 95-119.
(97) Percival, M. D.; Ouellet, M.; Campagnolo, C.; Claveau, D.; Li, C. *Biochemistry* **1999**, *38*, 13574-13583.
(98) Yeh, J. I.; Claiborne, A.; Hol, W. G. J. *Biochemistry* **1996**, *35*, 9951-9957.
(99) Claiborne, A.; Miller, H.; Parsonage, D.; Ross, R. P. *FASEB J.* **1993**, *7*, 1483-1490.
(100) Salmeen, A.; Andersen, J. N.; Myers, M. P.; Meng, T. C.; Hinks, J. A.; Tonks, N. K.; Barford, D. *Nature* **2003**, *423*, 769-773.
(101) Yang, J.; Groen, A.; Lemeer, S.; Jans, A.; Slijper, M.; Roe, S. M.; den Hertog, J.; Barford, D. *Biochemistry* **2007**, *46*, 709-719.
(102) Wood, Z. A.; Schroder, E.; Harris, J. R.; Poole, L. B. *Trends Biochem. Sci.* **2003**, *28*, 32-40.
(103) Hofmann, B.; Hecht, H. J.; Flohe, L. *Biol. Chem.* **2002**, *383*, 347-364.
(104) Schroder, E.; Littlechild, J. A.; Lebedev, A. A.; Errington, N.; Vagin, A. A.; Isupov, M. N. *Structure Fold. Des.* **2000**, *8*, 605-615.
(105) Alphey, M. S.; Bond, C. S.; Tetaud, E.; Fairlamb, A. H.; Hunter, W. N. *J. Mol. Biol.* **2000**, *300*, 903-916.
(106) Seo, M. S.; Kang, S. W.; Kim, K.; Baines, I. C.; Lee, T. H.; Rhee, S. G. *J. Biol. Chem.* **2000**, *275*, 20346-20354.
(107) Lee, S. R.; Kwon, K. S.; Kim, S. R.; Rhee, S. G. *J. Biol. Chem.* **1998**, *273*, 15366-15372.
(108) Meng, T. C.; Fukada, T.; Tonks, N. K. *Mol. Cell* **2002**, *9*, 387-399.
(109) Nidetzky, B. *Biochem. Soc. Trans.* **2007**, *35*, 1588-1592.

(110) Choi, J.; Sullards, M. C.; Olzmann, J. A.; Rees, H. D.; Weintraub, S. T.; Bostwick, D. E.; Gearing, M.; Levey, A. I.; Chin, L. S.; Li, L. *J. Biol. Chem.* **2006**, *281*, 10816-10824.
(111) Cozzolino, M.; Amori, I.; Pesaresi, M. G.; Ferri, A.; Nencini, M.; Carri, M. T. *J. Biol. Chem.* **2008**, *283*, 866-874.
(112) Murakami, T.; Nojiri, M.; Nakayama, H.; Odaka, M.; Yohda, M.; Dohmae, N.; Takio, K.; Nagamune, T.; Endo, I. *Protein Sci.* **2000**, *9*, 1024-1030.
(113) Vivancos, A. P.; Castillo, E. A.; Biteau, B.; Nicot, C.; Ayte, J.; Toledano, M. B.; Hidalgo, E. *Proc. Natl. Acad. Sci. U. S. A.* **2005**, *102*, 8875-8880.
(114) Wood, Z. A.; Poole, L. B.; Karplus, P. A. *Science* **2003**, *300*, 650-653.
(115) Biteau, B.; Labarre, J.; Toledano, M. B. *Nature* **2003**, *425*, 980-984.
(116) Schroder, E.; Littlechild, J. A.; Lebedev, A. A.; Errington, N.; Vagin, A. A.; Isupov, M. N. *Structure* **2000**, *8*, 605-615.
(117) Thannickal, V. J.; Fanburg, B. L. *Am. J. Physiol. Lung Cell. Mol. Physiol.* **2000**, *279*, L1005-L1028.
(118) Martindale, J. L.; Holbrook, N. J. *J. Cell. Physiol.* **2002**, *192*, 1-15.
(119) Jeong, W.; Park, S. J.; Chang, T. S.; Lee, D. Y.; Rhee, S. G. *J. Biol. Chem.* **2006**, *281*, 14400-14407.
(120) Haendeler, J.; Hoffmann, J.; Tischler, V.; Berk, B. C.; Zeiher, A. M.; Dimmeler, S. *Nat. Cell Biol.* **2002**, *4*, 743-749.
(121) Meyer, D. J.; Kramer, H.; Ozer, N.; Coles, B.; Ketterer, B. *FEBS Lett.* **1994**, *345*, 177-180.
(122) Scharfstein, J. S.; Keaney, J. F.; Slivka, A.; Welch, G. N.; Vita, J. A.; Stamler, J. S.; Loscalzo, J. *J. Clin. Investig.* **1994**, *94*, 1432-1439.
(123) Ignarro, L. J.; Lippton, H.; Edwards, J. C.; Baricos, W. H.; Hyman, A. L.; Kadowitz, P. J.; Gruetter, C. A. *J. Pharmacol. Exp. Ther.* **1981**, *218*, 739-749.
(124) Lander, H. M.; Jacovina, A. T.; Davis, R. J.; Tauras, J. M. *J. Biol. Chem.* **1996**, *271*, 19705-19709.
(125) Lei, S. Z.; Pan, Z. H.; Aggarwal, S. K.; Chen, H. S. V.; Hartman, J.; Sucher, N. J.; Lipton, S. A. *Neuron* **1992**, *8*, 1087-1099.
(126) Bolotina, V. M.; Najibi, S.; Palacino, J. J.; Pagano, P. J.; Cohen, R. A. *Nature* **1994**, *368*, 850-853.
(127) Broillet, M. C.; Firestein, S. *Neuron* **1997**, *18*, 951-958.
(128) Xu, L.; Eu, J. P.; Meissner, G.; Stamler, J. S. *Science* **1998**, *279*, 234-237.
(129) Persichini, T.; Colasanti, M.; Lauro, G. M.; Ascenzi, P. *Biochem. Biophys. Res. Commun.* **1998**, *250*, 575-576.
(130) von Sonntag, C.; Schuchmann, H. P. In *Sulfur-centered reactive intermediates in chemistry and biology*; Chatgilialoglu, C., Asmus, K. D., Eds.; Plenum Press: New York, 1990; Vol. 197, pp 409-414.
(131) Buxton, G. V.; Greenstock, C. L.; Helman, W. P.; Ross, A. B. *J. Phys. Chem. Ref. Data* **1988**, *17*, 513-886.
(132) Oneill, P. *Radiat. Res.* **1983**, *96*, 198-210.
(133) Radi, R.; Beckman, J. S.; Bush, K. M.; Freeman, B. A. *J. Biol. Chem.* **1991**, *266*, 4244-4250.
(134) Persson, A. L.; Sahlin, M.; Sjoberg, B. M. *J. Biol. Chem.* **1998**, *273*, 31016-31020.

(135) Sun, X. Y.; Ollagnier, S.; Schmidt, P. P.; Atta, M.; Mulliez, E.; Lepape, L.; Eliasson, R.; Graslund, A.; Fontecave, M.; Reichard, P.; Sjoberg, B. M. *J. Biol. Chem.* **1996**, *271*, 6827-6831.
(136) Saez, G.; Thornalley, P. J.; Hill, H. A. O.; Hems, R.; Bannister, J. V. *Biochim. Biophys. Acta* **1982**, *719*, 24-31.
(137) Hartmann, H. J.; Sievers, C.; Weser, U. In *Metal Ions in Biological Systems, Vol 36*, 1999; Vol. 36, pp 389-413.
(138) Nordlund, N.; Reichard, P. *Annu. Rev. Biochem.* **2006**, *75*, 681-706.
(139) Wardman, P. In *Biothiols in health and disease*; Packer, L., Ed.; Marcel Dekker: New York, 1995, pp 1-19.
(140) Jourd'heuil, D.; Jourd'heuil, F. L.; Feelisch, M. *J. Biol. Chem.* **2003**, *278*, 15720-15726.
(141) Sevilla, M. D.; Becker, D.; Yan, M. *Int. J. Radiat. Biol.* **1990**, *57*, 65-81.
(142) Zhang, X. J.; Zhang, N.; Schuchmann, H. P.; Vonsonntag, C. *J. Phys. Chem.* **1994**, *98*, 6541-6547.
(143) Zhang, N.; Schuchmann, H. P.; Vonsonntag, C. *J. Phys. Chem.* **1991**, *95*, 4718-4722.
(144) Lal, M. *Radiat. Phys. Chem.* **1994**, *43*, 595-611.
(145) Tweeddale, H. J.; Kondo, M.; Gebicki, J. M. *Arch. Biochem. Biophys.* **2007**, *459*, 151-158.
(146) Xu, G. H.; Chance, M. R. *Chem. Rev.* **2007**, *107*, 3514-3543.
(147) Pogocki, D.; Schoneich, C. *Free Radic. Biol. Med.* **2001**, *31*, 98-107.
(148) Nauser, T.; Schoneich, C. *J. Am. Chem. Soc.* **2003**, *125*, 2042-2043.
(149) Akhlaq, M. S.; Schuchmann, H. P.; Vonsonntag, C. *Int. J. Radiat. Biol.* **1987**, *51*, 91-102.
(150) Kuschel, L.; Hansel, A.; Schoherr, R.; Weissbach, H.; Brot, N.; Hoshi, T.; Heinemann, S. H. *FEBS Lett.* **1999**, *456*, 17-21.
(151) Moskovitz, J.; Rahman, M. A.; Strassman, J.; Yancey, S. O.; Kushner, S. R.; Brot, N.; Weissbach, H. *J. Bacteriol.* **1995**, *177*, 502-507.
(152) Moskovitz, J.; Weissbach, H.; Brot, N. *Proc. Natl. Acad. Sci. U. S. A.* **1996**, *93*, 2095-2099.
(153) Sadanandom, A.; Poghosyan, Z.; Fairbairn, D. J.; Murphy, D. J. *Plant Physiol.* **2000**, *123*, 255-263.
(154) Moskovitz, J.; Poston, J. M.; Berlett, B. S.; Nosworthy, N. J.; Szczepanowski, R.; Stadtman, E. R. *J. Biol. Chem.* **2000**, *275*, 14167-14172.
(155) Moskovitz, J.; Singh, V. K.; Requena, J.; Wilkinson, B. J.; Jayaswal, R. K.; Stadtman, E. R. *Biochem. Biophys. Res. Commun.* **2002**, *290*, 62-65.
(156) Lowther, W. T.; Brot, N.; Weissbach, H.; Matthews, B. W. *Biochemistry* **2000**, *39*, 13307-13312.
(157) Boschi-Muller, S.; Azza, S.; Sanglier-Cianferani, S.; Talfournier, F.; Van Dorsselear, A.; Branlant, G. *J. Biol. Chem.* **2000**, *275*, 35908-35913.
(158) Levine, R. L.; Berlett, B. S.; Moskovitz, J.; Mosoni, L.; Stadtman, E. R. *Mech. Ageing Dev.* **1999**, *107*, 323-332.
(159) Reddy, V. Y.; Pizzo, S. V.; Weiss, S. J. *J. Biol. Chem.* **1989**, *264*, 13801-13809.

(160) Reddy, V. Y.; Desrochers, P. E.; Pizzo, S. V.; Gonias, S. L.; Sahakian, J. A.; Levine, R. L.; Weiss, S. J. *J. Biol. Chem.* **1994**, *269*, 4683-4691.
(161) Gao, J.; Yin, D. H.; Yao, Y. H.; Sun, H. Y.; Qin, Z. H.; Schoneich, C.; Williams, T. D.; Squier, T. C. *Biophys. J.* **1998**, *74*, 1115-1134.
(162) Sun, H. Y.; Gao, J.; Ferrington, D. A.; Biesiada, H.; Williams, T. D.; Squier, T. C. *Biochemistry* **1999**, *38*, 105-112.
(163) Garner, M. H.; Spector, A. *Proc. Natl. Acad. Sci. U. S. A.* **1980**, *77*, 1274-1277.
(164) Buzy, A.; Bracchi, V.; Sterjiades, R.; Chroboczek, J.; Thibault, P.; Gagnon, J.; Jouve, H. M.; Hudryclergeon, G. *J. Protein Chem.* **1995**, *14*, 59-72.
(165) Schoneich, C. *Arch. Biochem. Biophys.* **2002**, *397*, 370-376.
(166) Hiller, K. O.; Masloch, B.; Gobl, M.; Asmus, K. D. *J. Am. Chem. Soc.* **1981**, *103*, 2734-2743.
(167) Schoneich, C.; Pogocki, D.; Wisniowski, P.; Hug, G. L.; Bobrowski, K. *J. Am. Chem. Soc.* **2000**, *122*, 10224-10225.
(168) Selkoe, D. J. *J. Neuropathol. Exp. Neurol.* **1994**, *53*, 438-447.
(169) Spires, T. L.; Hyman, B. T. *Rev. Neurosci.* **2004**, *15*, 267-278.
(170) Vickers, J. C.; Dickson, T. C.; Adlard, P. A.; Saunders, H. L.; King, C. E.; McCormack, G. *Prog. Neurobiol.* **2000**, *60*, 139-165.
(171) Pogocki, D. *Acta Neurobiol. Exp. (Warsz.)* **2003**, *63*, 131-145.
(172) Glass, R. S. In *Organosulfur Chemistry Ii*, 1999; Vol. 205, pp 1-87.
(173) Butterfield, D. A.; Bush, A. I. *Neurobiol. Aging* **2004**, *25*, 563-568.
(174) Watson, A. A.; Fairlie, D. P.; Craik, D. J. *Biochemistry* **1998**, *37*, 12700-12706.
(175) Dong, J.; Atwood, C. S.; Anderson, V. E.; Siedlak, S. L.; Smith, M. A.; Perry, G.; Carey, P. R. *Biochemistry* **2003**, *42*, 2768-2773.
(176) Jones, D. P.; Carlson, J. L.; Mody, V. C.; Cai, J. Y.; Lynn, M. J.; Sternberg, P. *Free Radic. Biol. Med.* **2000**, *28*, 625-635.
(177) Lusini, L.; Tripodi, S. A.; Rossi, R.; Giannerini, F.; Giustarini, D.; del Vecchio, M. T.; Barbanti, G.; Cintorino, M.; Tosi, P.; Di Simplicio, P. *Int. J. Cancer* **2001**, *91*, 55-59.
(178) Ghezzi, P.; Romines, B.; Fratelli, M.; Eberini, I.; Gianazza, E.; Casagrande, S.; Laragione, T.; Mengozzi, M.; Herzenberg, L. A.; Herzenberg, L. A. *Mol. Immunol.* **2002**, *38*, 773-780.
(179) Niwa, T.; Naito, C.; Mawjood, A. H. M.; Imai, K. *Clin. Chem.* **2000**, *46*, 82-88.
(180) Herzenberg, L. A.; DeRosa, S. C.; Dubs, J. G.; Roederer, M.; Anderson, M. T.; Ela, S. W.; Deresinski, S. C.; Herzenberg, L. A. *Proc. Natl. Acad. Sci. U. S. A.* **1997**, *94*, 1967-1972.
(181) Giustarini, D.; Dalle-Donne, I.; Colombo, R.; Petralia, S.; Giampaoletti, S.; Milzani, A.; Rossi, R. *Clin. Chem.* **2003**, *49*, 327-330.
(182) Piemonte, F.; Pastore, A.; Tozzi, G.; Tagliacozzi, D.; Santorelli, F. M.; Carrozzo, R.; Casali, C.; Damiano, M.; Federici, G.; Bertini, E. *Eur. J. Clin. Investig.* **2001**, *31*, 1007-1011.
(183) Al-Abed, Y.; VanPatten, S.; Li, H. W.; Lawson, J. A.; FitzGerald, G. A.; Manogue, K. R.; Bucala, R. *Mol. Med.* **2001**, *7*, 619-623.

(184) Takayama, F.; Tsutsui, S.; Horie, M.; Shimokata, K.; Niwa, T. *Kidney Int.* **2001**, *59*, S155-S158.
(185) Hilliquin, P.; Borderie, D.; Hernvann, A.; Menkes, C. J.; Ekindjian, O. G. *Arthritis. Rheum.* **1997**, *40*, 1512-1517.
(186) Padron, J.; Peiro, C.; Cercas, E.; Llergo, J. L.; Sanchez-Ferrer, C. F. *Biochem. Biophys. Res. Commun.* **2000**, *271*, 217-221.
(187) Stamler, J. S.; Jaraki, O.; Osborne, J.; Simon, D. I.; Keaney, J.; Vita, J.; Singel, D.; Valeri, C. R.; Loscalzo, J. *Proc. Natl. Acad. Sci. U. S. A.* **1992**, *89*, 7674-7677.
(188) Tyurin, V. A.; Liu, S. X.; Tyurina, Y. Y.; Sussman, N. B.; Hubel, C. A.; Roberts, J. M.; Taylor, R.; Kagan, V. E. *Circ. Res.* **2001**, *88*, 1210-1215.
(189) Stamler, J. S.; Simon, D. I.; Osborne, J. A.; Mullins, M. E.; Jaraki, O.; Michel, T.; Singel, D. J.; Loscalzo, J. *Proc. Natl. Acad. Sci. U. S. A.* **1992**, *89*, 444-448.
(190) Wilcox, K. C.; Zhou, L.; Jordon, J. K.; Huang, Y.; Yu, Y. B.; Redler, R. L.; Chen, X.; Caplow, M.; Dokholyan, N. V. *J. Biol. Chem.* **2009**, *284*, 13940-13947.
(191) Asahi, M.; Fujii, J.; Suzuki, K.; Seo, H. G.; Kuzuya, T.; Hori, M.; Tada, M.; Fujii, S.; Taniguchi, N. *J. Biol. Chem.* **1995**, *270*, 21035-21039.
(192) Fujiwara, N.; Nakano, M.; Kato, S.; Yoshihara, D.; Ookawara, T.; Eguchi, H.; Taniguchi, N.; Suzuki, K. *J. Biol. Chem.* **2007**, *282*, 35933-35944.
(193) Diilio, C.; Sacchetta, P.; Angelucci, S.; Zezza, A.; Tenaglia, R.; Aceto, A. *Cancer Lett.* **1995**, *91*, 19-23.
(194) Iuchi, Y.; Okada, F.; Onuma, K.; Onoda, T.; Asao, H.; Kobayashi, M.; Fujii, J. *Biochem. J.* **2007**, *402*, 219-227.
(195) Janssen-Heininger, Y.; Ckless, K.; Reynaert, N.; van der Vliet, A. *Am. J. Pathol.* **2005**, *166*, 649-652.
(196) Gabbita, S. P.; Aksenov, M. Y.; Lovell, M. A.; Markesbery, W. R. *J. Neurochem.* **1999**, *73*, 1660-1666.
(197) Krishnan, S.; Chi, E. Y.; Wood, S. J.; Kendrick, B. S.; Li, C.; Garzon-Rodriguez, W.; Wypych, J.; Randolph, T. W.; Narhi, L. O.; Biere, A. L.; Citron, M.; Carpenter, J. F. *Biochemistry* **2003**, *42*, 829-837.
(198) Hokenson, M. J.; Uversky, V. N.; Goers, J.; Yamin, G.; Munishkina, L. A.; Fink, A. L. *Biochemistry* **2004**, *43*, 4621-4633.
(199) WellsKnecht, M. C.; Lyons, T. J.; McCance, D. R.; Thorpe, S. R.; Baynes, J. W. *J. Clin. Investig.* **1997**, *100*, 839-846.
(200) Brovelli, A.; Seppi, C.; Castellana, A. M.; Derenzis, M. R.; Blasina, A.; Balduini, C. *Biomed. Biochim. Acta* **1990**, *49*, S218-S223.
(201) Seppi, C.; Castellana, M. A.; Minetti, G.; Piccinini, G.; Balduini, C.; Brovelli, A. *Mech. Ageing Dev.* **1991**, *57*, 247-258.
(202) Spector, A. *FASEB J.* **1995**, *9*, 1173-1182.
(203) Korlimbinis, A.; Truscott, R. J. W. *Biochemistry* **2006**, *45*, 1950-1960.
(204) Horwitz, J.; Bova, M. P.; Ding, L. L.; Haley, D. A.; Stewart, P. L. *Eye* **1999**, *13*, 403-408.
(205) Horwitz, J. *Proc. Natl. Acad. Sci. U. S. A.* **1992**, *89*, 10449-10453.

(206) Cherian, M.; Abraham, E. C. *Biochem. Biophys. Res. Commun.* **1995**, - *208*, 675- 679.
(207) Uversky, V. N.; Li, J.; Souillac, P.; Millett, I. S.; Doniach, S.; Jakes, R.; Goedert, M.; Fink, A. L. *J. Biol. Chem.* **2002**, *277*, 11970-11978.
(208) Glaser, C. B.; Yamin, G.; Uversky, V. N.; Fink, A. L. *Biochimica et Biophysica Acta (BBA) - Proteins & Proteomics* **2005**, *1703*, 157-169.
(209) Penner-Hahn, J. E. *Coord. Chem. Rev.* **2005**, *249*, 161-177.
(210) Zhang, H. H.; Hedman, B.; Hodgson, K. O. In *Inorganic Electronic Structure and Spectroscopy, Volume 1: Methodology*; Solomon, E. I., Lever, A. B. P., Eds.; John Wiley & Sons, 1999; Vol. 1, pp 514-554.
(211) Thompson, A.; Vaughan, D., Eds. *X-ray Data Booklet*; Lawrence Berkeley National Laboratory: Berkeley, 2001.
(212) Wende, H. *Rep. Prog. Phys* **2004**, *67*, 2105-2181.
(213) Stern, E. A. In *EXAFS, SEXAFS and XANES*; Koningsberger, D. C., Prins, R., Eds.; John Wiley & Sons: New York, 1988; Vol. 1.
(214) Shadle, S. E.; Penner-Hahn, J. E.; Schugar, H. J.; Hedman, B.; Hodgson, K. O.; Solomon, E. I. *J. Am. Chem. Soc.* **1993**, *115*, 767-776.
(215) George, G. N.; Gorbaty, M. L. *J. Am. Chem. Soc.* **1989**, *111*, 3182-3186.
(216) Pickering, I. J.; Prince, R. C.; Divers, T.; George, G. N. *FEBS Lett.* **1998**, *441*, 11 - 14.
(217) Teo, B. K. *Acc. Chem. Res.* **1980**, *13*, 412-419.
(218) Duke, P. J. *Synchrotron Radiation: Production and Properties*; Oxford University Press: Oxford, 2000.
(219) Hoffman, A. *The Physics of Synchrotron Radiation*; Cambridge University Press: Cambridge, 2004.
(220) Webb, S. M. *Phys. Scr.* **2005**, *T115*, 1011-1014.
(221) Ravel, B.; Newville, M. *J. Synch. Rad.* **2005**, *12*, 537-541.
(222) Newville, M. *J. Synch. Rad.* **2001**, *8*, 96-100.
(223) Zabinsky, S. I.; Rehr, J. J.; Ankudinov, A.; Albers, R. C.; Eller, M. J. *Phys. Rev. B.* **1995**, *52*, 2995-3009.
(224) Fontecave, M. *Cell. Mol. Life Sci.* **1998**, *54*, 684-695.
(225) Eklund, H.; Uhlin, U.; Farnegardh, M.; Logan, D. T.; Nordlund, P. *Prog. Biophys. Mol. Biol.* **2001**, *77*, 177-268.
(226) Halliwell, B.; Gutteridge, J. *Free Radicals in Biology and Medicine*; 3 ed.; Oxford University Press Inc.: New York, 1999.
(227) Wardman, P. In *S-Centered Radicals*; Alfassi, Z., Ed.; John Wiley & Sons Ltd.: Chichester, 1999, pp 289-309.
(228) Lancaster, J. R. **2008**, *19*, 68-72.
(229) Well, J. A.; Bolton, J. R.; Wertz, J. E. *Electron Paramagnetic Resonance - Elementary Theory and Practical Applications*; John Wiley & Sons Inc.: New York, 1994.
(230) Hoffman, B. M.; DeRose, V. J.; Doan, P. E.; Gurbiel, R. J.; Houseman, A. L. P. In *Biological Magnetic Resonance*; Berliner, L. J., Reuben, J., Eds.; Plenum: New York, 1993; Vol. 13, p 151.
(231) Graslund, A.; Sahlin, M. *Annu. Rev. Biophys. Biomol. Struct.* **1996**, *25*, 259-286.

(232) Thomann, H.; Bernardo, M. In *Biological Magnetic Resonance*; Berliner, L. J., Reuben, J., Eds.; Plenum: New York, 1993; Vol. 13, p 275.
(233) Carrington, A.; McLachlan, D. M. *Introduction to Magnetic Resonance*; Harper and Row: New York, 1969.
(234) Gilbert, B. C. In *Sulfur-Centered Reactive Intermediated in Chemistry and Biology*; Chatgilialoglu, C., Asmus, K. D., Eds.; Plenum: New York, 1990, p 135.
(235) Lassmann, G.; Kolberg, M.; Bleifuss, G.; Graslund, A.; Sjoberg, B. M.; Lubitz, W. *Phys. Chem. Chem. Phys.* **2003**, *5*, 2442-2453.
(236) Kolberg, M.; Bleifuss, G.; Graslund, A.; Sjoberg, B. M.; Lubitz, W.; Lendzian, F.; Lassmann, G. *Arch. Biochem. Biophys.* **2002**, *403*, 141-144.
(237) Nelson, D. J.; Petersen, R. L.; Symons, M. C. R. *Journal of the Chemical Society Perkin Transactions 2* **1977**, 2005-2015.
(238) Winkler, J. R.; Gray, H. B. *Chem. Rev.* **1992**, *92*, 369-379.
(239) Donaire, A.; Salgado, J.; Moratal, J. M. *Biochemistry* **1998**, *37*, 8659-8673.
(240) Sjolin, L.; Tsai, L. C.; Langer, V.; Pascher, T.; Karlsson, G.; Nordling, M.; Nar, H. *Acta Crystallogr. Sect. D Biol. Crystallogr.* **1993**, *49*, 449-457.
(241) Wrighton, M.; Morse, D. L. *J. Am. Chem. Soc.* **1974**, *96*, 998-1003.
(242) Sullivan, B. P.; Meyer, T. J. *J. Chem. Soc., Chem. Commun.* **1984**, 1244-1245.
(243) PeakFit4.12; SeaSolve Software Inc., 2003.
(244) Chang, I. J.; Gray, H. B.; Winkler, J. R. **1991**, *113*, 7056-7057.
(245) Dey, A.; Okamura, T.; Ueyama, N.; Hedman, B.; Hodgson, K. O.; Solomon, E. I. *J. Am. Chem. Soc.* **2005**, *127*, 12046-12053.
(246) Brot, N.; Weissbach, H. *Arch. Biochem. Biophys.* **1983**, *223*, 271-281.
(247) Takemoto, L.; Horwitz, J.; Emmons, T. *Curr. Eye Res.* **1992**, *11*, 651-655.
(248) Andley, U. P. *Prog. Retin. Eye Res.* **2007**, *26*, 78-98.
(249) Hanson, S. R. A.; Hasan, A.; Smith, D. L.; Smith, J. B. *Exp. Eye Res.* **2000**, *-71*, - 207.
(250) Taylor, H. R.; West, S. K.; Rosenthal, F. S.; Munoz, B.; Newland, H. S.; Abbey, H.; Emmett, E. A. *N. Engl. J. Med.* **1988**, *319*, 1429-1433.
(251) Sliney, D. H. *Investigative Ophthalmology & Visual Science* **1986**, *27*, 781-790.
(252) McCarty, C. A.; Taylor, H. R. *Investigative Ophthalmology & Visual Science* **1996**, *37*, 1720-1723.
(253) Dong, X. Q.; Ayala, M.; Lofgren, S.; Soderberg, P. G. *Invest. Ophthalmol. Vis. Sci.* **2003**, *44*, 1150-1154.
(254) Merriam, J. C.; Lofgren, S.; Michael, R.; Soderberg, P.; Dillon, J.; Zheng, L.; Ayala, M. *Invest. Ophthalmol. Vis. Sci.* **2000**, *41*, 2642-2647.
(255) Azzam, N.; Levanon, D.; Dovrat, A. *Exp. Gerontol.* **2004**, *39*, 139-146.
(256) Giblin, F. J.; Leverenz, V. R.; Padgaonkar, V. A.; Unakar, N. J.; Dang, L.; Lin, L. R.; Lou, M. F.; Reddy, V. N.; Borchman, D.; Dillon, J. P. *Exp. Eye Res.* **2002**, *75*, 445-458.
(257) Marciniak, B.; Bobrowski, K.; Hug, G. L.; Rozwadowski, J. *J. Phys. Chem.* **1994**, *98*, 4854-4860.

(258) Bobrowski, K.; Marciniak, B.; Hug, G. L. *J. Am. Chem. Soc.* **1992**, *114*, 10279-10288.
(259) Foote, C. S.; Peters, J. W. *J. Am. Chem. Soc.* **1971**, *93*, 3795-&.
(260) Sysak, P. K.; Foote, C. S.; Ching, T. Y. *Photochem. Photobiol.* **1977**, *26*, 19-27.
(261) Baciocchi, E.; Del Giacco, T.; Elisei, F.; Gerini, M. F.; Guerra, M.; Lapi, A.; Liberali, P. *J. Am. Chem. Soc.* **2003**, *125*, 16444-16454.
(262) Kennepohl, P.; Wasinger, E. C.; George, S. D. *J. Synch. Rad.* **2009**, *16*, 484-488.
(263) Malinowski, E. R. *Factor Analysis in Chemistry*; 2nd ed.; Wiley: New York, 1991.
(264) Rompel, A.; Cinco, R. M.; Latimer, M. J.; McDermott, A. E.; Guiles, R. D.; Quintanilha, A.; Krauss, R. M.; Sauer, K.; Yachandra, V. K.; Klein, M. P. *Proc. Natl. Acad. Sci. U. S. A.* **1998**, *95*, 6122-6127.
(265) Kopoldov.J; Liebster, J.; Gross, E. *Radiat. Res.* **1967**, *30*, 261-&.
(266) Martin-Diaconescu, V.; Kennepohl, P. *J. Am. Chem. Soc.* **2007**, *129*, 3034-3035.
(267) Saidel, L. J.; Godfarb, R. A.; Waldman, S. *J. Biol. Chem.* **1952**, *197*, 285-291.
(268) Faller, P.; Vasak, M. *Inorg. Chim. Acta* **1998**, *272*, 150-152.
(269) Harvey, G. R.; Russell, L. F. *Geophys. Res. Lett.* **1986**, *13*, 49-51.
(270) Davies, M. J.; Truscott, R. J. W. *J. Photochem. Photobiol. B Biol.* **2001**, *63*, 114-125.
(271) Small, G. W.; Rabins, P. V.; Barry, P. P.; Buckholtz, N. S.; DeKosky, S. T.; Ferris, S. H.; Finkel, S. I.; Gwyther, L. P.; Khachaturian, Z. S.; Lebowitz, B. D.; McRae, T. D.; Morris, J. C.; Oakley, F.; Schneider, L. S.; Streim, J. E.; Sunderland, T.; Teri, L. A.; Tune, L. E. *Journal of the American Medical Association* **1997**, *278*, 1363-1371.
(272) Rogaeva, E. *NeuroMol. Med.* **2002**, *2*, 1-10.
(273) Lindsay, J.; Laurin, D.; Verreault, R.; Hebert, R.; Helliwell, B.; Hill, G. B.; McDowell, I. *Am. J. Epidemiol.* **2002**, *156*, 445-453.
(274) Hardy, J. A.; Higgins, G. A. *Science* **1992**, *256*, 184-185.
(275) McLean, C. A.; Cherny, R. A.; Fraser, F. W.; Fuller, S. J.; Smith, M. J.; Beyreuther, K.; Bush, A. I.; Masters, C. L. *Ann. Neurol.* **1999**, *46*, 860-866.
(276) Cherny, R. A.; Legg, J. T.; McLean, C. A.; Fairlie, D. P.; Huang, X. D.; Atwood, C. S.; Beyreuther, K.; Tanzi, R. E.; Masters, C. L.; Bush, A. I. *J. Biol. Chem.* **1999**, *274*, 23223-23228.
(277) Hung, L. W.; Ciccotosto, G. D.; Giannakis, E.; Tew, D. J.; Perez, K.; Masters, C. L.; Cappai, R.; Wade, J. D.; Barnham, K. J. *J. Neurosci.* **2008**, *28*, 11950-11958.
(278) Rauk, A. **2009**, *38*, 2698-2715.
(279) Dahlgren, K. N.; Manelli, A. M.; Stine, W. B.; Baker, L. K.; Krafft, G. A.; LaDu, M. J. *J. Biol. Chem.* **2002**, *277*, 32046-32053.
(280) Takahashi, S.; Takahashi, I.; Sato, H.; Kubota, Y.; Yoshida, S.; Muramatsu, Y. *Biol. Trace Elem. Res.* **2001**, *80*, 145-158.

(281) Maynard, C. J.; Cappai, R.; Volitakis, I.; Cherny, R. A.; White, A. R.; Beyreuther, K.; Masters, C. L.; Bush, A. I.; Li, Q. X. *J. Biol. Chem.* **2002**, *277*, 44670-44676.
(282) Smith, D. G.; Cappai, R.; Barnham, K. J. *Biochim. Biophys. Acta, Biomembr.* **2007**, *1768*, 1976-1990.
(283) Barnham, K. J.; Bush, A. I. *Curr. Opin. Chem. Biol.* **2008**, *12*, 222-228.
(284) Atwood, C. S.; Huang, X. D.; Moir, R. D.; Tanzi, R. E.; Bush, A. I. In *Metal Ions in Biological Systems, Vol 36*, 1999; Vol. 36, pp 309-364.
(285) Lovell, M. A.; Robertson, J. D.; Teesdale, W. J.; Campbell, J. L.; Markesbery, W. R. *J. Neurol. Sci.* **1998**, *158*, 47-52.
(286) Gutteridge, J. M. C. *Biochem. J.* **1984**, *218*, 983-985.
(287) Scott, L. E.; Orvig, C. *Chem. Rev.* **2009**, *109*, 4885-4910.
(288) Zatta, P.; Drago, D.; Bolognin, S.; Sensi, S. L. *Trends Pharmacol. Sci.* **2009**, *30*, 346-355.
(289) Deibel, M. A.; Ehmann, W. D.; Markesbery, W. R. *J. Neurol. Sci.* **1996**, *143*, 137-142.
(290) Atwood, C. S.; Scarpa, R. C.; Huang, X. D.; Moir, R. D.; Jones, W. D.; Fairlie, D. P.; Tanzi, R. E.; Bush, A. I. *J. Neurochem.* **2000**, *75*, 1219-1233.
(291) Bush, A. I. *Trends Neurosci.* **2003**, *26*, 207-214.
(292) Bush, A. I.; Pettingell, W. H.; Multhaup, G.; Paradis, M. D.; Vonsattel, J. P.; Gusella, J. F.; Beyreuther, K.; Masters, C. L.; Tanzi, R. E. *Science* **1994**, *265*, 1464-1467.
(293) Miura, T.; Suzuki, K.; Kohata, N.; Takeuchi, H. *Biochemistry* **2000**, *39*, 7024-7031.
(294) Atwood, C. S.; Moir, R. D.; Huang, X. D.; Scarpa, R. C.; Bacarra, N. M. E.; Romano, D. M.; Hartshorn, M. K.; Tanzi, R. E.; Bush, A. I. *J. Biol. Chem.* **1998**, *273*, 12817-12826.
(295) Smith, M. A.; Harris, P. L. R.; Sayre, L. M.; Perry, G. *Proc. Natl. Acad. Sci. U. S. A.* **1997**, *94*, 9866-9868.
(296) Cuajungco, M. P.; Goldstein, L. E.; Nunomura, A.; Smith, M. A.; Lim, J. T.; Atwood, C. S.; Huang, X. D.; Farrag, Y. W.; Perry, G.; Bush, A. I. *J. Biol. Chem.* **2000**, *275*, 19439-19442.
(297) Schubert, D.; Chevion, M. *Biochem. Biophys. Res. Commun.* **1995**, *216*, 702-707.
(298) Huang, X. D.; Cuajungco, M. P.; Atwood, C. S.; Hartshorn, M. A.; Tyndall, J. D. A.; Hanson, G. R.; Stokes, K. C.; Leopold, M.; Multhaup, G.; Goldstein, L. E.; Scarpa, R. C.; Saunders, A. J.; Lim, J.; Moir, R. D.; Glabe, C.; Bowden, E. F.; Masters, C. L.; Fairlie, D. P.; Tanzi, R. E.; Bush, A. I. *J. Biol. Chem.* **1999**, *274*, 37111-37116.
(299) Huang, X. D.; Atwood, C. S.; Hartshorn, M. A.; Multhaup, G.; Goldstein, L. E.; Scarpa, R. C.; Cuajungco, M. P.; Gray, D. N.; Lim, J.; Moir, R. D.; Tanzi, R. E.; Bush, A. I. *Biochemistry* **1999**, *38*, 7609-7616.
(300) Barnham, K. J.; Ciccotosto, G. D.; Tickler, A. K.; Ali, F. E.; Smith, D. G.; Williamson, N. A.; Lam, Y. H.; Carrington, D.; Tew, D.; Kocak, G.; Volitakis, I.; Separovic, F.; Barrow, C. J.; Wade, J. D.; Masters, C. L.; Cherny, R. A.; Curtain, C. C.; Bush, A. I.; Cappai, R. *J. Biol. Chem.* **2003**, *278*, 42959-42965.

(301) Hureau, C.; Faller, P. *Biochimie* **2009**, *91*, 1212-1217.
(302) Tabner, B. J.; El-Agnaf, O. M. A.; Turnbull, S.; German, M. J.; Paleologou, K. E.; Hayashi, Y.; Cooper, L. J.; Fullwood, N. J.; Allsop, D. *J. Biol. Chem.* **2005**, *280*, 35789-35792.
(303) Hardy, J.; Selkoe, D. J. *Science* **2002**, *297*, 353-356.
(304) Opazo, C.; Huang, X. D.; Cherny, R. A.; Moir, R. D.; Roher, A. E.; White, A. R.; Cappai, R.; Masters, C. L.; Tanzi, R. E.; Inestrosa, N. C.; Bush, A. I. *J. Biol. Chem.* **2002**, *277*, 40302-40308.
(305) Markesbery, W. R. *Free Radic. Biol. Med.* **1997**, *23*, 134-147.
(306) Liochev, S. I. In *Metal Ions in Biological Systems, Vol 36*, 1999; Vol. 36, pp 1-39.
(307) Varadarajan, S.; Yatin, S.; Aksenova, M.; Butterfield, D. A. *J. Struct. Biol.* **2000**, *130*, 184-208.
(308) Ali, F. E.; Separovic, F.; Barrow, C. J.; Cherny, R. A.; Fraser, F.; Bush, A. I.; Masters, C. L.; Barnham, K. J. *J. Pept. Sci.* **2005**, *11*, 353-360.
(309) Curtain, C. C.; Ali, F.; Volitakis, I.; Cherny, R. A.; Norton, R. S.; Beyreuther, K.; Barrow, C. J.; Masters, C. L.; Bush, A. I.; Barnham, K. J. *J. Biol. Chem.* **2001**, *276*, 20466-20473.
(310) Varadarajan, S.; Kanski, J.; Aksenova, M.; Lauderback, C.; Butterfield, D. A. *J. Am. Chem. Soc.* **2001**, *123*, 5625-5631.
(311) Pogocki, D.; Schoneich, C. *Chem. Res. Toxicol.* **2002**, *15*, 408-418.
(312) Kuo, Y. M.; Kokjohn, T. A.; Beach, T. G.; Sue, L. I.; Brune, D.; Lopez, J. C.; Kalback, W. M.; Abramowski, D.; Sturchler-Pierrat, C.; Staufenbiel, M.; Roher, A. E. *J. Biol. Chem.* **2001**, *276*, 12991-12998.
(313) Varadarajan, S.; Yatin, S.; Kanski, J.; Jahanshahi, F.; Butterfield, D. A. *Brain Res. Bull.* **1999**, *50*, 133-141.
(314) Sanaullah; Wilson, G. S.; Glass, R. S. *J. Inorg. Biochem.* **1994**, *55*, 87-99.
(315) Jiang, D. L.; Men, L. J.; Wang, J. X.; Zhang, Y.; Chickenyen, S.; Wang, Y. S.; Zhou, F. M. *Biochemistry* **2007**, *46*, 9270-9282.
(316) Schoneich, C.; Pogocki, D.; Hug, G. L.; Bobrowski, K. *J. Am. Chem. Soc.* **2003**, *125*, 13700-13713.
(317) Glass, R. S.; Hug, G. L.; Schoneich, C.; Wilson, G. S.; Kuznetsova, L.; Lee, T. M.; Ammam, M.; Lorance, E.; Nauser, T.; Nichol, G. S.; Yamamoto, T. *J. Am. Chem. Soc.* **2009**, *131*, 13791-13805.
(318) Pogocki, D.; Serdiuk, K.; Schoneich, C. *J. Phys. Chem. A* **2003**, *107*, 7032-7042.
(319) Schiewe, A. J.; Margol, L.; Soreghan, B. A.; Thomas, S. N.; Yang, A. J. *Pharm. Res.* **2004**, *21*, 1094-1102.
(320) Guilloreau, L.; Damian, L.; Coppel, Y.; Mazarguil, H.; Winterhalter, M.; Faller, P. *J. Biol. Inorg. Chem.* **2006**, *11*, 1024-1038.
(321) da Silva, G. F. Z.; Lykourinou, V.; Angerhofer, A.; Ming, L. J. *Biochim. Biophys. Acta* **2009**, *1792*, 49-55.
(322) Nadal, R. C.; Rigby, S. E. J.; Viles, J. H. *Biochemistry* **2008**, *47*, 11653-11664.
(323) Pogocki, D. *Chem. Res. Toxicol.* **2004**, *17*, 325-329.

(324) Karr, J. W.; Kaupp, L. J.; Szalai, V. A. *J. Am. Chem. Soc.* **2004**, *126*, 13534-13538.
(325) Syme, C. D.; Nadal, R. C.; Rigby, S. E. J.; Viles, J. H. *J. Biol. Chem.* **2004**, *279*, 18169-18177.
(326) Syme, C. D.; Viles, J. H. *Biochim. Biophys. Acta* **2006**, *1764*, 246-256.
(327) Stellato, F.; Menestrina, G.; Dalla Serra, M.; Potrich, C.; Tomazzolli, R.; Meyer-Klaucke, W.; Morante, S. *Eur. Biophys. J.* **2006**, *35*, 340-351.
(328) Minicozzi, V.; Stellato, F.; Comai, M.; Serra, M. D.; Potrich, C.; Meyer-Klaucke, W.; Morante, S. *J. Biol. Chem.* **2008**, *283*, 10784-10792.
(329) Streltsov, V. A.; Titmuss, S. J.; Epa, V. C.; Barnham, K. J.; Masters, C. L.; Varghese, J. N. *Biophys. J.* **2008**, *95*, 3447-3456.
(330) Shearer, J.; Szalai, V. A. *J. Am. Chem. Soc.* **2008**, *130*, 17826-17835.
(331) Mantri, Y.; Fioroni, M.; Baik, M. H. *J. Biol. Inorg. Chem.* **2008**, *13*, 1197-1204.
(332) Dorlet, P.; Gambarelli, S.; Faller, P.; Hureau, C. *Angew. Chem.* **2009**, *48*, 9273-9276.
(333) Dong, J. J.; Shokes, J. E.; Scott, R. A.; Lynn, D. G. *J. Am. Chem. Soc.* **2006**, *128*, 3540-3542.
(334) Zirah, S.; Kozin, S. A.; Mazur, A. K.; Blond, A.; Cheminant, M.; Segalas-Milazzo, I.; Debey, P.; Rebuffat, S. *J. Biol. Chem.* **2006**, *281*, 2151-2161.
(335) Danielsson, J.; Pierattelli, R.; Banci, L.; Graslund, A. *FEBS J.* **2007**, *274*, 46-59.
(336) Drochioiu, G. *Eur. J. Mass Spectrom.* **2009**, *15*, 651-659.
(337) Newville, M.; Livins, P.; Yacoby, Y.; Rehr, J. J.; Stern, E. A. *Phys. Rev. B.* **1993**, *47*, 14126-14131.
(338) Binsted, N.; Strange, R. W.; Hasnain, S. S. *Biochemistry* **1992**, *31*, 12117-12125.
(339) Kau, L. S.; Spirasolomon, D. J.; Pennerhahn, J. E.; Hodgson, K. O.; Solomon, E. I. *J. Am. Chem. Soc.* **1987**, *109*, 6433-6442.
(340) Karr, J. W.; Szalai, V. A. *J. Am. Chem. Soc.* **2007**, *129*, 3796-3797.
(341) Hureau, C.; Coppel, Y.; Dorlet, P.; Solari, P. L.; Sayen, S.; Guillon, E.; Sabater, L.; Faller, P. *Angew. Chem.* **2009**, *48*, 9522-9525.
(342) Kowalik-Jankowska, T.; Ruta, M.; Wisniewska, K.; Lankiewicz, L. *J. Inorg. Biochem.* **2003**, *95*, 270-282.
(343) Ma, Q. F.; Hu, J.; Wu, W. H.; Liu, H. D.; Du, J. T.; Fu, Y.; Wu, Y. W.; Lei, P.; Zhao, Y. F.; Li, Y. M. *Biopolymers* **2006**, *83*, 20-31.
(344) Karr, J. W.; Akintoye, H.; Kaupp, L. J.; Szalai, V. A. *Biochemistry* **2005**, *44*, 5478-5487.
(345) Chaboy, J.; Munoz-Paez, A.; Merkling, P. J.; Marcos, E. S. *J. Chem. Phys.* **2006**, *124*.
(346) Fulton, J. L.; Hoffmann, M. M.; Darab, J. G.; Palmer, B. J.; Stern, E. A. *J. Phys. Chem. A* **2000**, *104*, 11651-11663.
(347) Westre, T. E.; Kennepohl, P.; DeWitt, J. G.; Hedman, B.; Hodgson, K. O.; Solomon, E. I. *J. Am. Chem. Soc.* **1997**, *119*, 6297-6314.
(348) Bush, A. I.; Tanzi, R. E. *Neurotherapeutics* **2008**, *5*, 421-432.

APPENDIX A: DNA SEQUENCING OUTPUT

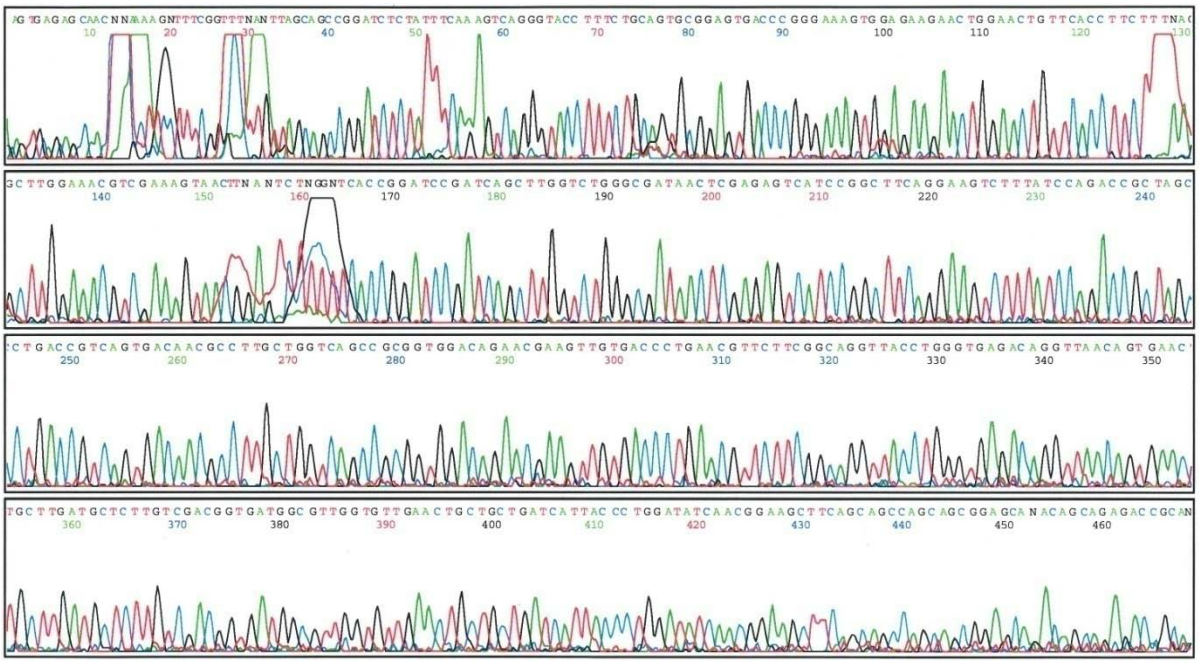

Figure A.0.1 DNA sequence of Y108C^{m}

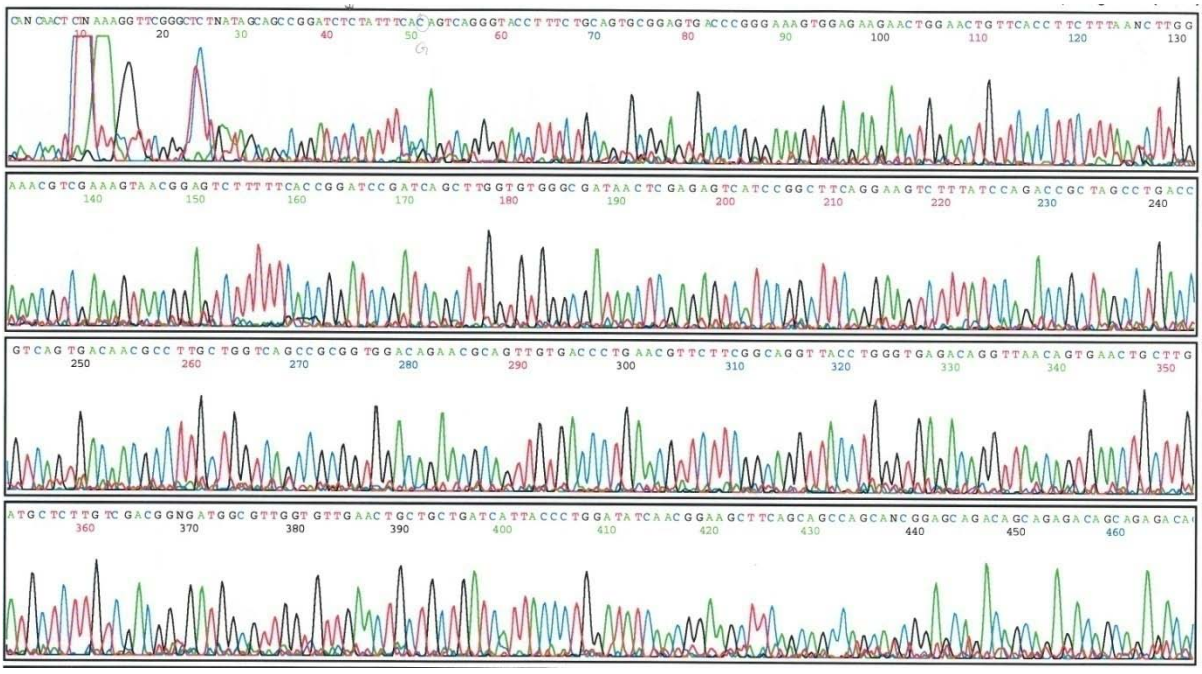

Figure A.0.2 DNA sequence of W48C^{m}

APPENDIX B: RHENIUM-LABELED AZURIN DATA

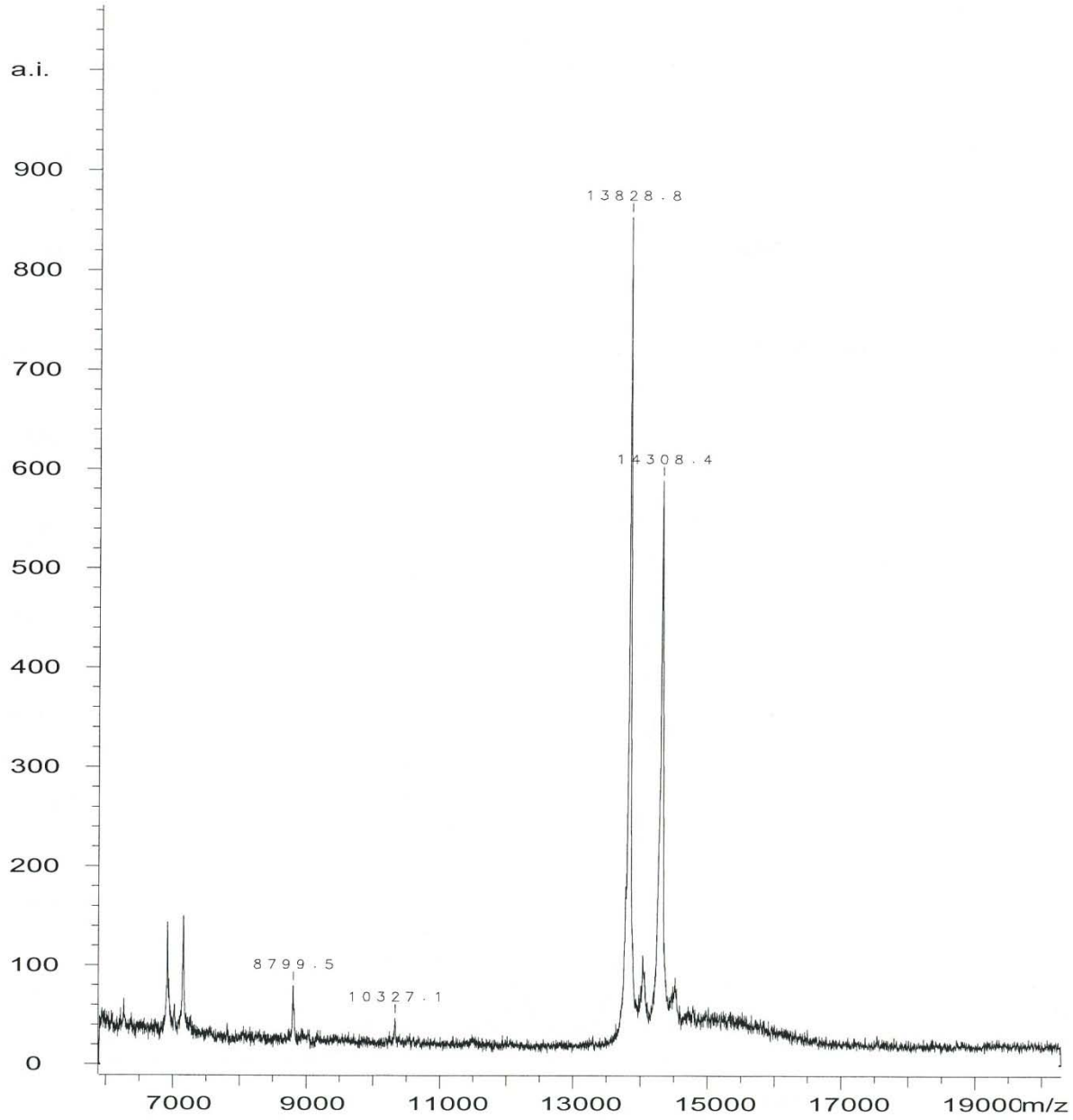

Figure B.0.3 MALDI-TOF result of Re-labeled Y108C and unlabeled Y108C before purification.

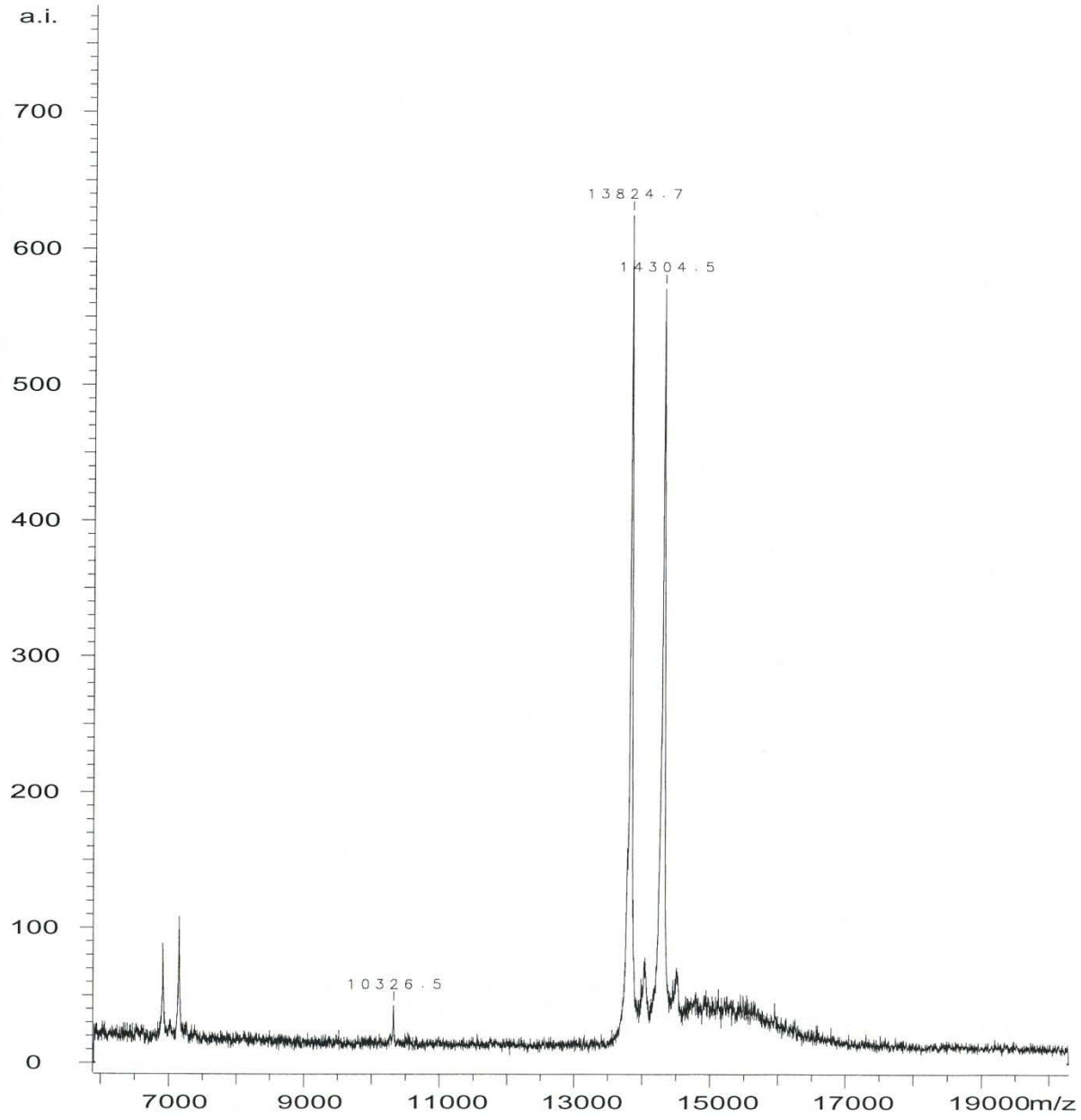

Figure B.0.4 MALDI-TOF result of Re-labeled W48C and unlabeled W48C before purification.

APPENDIX C: LIST OF PUBLICATIONS

1. Karunakaran-Datt, A. and Kennepohl, P., "Redox Photochemistry of Methionine by Sulfur K-edge X-ray Absorption Spectroscopy: Potential Implications for Cataract Formation" *J. Am. Chem. Soc.* **2009**, *131*, 3577-3582. (The work presented in Chapter 4 corresponds to this publication)

2. Karunakaran-Datt, A., Martin-Diaconescu, V., and Kennepohl, P. *Chem. Soc. Rev.* In preparation. (Majority of the Chapter 1 will be published as a major component of a broader review article with additional contributions from Vlad Martin-Diaconescu)

3. Karunakaran-Datt, A. and Kennepohl, P., "Redox-active Metal Binding in Amyloid-β and Its Potential Role in Oxidation of Met_{35}" In preparation. (The work presented in Chapter 5 and 6 corresponds to this publication)

4. Karunakaran-Datt, A. and Kennepohl, P. "Protein Sulfur-Centred Radicals: a Sulfur K-edge XAS Detection Method" In preparation. (The work presented in Chapter 3 corresponds to this publication)